



# LUND UNIVERSITY

Reaction Mechanisms and Dynamics in the Early Stage of High- $\kappa$  Oxide Atomic Layer Deposition

Investigations by In Situ and Operando X-ray Photoemission Spectroscopy

D Acunto, Giulio

2022

[Link to publication](#)

*Citation for published version (APA):*

D Acunto, G. (2022). *Reaction Mechanisms and Dynamics in the Early Stage of High- $\kappa$  Oxide Atomic Layer Deposition: Investigations by In Situ and Operando X-ray Photoemission Spectroscopy*. Lund University.

*Total number of authors:*

1

## General rights

Unless other specific re-use rights are stated the following general rights apply:

Copyright and moral rights for the publications made accessible in the public portal are retained by the authors and/or other copyright owners and it is a condition of accessing publications that users recognise and abide by the legal requirements associated with these rights.

- Users may download and print one copy of any publication from the public portal for the purpose of private study or research.
- You may not further distribute the material or use it for any profit-making activity or commercial gain
- You may freely distribute the URL identifying the publication in the public portal

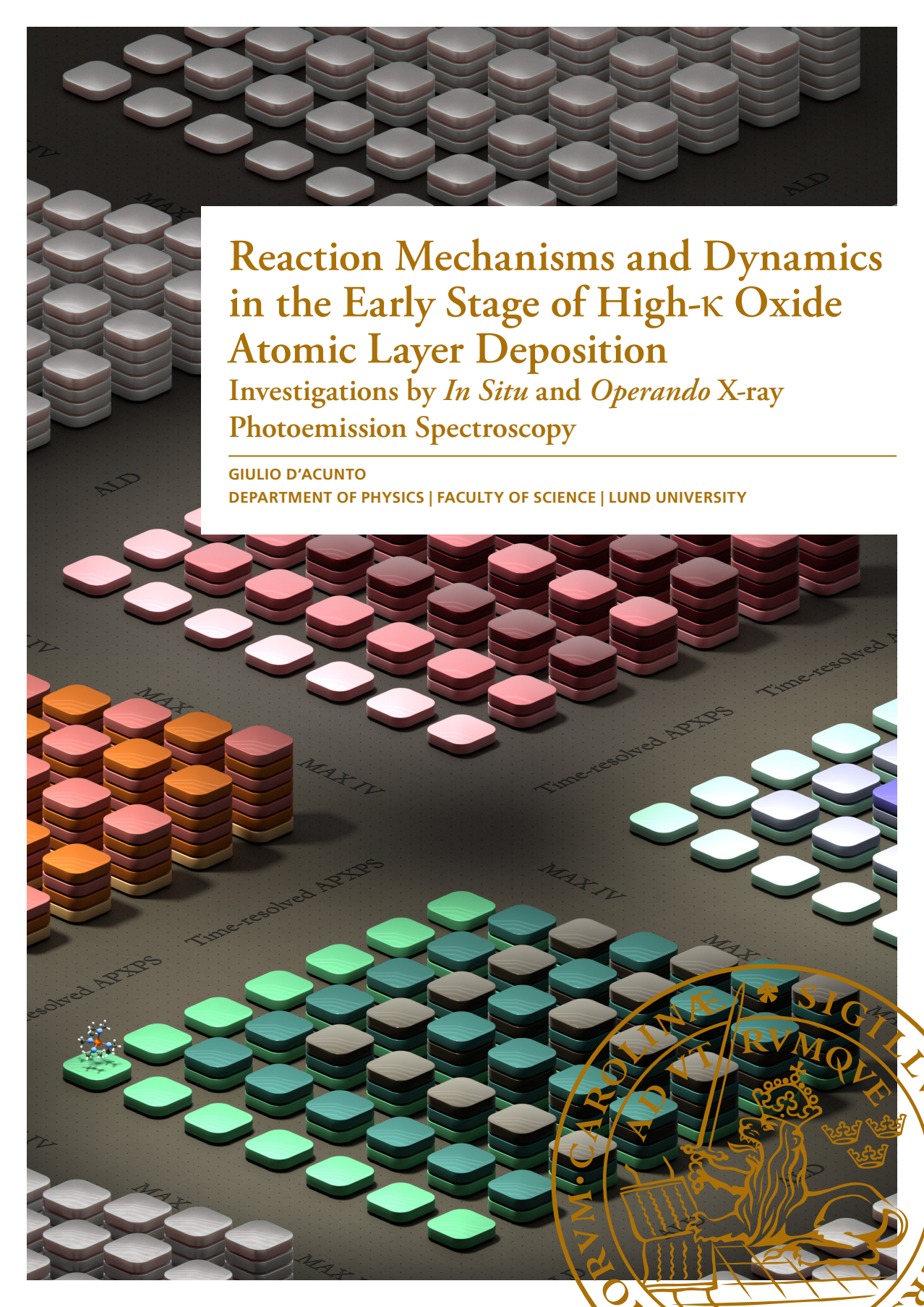
Read more about Creative commons licenses: <https://creativecommons.org/licenses/>

## Take down policy

If you believe that this document breaches copyright please contact us providing details, and we will remove access to the work immediately and investigate your claim.

LUND UNIVERSITY

PO Box 117  
221 00 Lund  
+46 46-222 00 00

A 3D visualization of the atomic layer deposition (ALD) process. The image shows a grid of square blocks representing atoms, arranged in layers. The blocks are colored in a gradient from white to red, orange, yellow, green, and blue, representing different chemical species or states. The text "ALD" is visible on the surface. A white box with a gold border contains the title and author information.

# Reaction Mechanisms and Dynamics in the Early Stage of High- $\kappa$ Oxide Atomic Layer Deposition

Investigations by *In Situ* and *Operando* X-ray  
Photoemission Spectroscopy

GIULIO D'ACUNTO

DEPARTMENT OF PHYSICS | FACULTY OF SCIENCE | LUND UNIVERSITY





Reaction Mechanisms and Dynamics in the Early  
Stage of High- $\kappa$  Oxide  
Atomic Layer Deposition

Investigations by *In Situ* and *Operando*  
X-ray Photoemission Spectroscopy

Giulio D'Acunto



**LUND**  
UNIVERSITY

DOCTORAL DISSERTATION

by due permission of the Faculty of Science, Lund University, Sweden.

To be defended in the Rydberg Lecture Hall at the  
Department of Physics on Friday, the 20<sup>th</sup> of May 2022 at 13:15.

*Faculty opponent*

Prof. Stacey Bent, Stanford University



<b>Organisation</b> LUND UNIVERSITY  <b>Author:</b> Giulio D'Acunto	<b>Document name</b> DOCTORAL DISSERTATION	
	<b>Date of issue</b> 2022-05-20	
	Sponsoring organisation	
<b>Reaction Mechanisms and Dynamics in the Early Stage of High-κ Oxide Atomic Layer Deposition - Investigations by In Situ and Operando X-ray Photoemission Spectroscopy</b>		
<p>Atomic layer deposition (ALD) is an outstanding deposition technique to deposit highly conformal and uniform thin films with atomic precision. In particular, ALD of transition metal oxide layers from metal amido complexes and water finds its way in several technological fields, including green energy devices and in the semiconductor industry. These ALD reactions are believed to follow a reaction scheme based on the ligand exchange mechanism, in which the surface on which deposition takes place plays a largely static role and the ligands of the used precursor are chemically unchanged during the reaction. To address the correctness of the model, time-resolved <i>in situ</i> and <i>operando</i> ambient pressure x-ray photoelectron spectroscopy (APXPS) technique was employed during the ALD of HfO<sub>2</sub> on InAs covered by a thermal or native oxide, TiO<sub>2</sub>(101) and oxidised as well as clean Si(111).</p> <p>The classic ligand exchange reaction mechanism does not adequately describe the reaction path in any of the investigated sample systems. In particular, ALD of HfO<sub>2</sub> on SiO<sub>2</sub> follows a bimolecular reaction mechanism based on the insertion of an hydrogen atom of one of the ligands in an amido complex dimer. As a result of its bimolecular nature, this reaction can take place only on a SiO<sub>2</sub> surface of a sufficiently high coverage of physisorbed complexes. Similarly, on TiO<sub>2</sub> the early stage of the reaction is based on dissociative adsorption, followed by an intra- and inter- molecular reaction path, leading to the formation of new sets of surface species never before identified in any of the previous ALD models.</p> <p>For easily reducible surfaces, such as InAs oxide and TiO<sub>2</sub>, evidence is found for HfO<sub>x</sub> formation already during the first ALD half-cycle, due to the transfer of O atoms from the surface to the metal complex. Clearly, this contradicts the static role of the surface in standard ALD models. Interestingly, in the case of InAs covered by a thermal or native oxide, this phenomenon, which lies behind the so-called self-cleaning effect, guarantees a sharp interface between the III-V material and HfO<sub>2</sub>, which is a prerequisite for next generation MOSFETs.</p> <p>These results open new doors for improving devices based on ALD. Time-resolved <i>in situ</i> and <i>operando</i> APXPS allows to follow the kinetics and mechanisms involved in ALD, in real time at second time resolution with significant benefit for the further improvement of general understanding of ALD reactions.</p>		
<b>Key words:</b> atomic layer deposition (ALD), high-k oxide, in situ and operando study, XPS, APXPS.		
Classification system and/or index terms (if any)		
Supplementary bibliographical information	<b>Language</b> English	
ISSN and key title	<b>ISBN</b> 978-91-8039-229-7 978-91-8039-230-3	
Recipient's notes	<b>Number of pages</b> 126	Price

I, the undersigned, being the copyright owner of the abstract of the above-mentioned dissertation, hereby grant to all reference sources permission to publish and disseminate the abstract of the above-mentioned dissertation.

Signature 

Date 2022-04-07

Reaction Mechanisms and Dynamics in the Early  
Stage of High- $\kappa$  Oxide  
Atomic Layer Deposition

Investigations by *In Situ* and *Operando*  
X-ray Photoemission Spectroscopy

Giulio D'Acunto



**LUND**  
UNIVERSITY

### **Cover photo**

Artistic representation of ALD. The different shades of colours represent the systems already studied. The white dowels, kept on the side and slightly in the dark, represent the endless possibilities of the technique and the materials that can deposit.

Pages i-104 © Giulio D'Acunto

Paper I © Licensed under CC-BY. Published by American Chemical Society.

Paper II © The authors.

Paper III © Licensed under CC-BY 3.0. Published by The Royal Society of Chemistry.

Paper IV © The authors.

Paper V © The authors.

Paper VI © The authors.

Paper VII © Licensed under CC-BY. Published by Journal of Synchrotron Radiation

Paper VIII © The authors.

Division of Synchrotron Radiation Research  
Department of Physics, Faculty of Science  
Lund University

### **ISBN**

978-91-8039-229-7 (electronic)

978-91-8039-230-3 (print)

Printed in Sweden by Media-Tryck, Lund University  
Lund 2022



Media-Tryck is a Nordic Swan Ecolabel certified provider of printed material. Read more about our environmental work at [www.mediatryck.lu.se](http://www.mediatryck.lu.se)

**MADE IN SWEDEN** 

# Table of Contents

List of publications .....	VII
Popular Scientific Summary .....	XIII
Sommario Divulgativo .....	XVII
Acknowledgements .....	XXI
<b>1 Introduction .....</b>	<b>1</b>
1.1 A brief story of a device .....	1
1.2 Motivation .....	6
1.3 This thesis .....	8
<b>2 Atomic Layer Deposition .....</b>	<b>9</b>
2.1 Why ALD and what it is .....	9
2.2 Current understanding .....	10
2.2.1 Ligand exchange model and other known reactions .....	13
2.3 ALD for the semiconductor industry .....	15
2.3.1 High- $\kappa$ oxides .....	15
2.3.2 Beyond silicon era - III-V semiconductors .....	17
<b>3 Techniques .....</b>	<b>21</b>
3.1 X-ray Photoemission Spectroscopy .....	21
3.1.1 The theory of photoemission .....	22
3.1.2 Practical approach .....	27
3.2 Small guide to analysing XPS data .....	31

<b>4</b>	<b>MAX IV Light Source.....</b>	<b>39</b>
4.1	Beamlines .....	43
4.1.1	Flux and resolution.....	45
4.2	Endstation.....	47
4.3	Practical guide to do a beamtime.....	55
<b>5</b>	<b>Insights from <i>in situ</i> and <i>operando</i> APXPS.....</b>	<b>61</b>
5.1	New surface species: the origin.....	61
5.2	The surface, does it do something? .....	64
5.3	Convolution of reaction mechanisms.....	74
5.4	Consideration on APXPS for ALD experiments.....	76
5.5	Adsorption of ethanol on rutile TiO <sub>2</sub> (110).....	78
<b>6</b>	<b>Other related research .....</b>	<b>81</b>
6.1	Fast process, smart setup I.....	81
6.2	Fast(er) process, smart setup II .....	83
6.3	Graphene vs. hBN.....	84
<b>7</b>	<b>Outlook.....</b>	<b>87</b>
7.1	Steady state during ALD .....	88
7.2	Graphene and ALD.....	89
<b>8</b>	<b>Concluding remarks .....</b>	<b>93</b>
<b>9</b>	<b>References.....</b>	<b>95</b>



# List of publications

This thesis is based on the following publications, referred by their Roman numerus. My involvement is well represented by the position of my name in the author list.

## **I. Atomic Layer Deposition of Hafnium Oxide on InAs: Insight from Time-Resolved in Situ Studies**

G. D'Acunto, A. Troian, E. Kokkonen, F. Rehman, Y.-P. Liu, S. Yngman, Z. Yong, S. R. McKibbin, T. Gallo, E. Lind, J. Schnadt, R. Timm

*ACS Applied Electronic Materials* 2, 3915–3922 (2020)

I was the main responsible for analysing all the data and writing the manuscript. Since the experiment was carried out briefly after my start of PhD, I was not the main responsible for planning and preparing the ambient pressure x-ray photoemission spectroscopy measurements.

## **II. Time evolution of surface species during the ALD of a high- $\kappa$ oxide on an InAs thermal oxide**

G. D'Acunto, P. Shayesteh, E. Kokkonen, V. Boix de la Cruz, F. Rehman, N. Mosahebfard, E. Lind, J. Schnadt, R. Timm

*Submitted to Applied Surface Science*

I was the main responsible for planning, preparing, and leading the ambient pressure x-ray photoemission spectroscopy experiment. I analysed all the data and wrote the manuscript.

## **III. Oxygen relocation during HfO<sub>2</sub> ALD on InAs**

G. D'Acunto, E. Kokkonen, P. Shayesteh, V. Boix de la Cruz, F. Rehman, Z. Mosahebfard, E. Lind, J. Schnadt, R. Timm

*Faraday Discussion, in press, 2022*

I was the main responsible for planning, preparing and leading the ambient pressure x-ray photoemission spectroscopy experiment. I analysed all the data and wrote the manuscript.

**IV. Role of temperature, pressure, and surface oxygen migration in the initial atomic layer deposition of HfO<sub>2</sub> on anatase TiO<sub>2</sub>(101)**

G. D'Acunto, R. Jones, L. Pérez Ramírez, P. Shayesteh, F. Rehman, E. Kokkonen, F. Lim, F. Bournel, J.-J. Gallet, R. Timm, J. Schnadt

*Submitted to Journal of Physical Chemistry C*

I was the main responsible for planning and preparing two of the three experiments carried out for this manuscript. I analysed all the data and wrote the manuscript.

**V. Bimolecular Reaction Mechanism in the Amido Complex-Based Atomic Layer Deposition of HfO<sub>2</sub>**

G. D'Acunto, R. Tsyshevsky, P. Shayesteh, J.-J. Gallet, F. Bournel, F. Rochet, I. Pinsard, R. Timm, A. Head, M. Kukla, J. Schnadt

*Submitted to Chemistry of Materials*

I inherited the data and a first draft from Dr Payam Shayesteh. I carried out the advanced parts of the data analysis and discussed the manuscript.

**VI. Following the evolution of the surface chemical species during the first ALD cycle of HfO<sub>2</sub> on Si(111)**

R. Jones, G. D'Acunto, R. Tsyshevsky, P. Shayesteh, J.-J. Gallet, F. Bournel, F. Rochet, I. Pinsard, R. Timm, A. Head, M. Kukla, J. Schnadt

*In manuscript*

As for paper V, Dr Rosemary Jones inherited the data from Dr Payam Shayesteh. I took part in the discussion of the analysis and the manuscript.

**VII. HIPPIE: a new platform for ambient-pressure X-ray photoelectron spectroscopy at the MAX IV Laboratory**

S. Zhu, M. Scardamaglia, J. Kundsén, R. Sankari, H. Tarawneh, R. Temperton, L. Pickworth, F. Cavalca, C. Wang, H. Tissot, J. Weissenrieder, B. Hagman, J. Gustafson, S. Kaya, F. Lindgren, I. Källquist, J. Maibach, M. Hahlin, V. Boix, T. Gallo, F. Rehman, G. D'Acunto, J. Schnadt, A. Shavorskiy

*Journal of Synchrotron Radiation* 28, 624-636 (2021)

During this PhD, I participated in many experiments at HIPPIE, both as a principal investigator and as a support. Some of these experiments have become part of the commissioning of the beamline. I provided comments and feedback throughout the article writing and submission process.

**VIII. AP-XPS study of the adsorption of ethanol on rutile TiO<sub>2</sub> (110)**

R. Jones, G. D'Acunto, P. Shayesteh, F. Rehman, J. Schnadt

*Submitted to Journal of Physical Chemistry C*

I participated in the APXPS beamtime, discussed the analysis of the data and I took part in the discussion of the manuscript.

Publication to which I have contributed, but which are not included in this thesis, however, these papers will be referenced in the thesis:

**IX. Comparative study of copper oxidation protection with graphene and hexagonal boron nitride**

M. Scardamaglia, V. Boix, G. D'Acunto, C. Struzzi, N. Reckinger, X. Chen, A. Shivayogimath, T. Booth, J. Knudsen

*Carbon* 171, 610-617 (2021)

**X. Gas Pulse – X-ray Probe Ambient Pressure Photoelectron Spectroscopy with sub-millisecond time resolution**

A. Shavorskiy, G. D'Acunto, V. Boix, M. Scardamaglia, S. Zhu, R. Temperton, J. Schnadt, J. Knudsen

*ACS Applied Materials & Interfaces* 13, 47629-47641 (2021)

**XI. Stroboscopic operando spectroscopy of the dynamics in heterogeneous catalysis by event-averaging**

J. Knudsen, T. Gallo, V. Boix, M. Døvre Strømsheim, G. D'Acunto, C. Goodwin, H. Wallander, S. Zhu, M. Soldemo, P. Loemker, F. Cavalca, M. Scardamaglia, D. Degerman, A. Nilsson, P. Amann, A. Shavorskiy, J. Schnadt

*Nature Communications* 12, 1-8 (2021)

Publication to which I have contributed, but which are not included in this thesis:

**XII. Tuning oxygen vacancies and resistive switching properties in ultra-thin HfO<sub>2</sub> RRAM via TiN bottom electrode and interface engineering**

Z. Yong, K-M. Persson, M. Saketh Ram, G. D'Acunto, Y. Liu, S. Benter, J. Pan, Z. Li, M. Borg, A. Mikkelsen, L-E. Wernersson, R. Timm

*Applied Surface Science 551, 149386 (2021)*

**XIII. Area-selective Electron-beam induced deposition of Amorphous-BN<sub>x</sub> on graphene**

V. Boix, C. Struzzi, T. Gallo, N. Johansson, G. D'Acunto, Z. Yong, A. Zakharov, Z. Li, J. Schnadt, A. Mikkelsen, J. Knudsen

*Applied Surface Science 557, 149806 (2021)*

**XIV. Resonant X-ray photo-oxidation of light-harvesting iron (II/III) N-heterocyclic carbene complexes**

R.H. Temperton, M. Guo, G. D'Acunto, N. Johansson, N. W. Rosemann, O. Prakash, K. Wärnmark, J. Schnadt, J. Uhlig & Petter Persson

*Scientific Reports 11, 22144 (2021)*

**XV. Thickness and composition of native oxides and near-surface regions of Ni superalloys**

A. Larsson, G. D'Acunto, M. Vorobyova, G. Abbondanza, U. Lienert, Z. Hegedüs, A. Preobrajenski, L. R Merte, J. Eidhagen, A. Delblanc, J. Pan, E. Lundgren

*Journal of Alloys and Compounds 895, 162657 (2022)*



**XVI. Hydrogen plasma enhanced oxide removal on GaSb planar and nanowire surfaces**

Y.-P. Liu, S. Yngman, A. Troian, **G. D'Acunto**, A. Jönsson, J. Svensson, A. Mikkelsen, L.-E. Wernersson, R. Timm

*Applied Surface Science, in press, (2022)*

# Popular Scientific Summary

As physicists, we are often blamed for using terms and concepts that appear complicated to those who are not familiar with natural sciences. A saying of my hometown, Rome, tells “speak like you eat” and it is used as an invitation to choose a lexicon that everyone can easily understand. In the case of physicists, the fault is, in my opinion, just the physicists’ because they should adjust and explain in a simple and clear manner what physics disguises and what it can unveil.

It is common knowledge that the technological progress of the last few decades are impressive. Phones with cameras, drones, ever-present wi-fi connection, self-driving cars are just some of the most recent inventions. However, many must have noticed already that a new phone bought 10 years ago would have a huge increase in functions compared to the previous model. Lately, instead, nothing substantial has changed in new smartphones in comparison to their previous versions, besides some slight aesthetic difference. And this is true for phones, but also for televisions, computers, watches, appliances, and so on.

Limiting the explanation of this phenomenon to a mere economic matter may be wrong. Planned obsolescence is, of course, a timely topic, that has been recently condemned by the EU. The big problem is, however, that building smaller and more powerful devices is getting harder and harder. A few basic concepts worthwhile knowing: when we talk about a chip, we refer to the heart of an electronic device, that it what is makes it fast, powerful, and pricey! Chips, in turn, are made of transistors, that are tiny devices that execute basic functions and operations. As one may imagine, the more transistors, the merrier! But how many? Talking numbers, the latest phone of the apple contains around 15 billion transistors. Last year’s model, they were 12 billion. These are huge quantities that are increasingly difficult to expand further. So, the current trend is not

as much to increase the number of transistors to fit into a device, but to make those which fit more efficient.

Here my research steps in. In these years, I have tried to understand how to develop or, using the proper term for it, “grow” new materials that can let the dimension of transistors shrink and, at the same time, make them more efficient. To do so, the right technique, largely adopted in most of tech sectors and beyond, is “atomic layer deposition”. The method allows, literally, to grow any kind of material at atomic precision, meaning that new materials can be built atom by atom. But how big is an atom? A few Ångströms. And how many atoms fit into a hair? Around 500 thousand.

The problem with the ALD technique is that it is not entirely clear how it works. We know it does, but we cannot figure out how so, precisely. Imagine to be in a kitchen to make a cake. You have the ingredients, which for a physicist would be the molecules, you have an oven, which corresponds to a reactor, you mix everything, following the instructions, you put the cake in the oven, and, after some tens of minutes, you take it out. The cake comes out well, it tastes good, but it could improve. How so? The secret is to understand what happens inside the oven. How do butter molecules bond with the eggs and flours? What is the role of temperature? And time? What oven mode is the most appropriate? This is just the kind of questions my dissertation poses, in regard to the process of growing one specific material, called hafnium oxide.

In the case of hafnium, to unveil what happens “inside the oven”, an electron storage ring (also called synchrotron light source) is necessary, as well as a beamline, and a particular oven. An electron storage ring, as the name suggests, is a large ring, about 600 metres circumference (about two football courts), in which electrons run. Electrons are charged particles, which travel, inside the ring, at a speed close to that of light (very fast!). To give an example, for an electron to travel from Lund to Rome it would take about the same time as it would take a bee to strike its wings once (5 thousandth second). Inside the synchrotron, electrons make around 500

thousand laps per second. Now, there is one thing hard to explain “like I eat”: every time electrons change trajectory, every time they make a turn, they lose energy in the form of light. We take such a light, in the beamline, and use it as a probe to control, in real time, how molecules interact with each other and with the surface, and, adjusting the parameters, different results are obtained. Comparing this with the previous example, our cake is the hafnium oxide, that promises to overturn the tech sector, so much so that a leading tech company has started using it to improve and miniaturise their devices.

To conclude, this thesis aspires to offer now insights and ideas on how to progress in the understanding of the atomic deposition of oxides that appear highly relevant for technological application. Moreover, it suggests a new approach to look at reactions as they happen, impossible until recently.





## Sommario Divulgativo

In quanto fisici, veniamo spesso rimproverati di usare termini e concetti che, per un non addetto alle scienze, risultano complicati. Un detto della mia città, Roma, recita: “parla come magni” e si usa per invitare qualcuno a scegliere un lessico comprensibile a tutti. Nel caso dei fisici, la colpa, a mio avviso, è prettamente nostra, in quanto è compito nostro, e non degli altri, adeguarci nello spiegare in modo semplice e chiaro ciò che la fisica nasconde e ciò che può rivelare. Perciò, per raccontare questa tesi, ho cercato di utilizzare esempi alla portata di tutti.

É abbastanza noto che i progressi fatti negli ultimi decenni nel campo della tecnologia siano impressionanti. Telefoni con videocamere, droni, wi-fi ovunque, macchine che si guidano da sole sono solo alcune recenti invenzioni. Tuttavia, in molti avranno già notato che quando si comprava un telefono nuovo 10 anni fa, le sue funzionalità rispetto al modello precedente erano abissali. Negli ultimi tempi, invece, al di là di qualche lieve modifica estetica, non sembra cambiare chissà che. E questa cosa vale per i telefoni, ma anche per i TV, i computer, gli orologi, gli elettrodomestici, etc.

Ridurre la spiegazione di questo fenomeno a un mero fatto economico, potrebbe essere una cantonata. Certo, esiste la strategia dell'obsolescenza programmata – peraltro condannata non molto tempo fa dall'UE. Il grande problema, tuttavia, è che sta diventando via via più difficile costruire apparecchi sempre più piccoli e allo stesso tempo più potenti. È necessario conoscere alcuni concetti chiave: quando si parla di chip, si parla del cuore di un apparecchio elettronico, ciò che lo rende veloce, potente, costoso! Le componenti dei chip sono i transistor, piccoli dispositivi che eseguono funzioni e operazioni base. Come potete immaginare, più ce ne sono, meglio è! Ma quanti sono? Numeri alla mano, un telefono della mela, l'ultimo, contiene circa 15 miliardi di transistor. Il modello dell'anno scorso ne aveva solo 12 miliardi. Sono tanti, e sta diventando sempre più difficile renderli

più piccoli. Perciò, quello che si sta provando a fare ora, non è tanto aumentare il numero di transistor, ma rendere quelli presenti più efficienti.

È qui che la mia ricerca entra in gioco. Durante questi anni ho cercato di capire come realizzare o, utilizzando il termine tecnico, crescere nuovi materiali che permettano di diminuire ulteriormente la dimensione dei transistor e renderli più efficienti. Per farlo, esiste una tecnica, molto utilizzata in quasi tutti i settori tecnologici e non, chiamata deposizione atomica a strati (in inglese, *atomic layer deposition*), che permette di crescere ogni tipo di materiale con un controllo a livello atomico, cioè si realizzano nuovi materiali atomo per atomo. Ma quanto è grande un atomo? Pochi Ångström. Quanti atomi entrano nel diametro di un capello? Circa 500 mila.

Il problema di questa tecnica è capire nel dettaglio come funziona. Si sa che funziona, ma non è chiaro esattamente come. Immaginatevi di trovarvi in cucina per cucinare una torta. Avete gli ingredienti, che per un fisico come me sono le molecole, avete un forno, che corrisponde a un reattore, mischiate tutto, seguite le istruzioni, infornate, e dopo alcune decine di minuti sfornate la teglia. La torta è venuta buona, ma poteva venire meglio. Cosa sarà successo? Il segreto è capire cosa succede dentro il forno. Come si legano le molecole del burro a quelle delle uova e della farina? Che ruolo ha la temperatura? E il tempo? Che tipo di funzione del forno è più adeguata? Questo è esattamente il tipo di domande che la mia tesi indaga, in un processo di crescita di un materiale specifico, chiamato ossido di afnio.

Nel caso dell'afnio, per capire cosa succede "all'interno del forno", è necessario avere a disposizione un sincrotrone, una linea di luce, e un forno apposito per essere montato lì. Un sincrotrone non è altro che un grande anello, circa 600 metri di circonferenza (come il perimetro di due campi da calcio), dove si fanno girare elettroni, che sono particelle cariche, a velocità prossime a quella della luce (tanto veloce!). Per fare un esempio, un elettrone viaggerebbe da Lund a Roma nello stesso tempo in cui un'ape sbatte le ali una volta (5 millesimi di secondo). Nel sincrotrone, gli elettroni fanno circa

500 mila giri dell'anello ogni secondo. Ora, c'è una cosa che non è facile spiegare "come mangio": ogni volta che gli elettroni cambiano traiettoria, perdono energia e la perdono sotto forma di luce. La "linea di luce", chiamata *beamline*, non fa altro che prendere questa luce e usarla come sonda per controllare, in tempo reale, come le molecole interagiscono tra di loro e con la superficie e come, modificando i parametri, si ottengono risultati diversi. La torta nell'esempio precedente, come detto, è un ossido di afnio, che promette di rivoluzionare il settore tecnologico. Un colosso dei processori, infatti, già inizia a utilizzarlo per migliorare e miniaturizzare i suoi dispositivi.

Perciò, per concludere, questa tesi fornisce nuovi punti di vista e nuove idee su come è possibile migliorare la deposizione di ossidi che sono altamente rilevanti da un punto di vista tecnologico. Inoltre, fornisce un nuovo approccio per "guardare" le reazioni mentre avvengono in tempo reale, impossibile fino a poco tempo fa.



# Acknowledgements

Thank you all, brilliant people who have always helped me in one way or another during this PhD journey.

Probably, I owe almost everything I know, and everything I am in academia, to Professor Joachim Schnadt. I would fill pages and pages if I had to name all the positive things for which I am grateful, like the opportunities and the trust he has given and shown me, and the time he found to answer my endless questions, even though his calendar is always full. In our discussion, he was almost always right, although sometimes, few times, I “won”. Certainly, it is important to write that he is the best supervisor I could have had. I feel I have grown so much under his "wings", and now I feel ready to leave the "nest" with all his teaching and ways of seeing things.

I am part of a lucky class of PhDs, as I also had two other supervisors, Dr Rainer Timm and Dr Jan Knudsen. I felt and sensed their trust more than once during this years and for that, I am grateful. Rainer is the one you want to have while writing an article; his comments are like water in the desert, necessary. Jan, with his energy, has taught me a lot of what I know about Synchrotron light source. They both have given me confidence and help when I needed it.

SLJUS is not only my supervisors, and I am thankful also to Professors Mathieu Gisselbrecht and Edvin Lundgren for the meaningful conversations.

The guys from MAX IV! Andrey, Suyun, Mattia, Esko, Robert and Calley. We've done so many beamtimes together. These people have fixed many things I've broken, with experience! There are places where you go, and you feel happy about it. Well, this happens when I do beamtimes with their help at MAX IV light source.

There are so many people at SLJUS to whom I am grateful. Virginia, who has always found time to help me even though we are in different

research projects, together we did a lot! Sanna, Hanna, Giuseppe, Sandra, Alfred, Lukas, Yen-Po, Payam, Ahmed, Claudiu, Stefano, and Andrea I spent a lot of time with you, complaining about something wrong with my fits or my experiments, and enjoying weekends in the woods. Then, like a big family, I also must thank their respective children, new born and coming, and partners! I own something to Yi, who has always balanced the tidiness of our office.

When it comes to chemistry, the to-go person for me has been Rosie, and for this I would like to thank her.

Patrik! Grande Patrik! I had so many nice chats with him. I am known to be a mess with bureaucracy, and without him, most likely, I would be lost and submerged in paperwork.

Then there are my friends - gruppo caccia - from La Sapienza. They are always present and deserve a special appreciation! Since the first year of the bachelor's, back in 2012 (10 years ago!) we have always been united, bearing the dream of working together again! I have shared all the joys and sorrows of academic life with them!

I am grateful to my adoptive family, Claudia, Marina Virginia, and Mattia. I arrived here in Sweden all by myself (but thanks to them), and they took such good care of me! Vi voglio bene!

Grazie to all my friends in Rome, who are a part of the family that you choose, that you know and knows you, that accepts you as you are and I know they will be there no matter what.

To my family. To my beloved mom and dad, my funny sister, and my beautiful niece Elena, who have always supported me! Grazie a tutti!

Finally, Valeria. Valeria is my strength, and my smile, and part of my heart!

Thank you.

# 1 Introduction

"Be faster, be smaller, be cheaper."  
-A New Electronics Device-

## 1.1 A brief story of a device

The technology behind many of today's everyday devices such as drones, phones, satellites, etc builds upon successive steps of small technological advancements. To define the first-ever step is a matter of choice. We can go back to the discovery of the electron, or even further back when, in 600 BC, a Greek mathematician and philosopher called Talete noticed he could attract small pieces of paper with an amber after having rubbed it with fur. However, if we chose 600 BC as the beginning of this thesis, probably, this story will not fit in this thesis. Here, I would like to begin by shortly

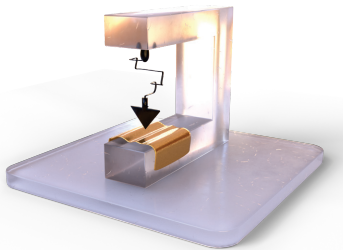


Figure 1.1 Render of the first transistor ever assembled in 1947 by Walter Brattain.

introducing one of the most significant discoveries of the 20<sup>th</sup> century. On December 16, 1947, at Bell Labs in Murray Hill, New Jersey, physicist Walter Brattain, with the help of a germanium plate, a plastic triangle, gold foil, and a paper clip, built the first ever transistor (Figure 1.1). The alternative to unreliable and bulky vacuum tubes was born. It only took

a few years for him and his colleagues, John Bardeen and William Shockley, dressed in smoking jackets, to hear the trumpets play for them and from a distant microphone the words:

*"Your Majesties, Your Royal Highnesses, Ladies and Gentlemen, it is a great honour to introduce the Nobel laureate in physics,[...], for their research on semiconductors and their discovery of the transistor effect."*

as they prepared to accept their Nobel prize in 1956 for their ground breaking discovery<sup>1</sup>. A simple idea that changed science and our history, forever.

Aug. 27, 1963      DAWON KAHNG      3,102,230  
ELECTRIC FIELD CONTROLLED SEMICONDUCTOR DEVICE  
Filed May 31, 1960

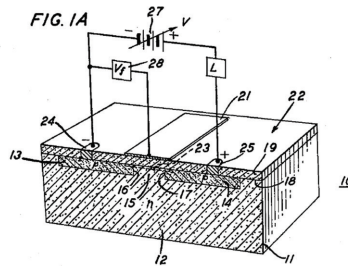


Figure 1.2 Figure from the Dawon Kahng's U.S. patent office. Source: United States Patent and Trademark Office, [www.uspto.gov](http://www.uspto.gov), ref [4]

In the past 70 years, great effort has been made to improve the performance of the transistor. If the first-ever transistor was a point-contact transistor<sup>2</sup>, then the second generation was developed<sup>a</sup> using a "sandwich"-like approach in 1951 by Shockley. The first generation of transistors were based on germanium, but this was later replaced by silicon which is a more stable and cheaper material<sup>3</sup>. In 1960 probably the most significant jump in the evolution of transistors was made at Bell Labs by Mohamed Atalla and

<sup>a</sup> The second generation was developed partially in secret, which was due to the fact that Shockley's name was not included in the patent for the first point contact design transistor, presumably.



Dawon Kahng. Their discovery was the field-effect transistor, specifically the metal-oxide-semiconductor field-effect transistor, or MOSFET<sup>3,4</sup> (Figure 1.2), the most<sup>5</sup> manufactured object ever<sup>b</sup>. From that moment, the electronics industry changed drastically.

Today the challenges facing the semiconductor industry remain just as numerous but vastly different. One, in particular, is the downscaling of the integrated circuits, ICs, which are the building blocks of any electronic device. If one is to talk about the downscaling of electronic devices, it is necessary to mention a luminary engineer, Gordon Moore. If the title engineer was given to him by the university, he deserved the luminary one for his prediction, which would become commonly known as Moore's law. He says in his 1965 paper<sup>6</sup> aptly titled "Cramming more components onto integrated circuits":

"The future of integrated electronics is the future of electronics itself. [...]. The complexity for minimum component costs has increased at a rate of roughly a factor of two per year. Certainly, over the short term this rate can be expected to continue, if not to increase. Over the longer term, the rate of increase is a bit more uncertain, although there is no reason to believe it will not remain nearly constant for at least 10 years. That means by 1975, the number of components per integrated circuit for minimum cost will be 65,000. I believe that such a large circuit can be built on a single wafer."

Moore's law was accepted as the primary goal to follow by the entire semiconductor industry and, besides few exceptions and feature corrections, the relation that Moore was able to predict still can be considered valid nowadays.

---

<sup>b</sup> Numbers on the hand: Thinking about plastic bags, a rough estimation, given the actual number of plastic bags produced every year ( $5^{12}$ ), and the first plastic bag ever made (1965), gives around  $3 \cdot 10^{14}$  bags ever produced. However, in 2014, Jim Handy estimated the number of transistors ever produced to be  $3 \cdot 10^{21}$ . A number which can not be compared even with the estimated number of stars in the Milky way ("only" 400 billion!)

But what is a MOSFET, and why making it smaller is a challenge? A MOSFET is essentially a switch, and if the ICs are the building block of electronic devices, the MOSFETs are the fundamental building block of an IC. It consists of two terminals, where the resistance between the two is controlled by a gate. The most common material to build a MOSFET is silicon. Silicon is cheap, easy to work with, and extremely versatile; however, it also has limitations. Scientists realised that to overcome the limitations of silicon, new materials were needed. Silicon oxide has been commonly used as the gate in MOSFETs, but around 15 years ago, it began to be phased out in mass production. It is replaced by a different group of oxides with high (electrical) permittivity, the so-called high- $\kappa$  oxides<sup>7</sup>. These high-k oxides allowed Moore's law to continue to hold true with chips reduced to 45 nm in size. From here, the evolution of transistors kept developing, changing materials and architecture, going from fully silicon based MOSFET, to high- $\kappa$  FinFET<sup>c</sup>, and to gate-all-around FET (GAAFET) (depicted in Figure 1.3). Unfortunately, the exponential decrease in size is not feasible forever, and a new strategy is under development, named "More than Moore" by the International Technology Roadmap for Semiconductors<sup>8</sup>.

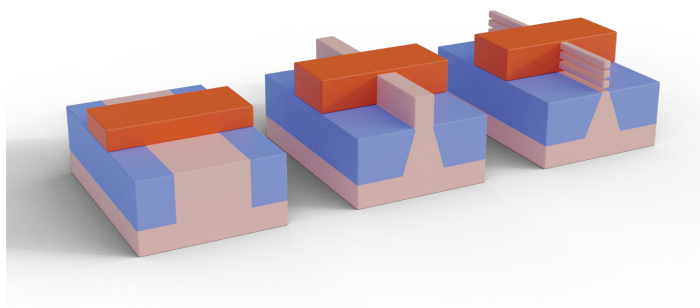


Figure 1.3 From left to right, sketches of a MOSFET, a FinFET and a GAAFET transistor. In blue is represented the body source and drain, in pink the channel and finally in orange the gate oxide.

---

<sup>c</sup> In this case the word "Fin" is not an acronym, but it described the shape of the channel, which, indeed, has a shape of a fin.

Meanwhile, what we can do as scientists, is to develop, enhance, and most importantly, understand how the current technology can be improved.

It is here that my research and thesis fits best. Previously, I briefly mentioned that one of the many possible changes one can make to improve the performance of devices, and make them smaller, is to use a high- $\kappa$  oxide as a gate. The reason for this move towards high- $\kappa$  oxides is quite simple: if one models the planar MOSFET, as sketched in Figure 1.3, as a capacitor, one finds that the capacitance is proportional to the dielectric constant  $\kappa$  and to the inverse of its thickness. This means that if one wants to increase the capacitance, one must either increase  $\kappa$  (by using a high- $\kappa$  oxide) or decrease its thickness. It is here that the main theme of this thesis is presented: atomic layer deposition (ALD). ALD, which will be explained in detail in chapter 2, is a deposition technique with the ability to control the thickness to the atomic level of the desired growth materials<sup>9-11</sup>. As it happens, high- $\kappa$  oxide can indeed be deposited with ALD<sup>12-17</sup>.

There are many research avenues towards the improvement of transistors. A particularly promising one is based on replacing the transistor's silicon body with materials that have superior electrical properties. The constraints of using silicon relate mainly to the operating voltage and charge carrier mobility. The former means the minimum energy required to let the transistor operate. The latter translates in the speed of the charges inside the device. It follows that the lower the operating voltage, the lower the power consumption, and the higher the charge carrier mobility, the faster the device. Overall, replacing silicon with other materials with improved electrical properties will allow for better devices regarding performance. III-V semiconductors, i.e. materials based on elements of the third and fifth columns in the periodic table, such as In, As, Ga and Sb, and all their alloys (InAs, GaSb, InGaSb ...), show significant promise<sup>18-20</sup> among possible candidates for such materials. However, even though the first ever InGaAs MOSFETs were demonstrated over thirty years ago<sup>3</sup>, only recently has there been significant progress. Some challenges in the usage of III-V

semiconductors in FET technology are the lack of a sharp interface between the III-V compound and the high- $\kappa$  compound, Fermi level pinning at the interface, and uncontrolled reoxidation of the III-V compound<sup>16,21,22</sup>. Here, the use of ALD for the deposition of high- $\kappa$  oxides on III-V semiconductors has been demonstrated<sup>12-14,23</sup>, to some extent, to overcome the problems listed above.

However, portraying ALD as the superhero that will solve the continuously increasing demand of more efficient devices, is a little disingenuous. If ALD was the real hero and everything perfectly understood, this PhD project would be obsolete. The following sections will elaborate on the underpinning motivations for this thesis.

## 1.2 Motivation

It is difficult to distill the motivation for this thesis into one succinct statement, especially when I consider all the experiments and experiences of the last four years. Probably, the ideal motivation I should have as a young researcher is to find the solution on the scaling down of the MOSFET, integrate them in IC, build devices that outperform the current used one, and understand how everything works. However, the motivation remains the same as it was when I started my bachelor's degree in physics, which is trying to find solutions to unanswered questions around us. If this is what motivates me to apply for a PhD position, here it comes what motivates this thesis.

In fairness, this project was given to me, when I started my PhD, from my supervisor Prof. Joachim Schnadt. The path was quite straightforward: I applied due to the exciting project and the vicinity of Lund University with MAX IV, I was selected and then, I started. Just after a month I had my first ever beamtime, my first time in a synchrotron with all the photons I needed to do my job. I was aware of my project, but what I was not fully aware was *why* I was doing that specific experiment. If at the beginning I was analysing

data, making fits and applying for beamtime, just for fun(!) and fulfilling my job, after probably a full year I truly understood the real *why* I was doing those experiment, fitting those complex data and applying for other beamtimes. To understand this *why* let's go back to the birth of ALD, in two neighbouring countries, Finland and the Soviet Union, between 1960 and 1970.

The Russians called and still call it molecular layering (ML), whilst for the rest of the world it started as atomic layer epitaxy but is now known as atomic layer deposition. To decide who was the "real" first, we need deep investigation and knowledge of Cyrillic, since most of the scientific papers that mention ML are written in Russian and not readily available. Different reviews on ALD suggest that the first full paper on ML<sup>24</sup> appeared in 1965; however, the first patent on ALE was submitted by Tuomo Suntola<sup>25</sup> in 1977. In his patent<sup>25</sup> (Figure 1.4) Suntola used the acronym ALE and described the deposition technique as a "*method for growing highly oriented compound thin films on a substrate by subjecting the substrate to the vapours [...] until the compound film reached a desired thickness*".

The story of ALD development is interesting, and a nice review describes the early steps of this technique<sup>26</sup>. Nowadays, ALD is used worldwide, not only for humidity sensors, the first-ever application of ALD, but also for medical applications, quantum devices, batteries, catalysis, fuel cells, and in

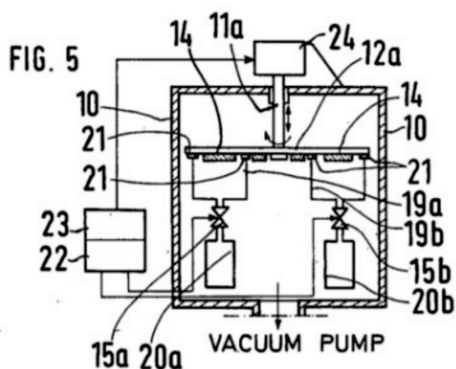


Figure 1.4 One of the Figures T. Suntola used in his original patent in 1977. In particular, this Figure shows an ALE apparatus. Source: United States Patent and Trademark Office, www.uspto.gov. From ref .[25].

the semiconductor industry<sup>11,27,28</sup>. My motivation and introduction sections meet here: Despite all, ALD still suffers from unknown surface reaction mechanisms and kinetics. Understanding these essential points will give us access to better semiconductor devices.

## 1.3 This thesis

In this thesis, I investigate a variety of systems, based mainly on the ALD of high- $\kappa$  oxide on several surfaces, using an innovative *in situ* and *operando* technique<sup>d</sup>. These studies focus on the role of the surface where the high- $\kappa$  oxide is deposited and how the experimental parameters, such as precursor pressure and temperature, can affect the surface.

The thesis will take a path, starting with a detailed introduction to ALD, based on the current understanding and possible real-world applications. Then, the main technique used is presented as well as an introduction to synchrotron radiation in general and the MAX IV synchrotron light source, preparing the reader for the results of the thesis. The final, two chapters, separated for the sake of the narrative, are based on selected works in which I was involved during my PhD (Papers IX, X and XI, only partially in this thesis). Finally, I will conclude this thesis with the outlook of this research and more generally the field of ALD.

---

<sup>d</sup> “Originally, the term *operando* refers to characterisation of a working catalyst under realistic pressure conditions (*in situ* in catalysis lingo) and the simultaneous acquisition of reaction data. The term *in situ*, is, however, used differently in the ALD community: it denotes that the sample is transferred from the ALD reactor into a characterisation instrument that is directly connected to the reactor. Hence, exposure to air is avoided, but the characterisation does not take place at the same time as the ALD film growth. We therefore employ the term *operando* to clearly distinguish the characterization during growth and at realistic pressure conditions from such *in situ* characterisation.” This is an extract of Paper V.

# 2 Atomic Layer Deposition

## 2.1 Why ALD and what it is

Atomic layer deposition (ALD) is an outstanding vapour phase technique used to deposit thin films in a controlled manner and with atomic-scale precision<sup>9,11,29</sup>. It can be viewed as a subcategory of chemical vapour deposition (CVD)<sup>30–33</sup>, but the working principles are slightly different. Put (very) simply, the difference between CVD and ALD can be summarised into one word: sequential. If CVD employs all the precursors simultaneously, ALD splits the precursors into two or more separate pulses.

As mentioned in the introduction of this thesis, ALD has shown great promise in the semiconductor industry, but its application is not limited to this field. As is visible in the inset of Figure 2.1, the areas where ALD is used range from physics and chemistry to chemical engineering and energy manufacturing. The growth in the number of publications of the two leading deposition techniques, CVD and ALD, demonstrates the continued interest in their development and use. Clearly, the leading deposition technique by far is CVD, but ALD, with its outstanding properties, starts to rise quite fast at the new millennium. A possible explanation to why it took almost 40 years to become popular may be the continuous demand for increasingly smaller devices, and several other applications where it found its way in, including energy storage<sup>34,35</sup>, solar energy devices<sup>36,37</sup>, and catalysis<sup>38</sup>. Both CVD and ALD are largely used in microelectronics, but only ALD has the capability to grow a uniform layer of a desired material with Ångström precision<sup>10</sup>. This statement is supported by the fact that the leading manufacturers in the microchip industry started using ALD for mass production right after a

conspicuous body of research was made available by laboratories and universities. In fact, in 2007, Intel<sup>39,40</sup> began to mass-produce transistors with  $\text{HfO}_2$  as gate oxide deposited via ALD.

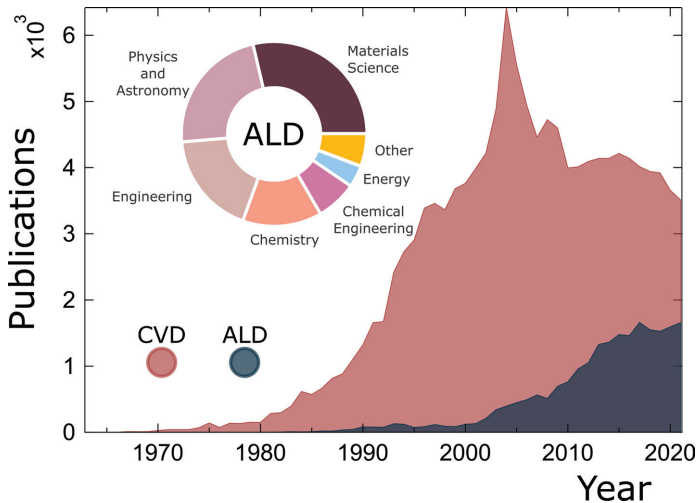


Figure 2.1 Number of publications per year of CVD and ALD reported in brick red and blue colour, respectively. A pie chart of documents on ALD by subject area is an inset. Data from Scopus.

The ideal ALD scheme, clarified later in this chapter, relies on the self-limiting adsorption and reaction of two, or more, vapor phase precursors with a substrate, in a sequential manner<sup>9,29</sup>. The exposure to the precursors leads, indeed, to the formation of no more than one monolayer of the desired materials. The lists of materials that can be grown via ALD spread from pure metals, to nitrides, from oxides, to sulphides<sup>27,29,41</sup>.

## 2.2 Current understanding

If one does a brief literature overview of ALD, a schematic similar to that in Figure 2.2 is easily found. This represents the commonly assumed ALD mechanism. First, the surface needs to have active sites where the precursor



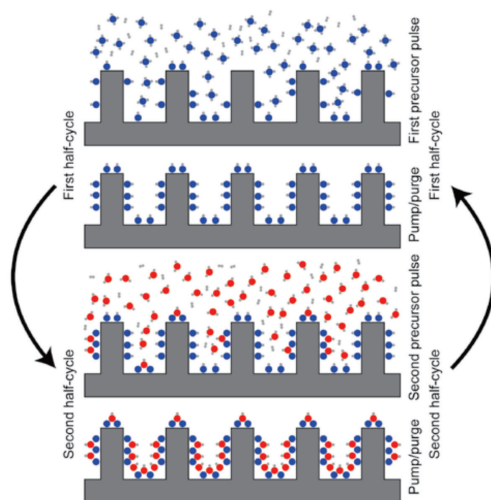


Figure 2.2 Ideal ALD scheme illustrating the two half-cycles, including an intermediate step of pump/purging. Image courtesy of Prof. Joachim Schnadt.

can interact. The type of interaction will depend on the type of process, but, as sketched in Figure 2.2, it is typically assumed to follow<sup>9</sup> the ligand exchange model<sup>c</sup>. When the first precursor saturates the surface fully and no active sites are left, a purging step with an inert gas is used. Once the first reaction is completed, also called half-cycle (if only two precursors are employed), the second precursor can be dosed. In the case of oxide ALD, one of the precursors, typically the second one, is often water<sup>9,42,43</sup>, but it can also be  $O_2$ ,  $O_3$ ,  $H_2O_2$ , or oxygen plasma. In the case of water, the molecules will again interact with adsorbed first precursors, so that a uniform, conformal, and defect-free monolayer is formed. Ideally, the second precursor will also prepare the surface for other ALD cycles, such as hydroxyl formation in the case of water as co-reactant, which will act as active sites.

This ideal scheme allows for a layer-by-layer growth, without defects; moreover, it appears to be completely independent of the type of substrate

<sup>c</sup> this is not the only reaction mechanism involved in ALD, but to our knowledge is the most evoked one when metal amido complexed and water are used as precursors.

used. There are two reasons why the surface on which ALD is performed is not often considered: i) the interface is really hard to analyse with *in situ* methods, and ii) ALD papers predominantly are looking at the steady state chemistry mechanisms. Yet, even if the scheme just presented gives a valid starting point on the mechanisms involved in ALD, in most cases, it is not clear if the ideal ALD scheme is correct or not with respect to the initial ALD cycles. Therefore, it is crucial to investigate in detail the surface species that occur during the deposition, the role of the support, and finally to build a separate reaction mechanism(s) for the initial ALD cycles.

Most of the thousands published papers on ALD are based on “*post mortem*” characterisation. ALD can be performed in a specifically designed reactor, where two or more, precursors flowed into the chamber in turn reacting with a heated surface. The final structure, resulting from  $N$  cycles of ALD, is then characterised by a number of techniques. However, this approach relies on *ex situ* characterisation which, sometimes, can leave a knowledge gap in the understanding of ALD, in particular where the substrate is concerned.

For this reason, this thesis uses *operando* and *in situ* methods which allow the characterisation of the ALD processes during ALD cycles. This approach makes possible to obtain a more detailed understanding of the kinetics, reaction mechanism, and surface species formation in ALD. However, as a drawback, the characterisation in real time is more time consuming and is limited in terms of pressure, precursor and temperature. Despite these challenges, by careful selection of precursor pairs new details on the ALD mechanism and kinetics can be elucidated.

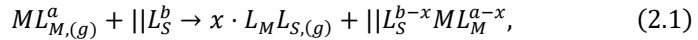
This thesis predominantly focuses on the ALD of transition metal-oxides, using transition metal-amido complexes and water as precursors. The current understanding is that ALD, using the aforementioned precursor pairing, proceeds via a ligand exchange reaction mechanism, which I will expand upon in the following section. New insight from *in situ* characterisation of this system is presented in Papers I to VI and Paper VIII.

### 2.2.1 Ligand exchange model and other known reactions

- Ligand exchange reaction mechanism

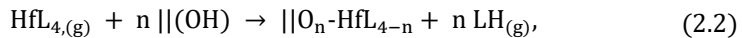
The ligand exchange reaction mechanism, as the name suggests, involves the exchange of ligands between two chemical species<sup>44</sup>. The ligand exchange reaction mechanism is the most commonly evoked reaction mechanism when transition metal amido complexes and water are used as precursors.

From a more general point of view, the ALD described by the ligand exchange reaction mechanism during the first half-cycle follows this equation:

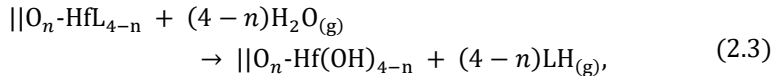


where  $M$  indicates the metal ion of the precursor,  $||$  the surface where the deposition occurs,  $L_{M,S}$  the ligands of the molecule and the surface, respectively, the superscripts  $a$  and  $b$  the number of ligands, and  $g$  the gas phase state. Equation 2.1 stands for the very first half-cycle of ALD. Note that the surface (e.g.  $\text{SiO}_2$ ,  $\text{TiO}_2$ , InAs oxide) plays a largely static role here. In my research, the precursor tetrakis(dimethyl-amido)-hafnium (TDMA-Hf) was used, which is part of the metal-amido complex family, in conjunction with water as the second precursor. The ligand exchange reaction mechanism for these two precursors, interacting with a surface covered by hydroxyl groups, can be written as follows:

*First half-cycle*

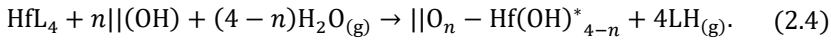


*Second half-cycle*



where the symbol  $||$  expresses a general surface, and  $L$  the ligand of the TDMA-Hf, i.e. the dimethyl-amido ligand (DMA).

In general, the overall reaction mechanism, describing the first cycle of ALD, can be written as:



There are several observations worth making:

- The surface, in this model, has a largely static role, since its only "contribution" is to be hydroxylated.
- The ligands remain intact, they are simply hydrogenated and 'leave' in gas phase.
- The two half-cycles follow only one reaction, and therefore only one timescale (e.g. for the second half-cycle, the removal of the surface species needs to follow the same characteristic time of the formation of hydroxyl).
- The reaction does not consider reactions between molecules of the same precursor.

In addition to the ligand exchange mechanism, two other mechanisms involved during ALD should be noted.

- Other possible reaction mechanisms in ALD

The first reaction mechanism I will discuss, a type of chemisorption process, is called dissociative adsorption, and takes place when a complex fragments<sup>44</sup>. Dissociative adsorption is typically triggered by an external source of energy, such as high temperature, plasma, or UV light. One of the most common phenomena is the dissociation of O<sub>2</sub>. Dissociation often occurs on metals, due to their high surface energy, defined by the excess of energy on the surface with respect to the bulk.

Several examples of dissociation reactions can be found in ALD reviews<sup>9,44-46</sup>, and also in Paper IV, where TDMAHf on anatase TiO<sub>2</sub> is performed. The initial reaction is well described by dissociative chemisorption. Outside of ALD, also in Papers XI and IX, dissociative

chemisorption of O<sub>2</sub> over a Pd(100)<sup>47</sup> and through the growth of graphene<sup>48</sup> on metal surfaces, are presented, respectively.

In addition to the mechanisms detailed previously physisorption is equally important when discussing the surface chemistry of ALD. Physisorption occurs when a molecule is adsorbed on a surface. The fundamental interacting force of physisorption is Van der Waals force. As it will be presented in detail later, the first step of ALD of HfO<sub>2</sub> on InAs, as well as the ALD of HfO<sub>2</sub> on SiO<sub>2</sub>, is physisorption, only later followed by other reactions. These are described in Papers I, II and V.

## 2.3 ALD for the semiconductor industry

As discussed in the preceding sections, ALD is used in a variety of technological fields, including that of semiconductors. Of particular relevance to this thesis is its use for the deposition of high- $\kappa$  oxides. I have already mentioned the example of ALD of the high- $\kappa$  oxide HfO<sub>2</sub>, but let me take a closer look on the properties of high- $\kappa$  oxides and why they are such promising materials. HfO<sub>2</sub>, as well as TiO<sub>2</sub>, and Al<sub>2</sub>O<sub>3</sub>, are dielectric materials, also known as high- $\kappa$  dielectrics.  $\kappa$  denotes the dielectric constant, which is a measure of a material's capability to hold charge under a potential.

I will discuss this concept more academically soon, and eventually I will discuss how to overcome the silicon era in the silicon-based devices. I will indicate how III-V semiconductors can be implemented in new devices and how they can increase the quality of their performance compared to silicon-based devices.

### 2.3.1 High- $\kappa$ oxides

When talking about high- $\kappa$  oxides,  $\kappa$  refers to the dielectric constant. One of the key features of dielectric materials is the permittivity. Permittivity tells about the ability of specific materials to be polarised. A related property of

the permittivity is the capacitance, which measures a material's ability to hold charge when a voltage is applied. The charge capacity of a material, defined as the ratio between the charge held on the conductor over the electrical potential, derived for a plate capacitor, can be expressed as follows:

$$C \propto \epsilon \cdot \frac{A}{d}, \quad (2.5)$$

where  $C$  is the capacitance,  $\epsilon$  the permittivity,  $A$  the area and  $d$  the thickness of the dielectric.  $\kappa$  is then defined as the ratio between the permittivity  $\epsilon$  of the material and the permittivity of the vacuum  $\epsilon_0$ . Therefore, equation 2.5 can be rewritten as:

$$C = \epsilon_0 \cdot \kappa \cdot \frac{A}{d}. \quad (2.6)$$

Obviously, if one's aim is to decrease the area while keeping the capacitance constant, one needs to increase or decrease the dielectric constant (quadratically). The most popular dielectric in the semiconductor industry is silicon oxide, which has a dielectric constant of about 3.9. However, when viewed in the context of other dielectrics such as  $\text{TiO}_2$ ,  $\text{ZrO}_2$  and  $\text{HfO}_2$  with  $\kappa$  values of 80, 25, and 24, one can see that the value of 3.9 of  $\text{SiO}_2$  is definitely small.

An important application of high- $\kappa$  oxides is in transistors, specifically MOSFETs. In almost any electronic device we can find them. Transistors can be seen as a switch; they either let the current pass through or they do not, and a small potential controls them. The schematic of a metal oxide semiconductor field-effect transistor (MOSFET) is depicted in Figure 2.3. If no bias voltage, or a small negative one, is applied to the gate, the resistance between source and drain is too high and therefore the MOSFET will be in an OFF state; if the bias becomes positive, the holes are pushed away from the semiconductor/insulator interface and electrons become the dominant charge carriers. If now a bias between source and drain is applied, the current will flow through the n-channel, and the MOSFET is in an ON state.

ON and OFF states are digital logic, and, the faster the switch, the better the device. Of course, the device's speed is not the only indicator for performance, power consumption also plays an important role.

### 2.3.2 Beyond silicon era - III-V semiconductors

Previously, I discussed the high- $\kappa$  dielectrics, and how they allow production of better devices, to “keep up” with their growing market demand. This section, instead, explores how it is conceivable to make them faster.

By far, the most commonly used material in the semiconductor industry is silicon. On the one hand, silicon is great: it is cheap<sup>f</sup>, easy to process, and stable at a vast range of temperatures; it, however, lacks in charge mobility. On the other hand, III-V compound semiconductors with their tuneable bandgap and excellent electron/hole mobility, appear to be great candidates to overcome the Si era.

The III-V semiconductors are alloys made from the third and fifth elements of the periodic table (Al, Ga, In and N, P, As, Sb). All compounds of these elements are semiconductors, and the bandgap varies within the possible permutation. In this thesis, I mainly work on InAs, although recently I performed an experiment on ALD of HfO<sub>2</sub> on GaSb<sup>g</sup>. InAs shows great potential for transistors in radio frequency applications<sup>49</sup>, especially for its narrow bandgap (0.43 eV *vs.* 1.17 eV of silicon) and its high electron mobility, which is 20 times higher than that of silicon<sup>50</sup>, while GaSb has a very high hole mobility.

However, a question needs to be posed: Why are we still using silicon-based devices?

---

<sup>f</sup> To give an absolute number, a wafer of silicon of 5 cm in diameter and 0.5 mm in thickness is about 1800 SEK (around 180 EUR), which gives a price of around 1000 SEK per cm<sup>2</sup>.

<sup>g</sup> the results are not part of this dissertation.

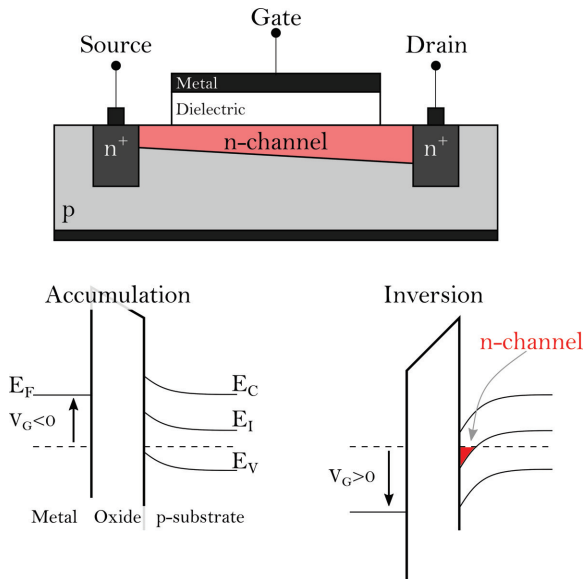


Figure 2.3 Top) sketch of a pMOSFET in an ON state. Bottom) total band diagram of metal oxide semiconductor interface when a small negative potential is applied to the gate (left), which leads the pMOSFET in accumulation; on the right, the total band diagram when a positive bias is applied. In red, n-channel formation. The p, in pMOSFET, indicates the type of semiconductor used as a body in the MOSFET.

Silicon is cheap!! InAs costs around three times more than silicon. However, there is also another physical explanation. That reason is found at the interface between the semiconductor and its oxide. Silicon has a sharp and defect-free interface with its oxide, which is not the case with III-V semiconductors. Extrinsic surface states due to defects in the interface<sup>21,22</sup>, such as adsorbates, are particularly harmful to the performance of the device since surface states, or defect states, exist in the bandgap. If the system is excited, the position of the band edges relative to the Fermi level gets pinned by the defect states, and electron transitions between the defect states and the conduction band become favourable, reducing the band bending necessary to form the n-channel, as shown in Figure 2.3.

ALD proved to be excellent at removing all the native oxide or thermal oxide and generating a sharp interface between the III-V semiconductors and a high- $\kappa$  oxide. In Papers I, II and III,  $\text{HfO}_2$  on InAs was studied, and they



show how a long pulse of TDMA-Hf is necessary if all the unwanted oxide should be removed and a single monolayer of high- $\kappa$  formed.



# 3 Techniques

## 3.1 X-ray Photoemission Spectroscopy

Photoemission spectroscopy (PES), also called photoelectron spectroscopy, is a powerful technique to investigate the chemical, elemental, and electronic properties of materials. The potential of x-ray photoelectron spectroscopy (XP) to become one of the most versatile methods to study surface chemistry has been realized since the first spectra were collected on thorium in Uppsala (Sweden) <sup>51</sup>. The idea of x-ray photoemission spectroscopy is based on the photoelectric effect, discovered by Heinrich Hertz in 1885, but only explained in 1905 by Einstein, who received the Nobel prize<sup>52</sup> in physics in 1921 for his explanation. It was only in 1967 that Kai Siegbahn published<sup>53</sup> a comprehensive study on x-ray photoemission spectroscopy (XPS) in his text entitled ESCA, which stands for electron spectroscopy for chemical analysis. Kai Siegbahn, for giving the key to XPS to the entire scientific community, was granted the Nobel prize<sup>54</sup> in physics in 1981, thanks to his contribution to the development of high-resolution electron spectroscopy.

In my research, XPS is profoundly and widely adopted in all publications collected in this thesis, except for Paper VII, that deals with the features of the synchrotron beamline that allows performing XPS. The processes involved during the photon-electron interaction will be elucidated briefly in the following paragraphs. The purpose is to cover the most important parameters needed to understand, analyse, and grasp conclusions from XPS data.

### 3.1.1 The theory of photoemission

Following a rationale of simplicity, the theory of photoemission can be summarised in four words: photon in, electron out. However, this simplistic way of imagining the processes during the photon-electron interaction can lead to a misunderstanding of the real core of XPS. To properly discuss the theory behind the photoemission process, it is essential to take a step back (in time) and briefly explain the photoelectric effect. Hertz noticed that electrons were escaping while shining ultraviolet light on a metal surface<sup>55</sup>. He also noticed that the electrons were ejected only when the frequency of the light would reach a certain threshold. The energy of the electron increased while increasing the photon energy. However, to explain the observed phenomena, Hertz needed to wait until 1905, when Albert Einstein published a paper<sup>56</sup> proving the hypothesis that light is carried in discrete quantised packets, which then explained the phenomena observed by Hertz.

Hertz's experiment was based on a vacuum tube containing two metal plates separated by a small distance. The whole experimental setup was connected to a potentiometer. Illuminating a plate with ultraviolet light, it generated a current in the circuit. The idea is to apply a potential such that the net current in the circuit was equal to zero.

Since the potential is equal to the energy of the electron (divided by the electron charge), one can obtain a dependence of the kinetic energy on the electrons with the energy of the incoming light:

$$E_k = h\nu_0 - \phi, \quad (3.1)$$

where  $h$  is the Planck constant,  $\nu_0$  is the frequency of the incoming photons, and  $\phi$  the minimum energy required to let an electron escape, also called work function.

However, the binding energy is missing here, which is essentially the energy of an electron with respect to the Fermi energy. Since Einstein and Hertz were only considering valence electrons, the binding energy  $E_B$ , by definition, was set to 0 eV. Including the binding energy, one can now rewrite equation 3.1 as:

$$E_k = h\nu - (E_B + \phi). \quad (3.2)$$

The main challenge is to understand what  $E_B$  is, and how photons can interact with matter. By evoking quantum mechanics, the photoemission process can be simply described via the three-step model<sup>57</sup>. It must be noted that the three-step model is an approximation; and fundamentally, photoemission is always a one-step process. First, a photon is absorbed by an electron, consequently excited to the unoccupied band structure of the solid; then, the excited electron travels inside the material and reaches the surface (second step); finally, in the third step, the electron crosses the surface as a plane wave and is released into the vacuum, where it can be finally detected.

The Hamiltonian of a single electron, immersed in a potential  $V(\mathbf{r})$  generated by the crystal, and in the presence of an external electromagnetic wave (field) of vector potential  $\mathbf{A}$  can be written as

$$\begin{aligned} H &= \frac{1}{2m} \left( \mathbf{p} - \frac{e}{c} \mathbf{A}(\mathbf{r}, t) \right)^2 + V(\mathbf{r}) \\ &= \frac{\mathbf{p}^2}{2m} + V(\mathbf{r}) - \frac{e}{2mc} [\mathbf{A}(\mathbf{r}, t) \cdot \mathbf{p} + \mathbf{p} \cdot \mathbf{A}(\mathbf{r}, t)] + \frac{e^2}{2mc^2} |\mathbf{A}(\mathbf{r}, t)|^2. \end{aligned} \quad (3.3)$$

The total Hamiltonian can be split into two terms  $H = H_0 + H_I$ , where  $H_0$  is the unperturbed part, and  $H_I$  describes the light-matter interaction:

$$H_0 = \frac{\mathbf{p}^2}{2m} + V(\mathbf{r}), \quad (3.4)$$

$$H_I = -\frac{e}{2mc} [\mathbf{A} \cdot \mathbf{p} + \mathbf{p} \cdot \mathbf{A}] + \frac{e^2}{2mc^2} |\mathbf{A}|^2. \quad (3.5)$$

The last term of the interaction Hamiltonian can be neglected for two reasons: it describes two-photons processes<sup>58</sup>, which are unlikely to happen, and for a sufficiently small field the term is anyway negligible. Moreover,

$$\mathbf{A} \cdot \mathbf{p} + \mathbf{p} \cdot \mathbf{A} = 2\mathbf{A} \cdot \mathbf{p} - i\hbar \nabla \cdot \mathbf{A}, \quad (3.6)$$

where the second term is set to 0, assuming that the photon wavevector is perpendicular to  $\mathbf{A}$ . However, this is just an approximation since the discontinuity of the dielectric function at the surface can lead to surface

photoemission. For now, one can still keep  $\nabla \cdot \mathbf{A} = 0$ , and finally write the total Hamiltonian as:

$$H = H_0 - \frac{e}{mc} (\mathbf{A} \cdot \mathbf{p}). \quad (3.7)$$

In time-dependent perturbation theory, the photocurrent produced from the excitation of electrons from the initial state  $i$  with wave function  $\psi_i$ , to the final state  $f$ , with wave function  $\psi_f$ , by a perturbation, can be calculated by the Fermi's Golden Rule, which states that the probability of transition from  $i$  to  $f$  will depend on the Hamiltonian of interaction<sup>58</sup> as:

$$w_{i \rightarrow f} = \frac{2\pi}{\hbar} |\langle \psi_f | H_I | \psi_i \rangle|^2 \delta(E_f - E_i - h\nu). \quad (3.8)$$

where  $w_{i \rightarrow f}$  is the transition probability, and the delta is needed to consider energy conservation. Concerning the matrix element  $\langle \psi_f | H_I | \psi_i \rangle$ , often also called  $M_{if}$ , one can observe:

- The wave functions can be described as Bloch waves, that oscillate rapidly on atomic distances.
- The amplitude of the potential  $\mathbf{A}$ ,  $A_0$  is considerably larger than the interatomic distance in a solid, which is a few Å. To give some numbers, a photon with an energy of 675 eV has a wavelength of around 18 Å. This allows to consider  $A$  as a constant.

With this in mind, one can solve the integral under the dipole approximation and write the transition probability as:

$$w_{i \rightarrow f} \propto |\langle \psi_f | r | \psi_i \rangle|^2 \delta(E_f - E_i - h\nu). \quad (3.9)$$

The main problem now is to understand and find an expression of the final and initial states  $\psi_i$  and  $\psi_f$ . The initial state can be expressed as a product of the wave function describing the electron that will be excited, and the wave function describing the remaining  $N-1$  electrons:

$$\psi_i(N) = \phi_{i,k} \cdot \psi_i(N-1), \quad (3.10)$$

where  $\phi_{i,k}$  is the photoelectron's wavefunction with quantum number  $k$ . The initial wave function has an energy of  $E(N)$ .

The final state can also be expressed as the product of the wavefunctions describing the photoemitted electron, with energy  $E_k$  and the wavefunction describing the remaining  $N-1$  electrons, with energy  $E(N-1)$ :

$$\psi_f(N) = \phi_{f,E_k} \cdot \sum_s \psi_{f,s}(N-1) , \quad (3.11)$$

where the sum over  $s$  describes all the possible final stats of the  $N-1$  system. Therefore, one can now write

$$\langle \psi_f | r | \psi_i \rangle = \langle \phi_{f,E_k} | r | \phi_{i,k} \rangle \cdot \sum_s \langle \psi_{f,s}(N-1) | \psi_i(N-1) \rangle , \quad (3.12)$$

where one assumes that  $H_I$  operates only on the single state electron.

From here, one can already notice something fascinating. The last term in equation 3.12 represents the overlap between the total wave function of the  $N-1$  electrons in the final and in the initial state. If one considers that the orbitals are locked in place and in energy, before and after the excitation,  $\psi_{f,s^*}(N-1) = \psi_i(N-1)$ , where  $s^*$  is the only state in the sum that gives a non-zero term, one obtains the so-called<sup>57</sup> “frozen orbital approximation”. This approximation allows to measure the negative Hartree-Fock energy, also called Koopmans' energy<sup>59</sup>, which represents the energy of a system where the electron-electron interaction is not considered<sup>57</sup>, or, in other words, it is the negative of the orbital energy of the photoemitted electron (before emission). In Figure 3.1, an XP spectrum with and without electron interaction is shown.

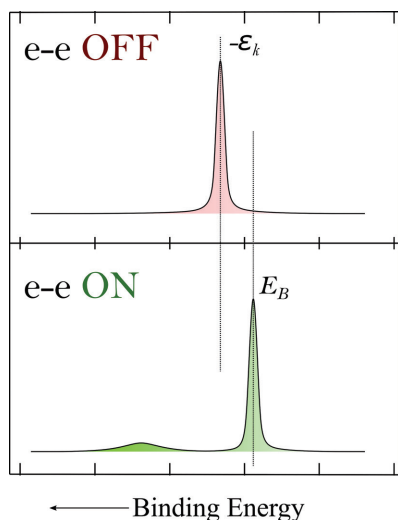


Figure 3.1 Schematic diagram of photoemission spectrum with electron electron interaction OFF (top), and ON (bottom). Interestingly, the centre of gravity of the two is identical. Adapted from [57].

It is evident that such an approximation, even if it gives a hint on how XPS works, needs a step forward to fully appreciate the photon-electron interaction and the creation of a core hole. If more than one coefficient in the sum over  $s$  in equation (3.12) lead to a non-zero value, this will be reflected by satellite lines in the spectra (c.f. Figure 3.1, bottom). I seldom encountered a satellite line since my systems are called “weakly correlated”. To define “correlation”, one can use a simple model introduced by Lafayette Hubbard<sup>60</sup>. The idea is to compare the Coulomb ( $U$ ) interaction with the valence band width ( $W$ ). If  $U \gg W$ , the system is strongly correlated; otherwise, it is weakly correlated.

One of the most important results that can be obtained through XPS is the chemical shift, which gives excellent information about the chemical environment of the photoemitting atom. One of the most often used textbook examples<sup>61</sup> for the chemical shift in the photoemission process, is the C 1s XP spectrum of ethyl trifluoroacetate, also called the ESCA



molecule, is shown in Figure 3.2. The chemical composition of the ESCA molecule is  $\text{CF}_3\text{-CO-O-CH}_2\text{-CH}_3$ , and four distinct chemical environments of carbon atoms can be identified. The image is illustrative since the binding energy of the four carbon atoms spread over more than 8 eV. Figure 3.2 is adapted from the original paper of U. Gelius et al.<sup>62</sup>.

In my manuscripts, the chemical shift is often used to discriminate the surface species present on the surface, as shown in the SI of Paper IV, where the N 1s was deconvolved with four components, representing the four surface species.

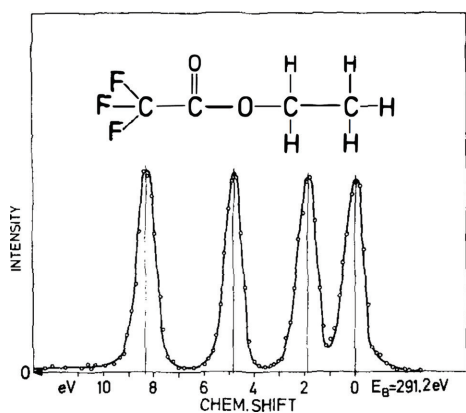


Figure 3.2 C 1s XP spectra of the ESCA molecule. Adapted from ref[62].

### 3.1.2 Practical approach

When collecting XP spectra, it is important to recall all the aspects that can and cannot affect a core level's intensity. Without indulging in details, the intensity of a core level peak can be expressed as:

$$I = N \cdot I_0 \cdot C \cdot \sigma \cdot T \cdot C_g \cdot F. \quad (3.13)$$

Here  $N$  is the number of photoemitting species in the volume probed by the x-ray beam,  $I_0$  is the energy-resolved and photoionisation cross section-corrected photocurrent for the particular core level into the solid angle of the electron energy analyser,  $C$  is a factor that takes into account the attenuation of the photoelectrons in the solid,  $\sigma$  is the subshell photoionisation cross

section,  $T$  represents the kinetic energy dependence of the transmission of the electron energy analyser,  $C_g$  describes the attenuation of the photoelectrons when immersed in gas, and, finally,  $F$  is the flux of the photon at a specific energy. Naturally,  $C_g$  needs to be considered only when experiments at an elevated pressure are conducted.

As it is evident from equation 3.13, several parameters need to be known while doing an XPS experiment. Some parameters such as the analyser slit and pass energy are hidden since they are contained in  $T$ ; they affect the intensity in the XP spectra.  $T$  is, however, typically unknown, and only seldom determined. Thus, it is often good practice to consider the ratio of intensities, as to remove the dependence of the unknown parameters. In the following, the factor  $C$  and the cross section  $\sigma$ , will be discussed in depth, since, among all possible parameters, they are the most interesting in terms of their physics. Moreover, these are only parameters that cannot, and should not, be considered the same when considering the ratio of core levels' intensity.

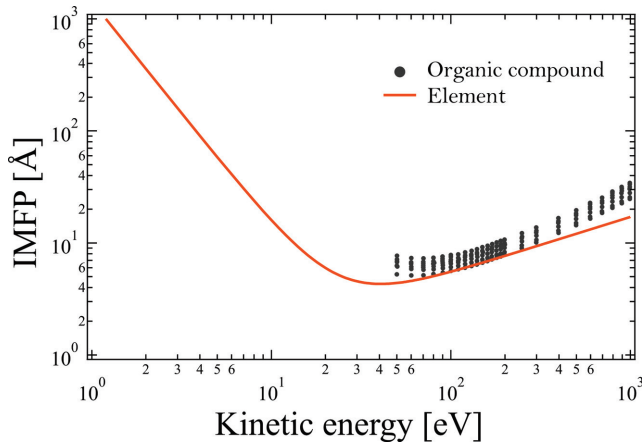


Figure 3.3 The inelastic mean free path of electrons travelling through various inorganic materials (orange), and organic compound (black dots). Adapted from ref [57] and ref [64].

$C$  strongly depends on the electron's inelastic mean free path (IMFP), which can be defined as the distance over which the probability of an electron

escaping from the solid loses  $1/e$  of its original value. Therefore,  $C$  can be expressed as an exponential function like  $e^{-d/\lambda}$ , where  $d$  is the depth in the solid from where a photoelectron can escape<sup>57</sup>, and  $\lambda$  is the inelastic mean free path;  $\lambda$  depends on several parameters, such as the density of the material, the depth the photoelectrons need to travel, the number of valance electrons, but, most importantly, the kinetic energy of the photoelectron. However, even if it may appear as a material-depending parameter,  $\lambda$  is, overall, found to follow the so-called “universal curve of surface science” shown in Figure 3.3. It is evident that the surface sensitivity of XPS (and any other technique based on the study of electrons) is due to the short IMFP of the photoelectrons. However, although the orange curve in Figure 3.3 is the best fit over the experimental parameter, in all my Papers, an approximation from Tanuma, Powell and Penn<sup>63</sup> was used to estimate the inelastic mean free path for HfO<sub>2</sub>, InAs, InAs Oxide, but also for TiO<sub>2</sub>. Figure 3.3 also shows experimental IMFP values for organic compound<sup>64</sup>.

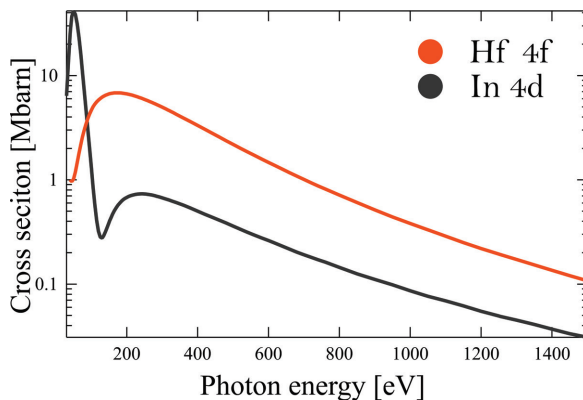


Figure 3.4 Atomic subshell photoionisation cross sections for 0-1500 eV, referred to In 4d (gray) and Hf 4f (orange). Adapted from Ref. [65].

This was used in Paper V, in which the thickness of the physisorbed TDMA-Hf molecules on the SiO<sub>2</sub> surface was calculated. Interestingly, the IMFP for elemental materials is slightly shorter than organic compounds.

At this point an interesting question arises. Is the IMFP really the important parameter for the factor  $C$ ? The answer is partly no, because the inelastic mean free path obviously only considers inelastic scattering. However, also elastic scattering should be taken into account, and therefore one should, in principal, use the electron attenuation length rather than the IMFP. The attenuation length is typically slightly shorter, around 90 % of the IMFP. This implies that the answer to the question is partly yes, because a difference of about 10 % in a decay exponential function can only be appreciate is few XP experiments.

Going back to the factors affecting the intensity of XP spectra, the cross section<sup>65</sup>  $\sigma$  is of utmost interest in regards to the research conducted during my doctoral years. Whilst the IMFP solely depends on electrons and materials properties, the cross section depends on the photon-electron interaction. Indeed, the cross section can be seen as the probability that a photon excites a specific transition. Therefore, different core levels of the same element can be excited with different probabilities. The cross sections also differ within elements on the sample, and before every experiment, it is essential to check whether it has an acceptable value. In Figure 3.4, the cross sections of Hf 4f and In 4d are shown as a function of the photon energy. If the scientist's goal is to enhance the signal of the Hf 4f line with respect the In 4d one, a photon energy higher than 200 eV is necessary. In this regard, it appears worthy to note why the cross sections of Hf 4f and In 4d have different "shapes". Suppose one assumes that the wave function describing the photoelectron is a plane wave, while the electron's wave function (before excitation) depends on its quantum numbers. In that case, the matrix element describing the photo-electron interaction will depend on the overlap between these two-wave functions. A minimum in the cross section is found

when a node<sup>h</sup> is met. This is the so-called Cooper minimum<sup>66</sup>, and it is well visible in the In 4d cross section in Figure 3.4 at around 150 eV.

## 3.2 Small guide to analysing XPS data

Needless to say, data handling is essential to any experimental research. Based on the insights collected during my work with XPS techniques and facilities, this final subsection aims at offering a small guide on how to manage XPS data, from the possible type of backgrounds to the possible line shapes, and eventually to the calibration of XP lines.

- **Background and line shapes**

First, it is crucial to check all the data gathered in order to develop a strategy to tackle them. Once all data are plotted, the iterative process can start. Should I remove the background before the fitting? Or should I also fit the background? Should I fit all the data together or should I handle them one by one? I have asked these questions to myself so many times! My experienced guess is, as often happens: it depends.

For simplicity, one can remove the background before fitting. Several types of background exist, “easy” ones are like a line, or a polynomial, others are more complicated, such as the Shirley<sup>67</sup> or Tougaard<sup>68</sup> backgrounds. It is important to know which background is more suited to your data.

The background originates from the loss of energy that photoelectrons experience when travelling inside a solid or gas. Such a loss of kinetic energy (therefore at high binding energy) is reflected by an increase of the background intensity. In Figure 3.5, a sketch of an overview spectrum of HfO<sub>2</sub> is displayed, in which different colours represent secondary electrons generated by any line.

---

<sup>h</sup> A wave function node occurs at points where the wave function is zero and therefore changes signs. The node can be found either in the radial or in the angular part of the wavefunction.

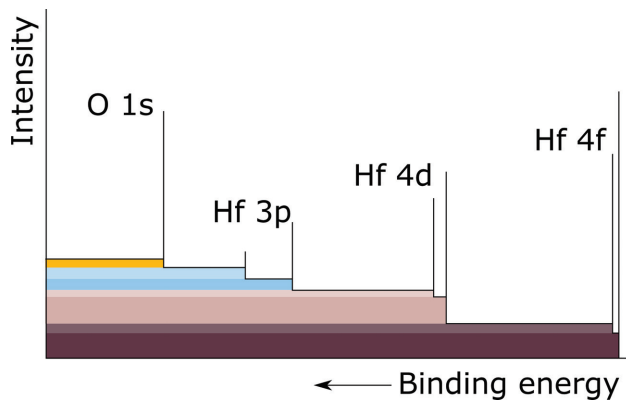


Figure 3.5 Schematic representation of a XPS background. Secondary electrons at low kinetic energy are not shown.

Sometimes, line backgrounds can be helpful when a preliminary analysis is required. However, one needs to be aware that a line background is affected by the initial and final point one chooses for the background. Therefore, it is not recommended to make any quantitative analysis in such a configuration. A very complex type of background shape is the Tougaard background. This background relies on the physics that generate the XPS background. It is typically based on several parameters that depend on the material from which the photoelectrons are generated. Therefore, to be used, quite some knowledge of the system is required. The last type of background, that also happens to be my favourite, is the Shirley background. The Shirley background, whose intensity at any given binding energy is proportional to the intensity of the total spectral area below the given binding energy, does not depend on material specific parameters. Therefore, it is less precise than the Tougaard background, but it does not require any heavy constraints<sup>i</sup> implemented by the user, thus eliminating the arbitrary problem explained before. The Shirley background is based on an algorithm:

---

<sup>i</sup> It still required a basic knowledge on the background since it can slightly change from where to where you are evaluating it.

$$S_n(E) = S_0(E) - k_n \int_{E_{min}}^{E_{max}} S_{n-1}(E') dE'. \quad (3.14)$$

In equation 3.14,  $k_n$  is defined by evaluating  $S_n(E_{min}) = 0$ . It typically requires 4 or 5 iterations until  $S_{n+1} \approx S_n$ .

Once the background is removed, it is time to fit the data. Fitting data can be done, as for the background, by using several different lineshapes: Gaussian, Lorentzian, a convolution of them called Voigt, and a Doniach-Šunjić<sup>69</sup>. The latter of the listed lineshapes, which was never used in the papers attached to this thesis, is particularly useful when dealing with a metal peak. Its intrinsic asymmetry already considers a final state effect: the creation of electron-hole pairs at the Fermi level.

Typically, it is assumed that one of the best lineshape to fit XP data is the Voigt function. It achieves the experimental broadening from the Gaussian and the lifetime broadening of the measured final state of the Lorentzian. However, and this is a big one, in most cases this is not quite accurate. In detail, during a photoemission process, one must take into consideration, in addition to the experimental and the core-hole lifetime broadening, the phonons. A phonon is a quasiparticle that describes the collective excitation in a system. Phonons, in contrast to vibrations, have a line shape characterised by a Gaussian distribution<sup>70</sup>. Moreover, in solid, there are typically too many lines around the same energy that makes it impossible to solve them. There are exceptions, such adsorbates on solid, where vibrational levels – and their Lorentzian broadening – can be resolved, as shown for  $C_2H_6$  on  $Ru(111)$ <sup>71</sup>.

Although using a Voigt does not add any meaning from a physical point of view compared to using a Gaussian, very often, and I speak from experience, it helps to get a fit with a chi-square – it is used to determine if the test hypothesis (fit) is representative of the experimental data- closer to one. The reason lies in the fact that by eliminating a background, of any form, errors can be made. These errors are more significant when the intensity is lower at a fixed energy. Consequently the tails of the peaks affect

the removal of one background more than another. Given that the big difference between a Gaussian and a Lorentzian are the tails of the distribution (this could make many statisticians and mathematicians turn up their noses), having the will to be able to choose the weight of each one, allows having a fit that "passes best for the experimental points".

Figure 3.6 shows an As 3d core level from an InAs sample. The background of choice is a Shirley background, which can be appreciated better in the inset. The data is fitted with three identical Voigt doublets, free to move in energy with respect to the main one, associated with As-In. There are three main parameters highlighted in the Figure: i) the chemical shift, which gives excellent information about the chemical environment in which the photoemitting atom is embodied, ii) the spin-orbit splitting and iii) the branching ratio, represented by the two vertical arrows.

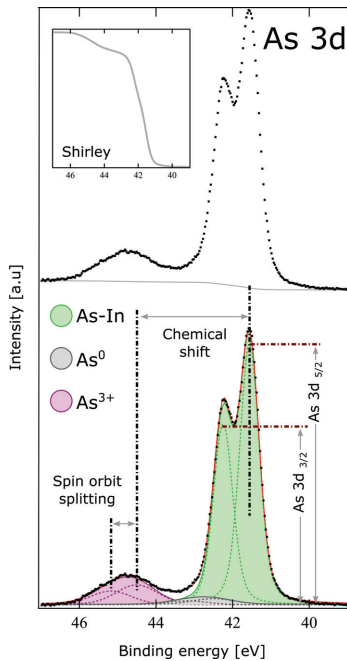


Figure 3.6 As 3d XPS spectra from an InAs sample thermally oxidised. Top) calibrated raw data and Shirley background. Bottom) raw data without background fitted with three doublets. Inset) the used Shirley background.



Theoretically, parameters ii and iii, namely the spin-orbit splitting and the branching ratio, are defined by the quantum numbers of the core electron. Regarding parameter ii, knowing the principal quantum number  $n$ , and its angular momentum  $L$ , as well as the spin, one can derive the total angular momentum  $J$  as  $L + S$ , where  $S$  is the multibody spin angular momentum. Since the coupling can be parallel or antiparallel, two main lines can be solved in energy. In the example presented in Figure 3.6, the total angular momentum for As 3d can be 3/2 and 5/2. The splitting in energy is in the order of eV, therefore it is possible to resolve them with XPS. It must be noted that the  $J$  value of 1/2 for s orbital is typically omitted since it is fixed.

The other important parameter is the branching ratio. It is defined as the ratio between the intensity of the two components in the doublet. As a general rule one can say that the ratio is reflected by the number of degenerative microstates unsolved with XPS. For any given  $j$  value there exist  $2j+1$  microstates sharing the same energy. Therefore the intensity ratio should be defined by the number of microstates for any given  $j$ . However, from experience, this is never the case. It gives a good indication on the ratio, but this rule does not take into account several other factors. For metal, for example, the internal Zeeman effect due to the coupling of the core and valance's open shells are typically neglected<sup>j</sup>, as well as "multiplet" effects, as described by de Groot<sup>72</sup>. He showed how the expected branching ratio of the  $L_2$  and  $L_3$  edges<sup>k</sup>, whose degeneracy should result in a value of 1/2, varies drastically as a function of the number of electrons in the 3d-band. His analysis is well described by crystal field theory, which explains the breaking in degeneracy of electrons states.

---

<sup>j</sup> Private conversation with Prof. Joachim Schnadt.

<sup>k</sup> When shining light to a sample, depending on the photon energy, the electron will either be promoted to the vacuum level (XPS), or to an unoccupied state (x-ray adsorption spectroscopy). An edge in XAS, which resembles a peak in XPS, is then named depending on which electron is excited. From the principal quantum number  $n=1, 2, 3$ , will correspond K-, L- and M-edges, respectively. Here,  $L_2$  and  $L_3$  refer to the  $2p_{1/2}$  and  $2p_{3/2}$  spin states.

- Calibration

In photoemission spectroscopy, the energies are typically referred to the Fermi level, and the scale is chosen either as binding energy or kinetic energy. I generally prefer to use the binding energy scale, since the absolute energy of the core level of interest is independent from the photon energy used. However, both scales are equally correct.

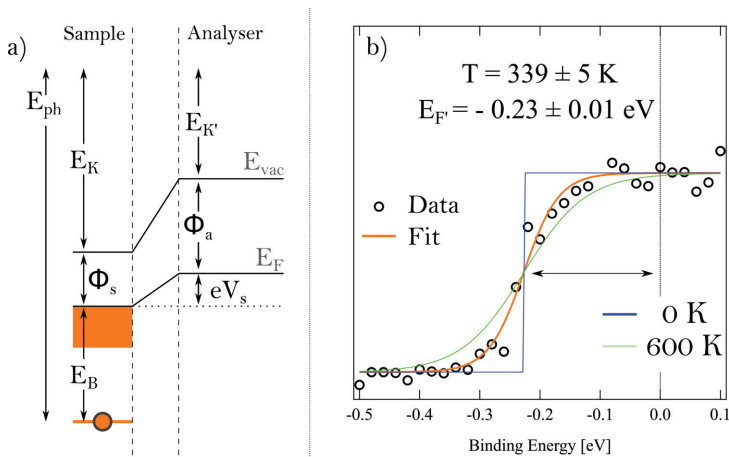


Figure 3.7 a) energy diagram involved the photoemission process. The  $E_B$  is defined by the energy of the electron to the fermi energy. b) Fermi edge of a graphene sample (circle) fitted with the Fermi-Dirac distribution (orange). Additional distribution at 0 K (blue) and 600 K (green) are also plotted. Data courtesy of Virginia Boix.

The main question to ask is: since all scales needs a reference point, how do I know where the 0 is on my scale? To help answer this question, one can use Figure 3.7. Place the sample one want to measure in electrical contact with the sample holder, which can be set to a potential  $V_s$ , as shown in Figure 3.7.  $V_s$  can be any potential, and it is generically placed at 0 V, with respect to the electron energy analyser (that is grounded). Illuminate the sample with photons, with energy  $E_{ph}$ , which will eject a core electron from an initial state with energy  $E_B$ . The kinetic energy of the photoelectron will be, as shown previously:

$$E_k = E_{ph} - E_B - \phi_s, \quad (3.15)$$

where  $\phi_s$  is the unknown work function of the sample defined by the energy difference between the Fermi edge and the vacuum level. However, the analyser has a work function too, which typically differs from that of the sample. Since the Fermi level of the sample will be shifted by  $eV_s$  with respect to the analyser's potential, to calculate the  $E_B$  of the core level, the only missing piece is the work function of the analyser (for an energy diagram, please see Figure 3.7 a). For non-metal surfaces, the most common method to determine it is to use a reference sample. Commonly, a Fermi edge of a metal is used. It is defined by the energy of the electrons in the higher occupied state and therefore it is used as the 0 eV in the binding energy scale. In the case of metal samples, the Fermi energy can be found by using the Fermi-Dirac distribution<sup>1</sup>:

$$f(E) = \frac{1}{e^{\frac{(E-E_f)}{k_B T}} + 1} \quad (3.16)$$

where  $k_B$  is the Boltzmann constant,  $T$  is the temperature, and  $E_f$  is the Fermi energy. For  $T=0$  K, the distribution shows a characteristic step function, while for  $T > 0$  K, it assumes a shape as shown in Figure 3.7 b.

Once  $E_f$  is determined and placed equal to 0 eV, the binding energy scale in XPS is calibrated. Unfortunately, in my research, I did not deal with metal surfaces, rather with semiconductors, that have a Fermi energy in between the sample's valence and conductive band. Therefore, other approaches needed to be used. We used a strip of gold attached to the sample older in good electrical contact with the sample on Paper II. Nevertheless, what is really in my research's interest is not the absolute value of binding energies but the relative binding energy between two or more core levels, or between different components of the same one.

---

<sup>1</sup> This is an approximation since the fermi energy distribution do not take into account the experimental resolution. However, the fermi energy is not affected.

There is another comment I would like to make regarding XPS calibration. I have often come across articles based on XPS measurement, which report having calibrated the XP spectra with the C 1s resulting from air contamination, also called adventitious carbon. Coached by my supervisor, I have always tried to avoid using absolute binding energies from data calibrated in such a way, but rather just making use of binding energy differences from such data. An article of Lars Hultman and Grzegorz Greczynski<sup>73</sup> covers very well, in a somewhat "bold" way, why calibrating the XP spectra to an adventitious carbon C 1s line is a rather unreliable way to perform a calibration. What I would like to report here, which is a summary of a summary of the article, is what surprised me the most: the position of the C 1s of the adventitious carbon, which it is not clear what is it, can vary by more than 2 eV according to the substrate in which it is deposited; in metallic surfaces, the C 1s of adventitious carbon, calibrated adequately with the Fermi edge, is reported between 284.5 eV up to 286.7 eV!

## 4 MAX IV Light Source

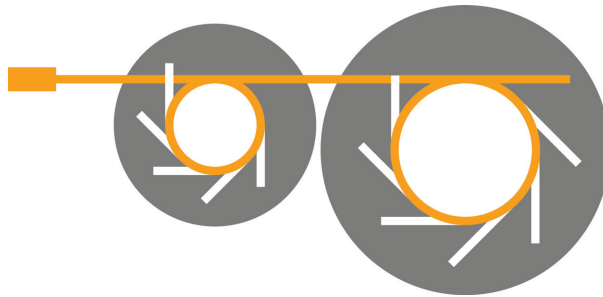


Figure 4.1 Schematic representation of the MAX IV synchrotron light source in Lund, Sweden. The electron path is in yellow, while the beamlines are in white. The left ring is the so-called "small ring" at 1.5 GeV, while the one on the right is the "large ring", at 3.0 GeV. The drawing is not to scale.

To find the first evidence in the history of x-rays, one needs to go back in time for more than 100 years. It was 1895 when Wilhelm Röntgen, accidentally discovered this unknown radiation.

*"In recognition of the extraordinary services he has rendered by the discovery of the remarkable rays subsequently named after him"*

he was awarded the Nobel prize<sup>74</sup> in physics in 1901. Several other scientists decided to investigate this new radiation, from William Henry Bragg<sup>54</sup>, Max von Laue<sup>75</sup>, to William Lawrence<sup>54</sup>. Eventually, they were also all awarded the Nobel Prize for the discovery of the interaction of the x-rays with the matter.

Historically, and still nowadays, the generation of x-rays is made by accelerating electrons towards a metal target in a vacuum tube. Then, x-rays are produced in two ways. The first occurs when a high-speed electron

approaches an atomic nucleus and is decelerated, giving rise to bremsstrahlung radiation. The second occurs when an incoming electron collides directly with one of the shell electrons, creating an electron vacancy. When the vacancy is filled with an electron from an outer shell, x-rays of discrete or characteristic energies are produced. However, even if the first generation of x-ray tubes led to outstanding results for that time, several improvements were made later. In 1940, at the University of Illinois, the first betatron of 2.3 MeV was built<sup>76</sup> by Kert. Its purpose was for nuclear research. The first synchrotron was constructed in the USA in 1947. It is interesting to cite a sentence from the abstract of the work<sup>77</sup> of Eldar et. al:

*“The radiation is seen as a small spot of brilliant white light by an observer looking into the vacuum tube tangent to the orbit and toward the approaching electrons”.*

It took almost 10 years for the scientific community to realise the potential advantages of synchrotron radiation for its own. Since the 1960s to today, four generations of synchrotron light sources have passed, and MAX IV, in Sweden, is the first of the latest generation, with high brilliance and small emittance. MAX IV is the first of the fourth generation since it is the first of the so-called diffraction-limited storage ring (DLSRs). This means that the emittance of the electron beam in the ring, is comparable with the emittance of the photon generated by the electron beam.

Today, the two most common sources of x-rays are synchrotrons light sources and x-ray tubes - the latter is the most common one. Although laboratory x-ray sources tend to lack in brilliance, which is defined as the number of photons generated per unit time, area, angle, and 0.1 % of the bandwidth, they are an efficient choice in terms of education, space, money, and availability, so that their use in higher education institutions should be encouraged. In addition to being excellent for chemical quantification and qualitative analysis, I personally think I was lucky to have had the opportunity to work in a laboratory equipped with an XPS lamp during my

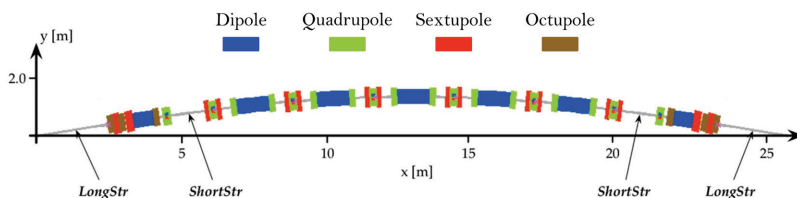


Figure 4.2 Schematic of one achromat used at the 3.0 GeV ring of MAX IV synchrotron light source. Dipoles are reported in blue, quadrupoles in red, sextuples in green, and octupoles in gold. Adopted from ref.[78].

master's degree at the Sapienza University of Rome. It was an old lamp, with a suboptimal resolution, but a working one. Given its age, it needed a lot of maintenance, which allowed me to take it apart, open it, fix it more than once. This persuaded me to understand its functioning and its internal components further. I think it must be present in every research institute to give the same opportunity I had to other students as well.

Synchrotrons light sources, instead, are dedicated facilities for generating x-rays. They offer optimal brilliance, around ten orders of magnitude higher than that of a standard x-ray source. Brilliance is not the only advantage that synchrotrons light sources have with respect to x-ray sources since the tunability of the photon energy is what makes a synchrotron several steps ahead of conventional x-ray tubes. When using a lamp, the energy is fixed and defined by the target element's energy level. Conversely, in a synchrotron light source, in principle, all the photon energies in the x-ray spectrum can be achieved. Synchrotrons light sources are built around several components, where several are similar to the ones at MAX IV. In the following, a list of components used at MAX IV are listed:

1. A source of electrons, generated, generally, by an electron gun based on a hot filament.
2. A linear accelerator (LINAC), where the generated electrons are accelerated up to 3 GeV in less 300 meters; The LINAC provides electrons continuously to the ring, in a manner that is called top-

up and that guarantees an almost constant electron beam current in the ring of 300 mA.

3. A storage ring, which contains the electrons. Magnetic devices are needed to keep the electrons travelling in the ring and to reduce the lateral spreading. MAX IV adopts a system of magnets placed in series, called achromats<sup>78</sup> (see Figure 4.2). The main components are:
  - i. Dipoles: also called bending magnets. They are necessary to turn the electron's trajectory and guarantee a close loop in the ring. In some synchrotrons light sources, such as Elettra in Italy, the photons generated in a dipole are used as the source of light in the beamline.
  - ii. Quadrupoles: These devices are needed to focus the electron beam.
  - iii. Sextupoles: once the quadrupole ejects the electrons, they need to be corrected for chromatic aberration<sup>m</sup>.
  - iv. Octupoles: once the sextupole ejects the electrons, they need to be corrected for higher order aberration.

What makes MAX IV special is the arrangement of the magnetic devices. All the magnets are inside a single unit, called magnet block, which guarantees tight alignment tolerance. Moreover, since the dipole and the quadrupole are machined out, the weight is contained. This allows to have magnet with a high natural frequency, therefore insensitive to typical “floor vibration”.

4. Undulators: they are based on a series of dipoles that constrain electrons' paths in a sinusoidal route. A similar device is a wiggler.

---

<sup>m</sup> The chromatic aberration is a phenomenon describing the failure of a lens to focus all the electron's energy to the same point.



They are structurally similar, but wigglers have a stronger magnetic field<sup>a</sup> (see Figure 4.3).

5. A radio frequency cavity, whose role is to restore the energy to those electrons which have lost part of it by emitting radiation. Electrons will receive boost in energy based on their speed: the higher the speed, the weaker the boost.
6. Beamline. Finally! We can find the beamlines just after the undulator, and they are built tangentially to the storage ring. Their role is to collimate the photons generated by the undulators and use them in several ways. They consist of several components, some of which will be detailed in the following section regarding two specific beamlines at MAX IV: HIPPIE and SPECIES and one at SOLEIL: TEMPO.

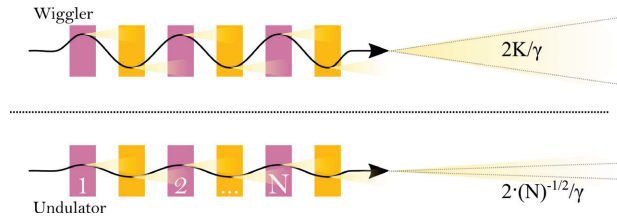


Figure 4.3 Wiggler (top) and undulator (bottom) schematics. The K value, proportional to the magnetic field of the dipoles, dominates in the output radiation in the Wiggler. Instead, the output radiation of an undulator is dominated by the inverse of the number of periods. The higher the number of periods, the smaller the divergence of the beam.

## 4.1 Beamlines

HIPPIE and SPECIES, as well as TEMPO, are soft x-ray beamlines on the 3.0 GeV and 1.5 GeV electron storage rings of the MAX IV, and SOLEIL

---

<sup>a</sup> The difference between the two in terms of photon flux will be presented later in this chapter.

electron storage rings, respectively, equipped with a novel ambient pressure x-ray photoemission spectroscopy instrument. There, is where I spent most of my time during my PhD, carrying out experiments that produced both valuable and frustrating results, the best of which constitutes the majority of the articles collected in this thesis. Needless to say, I feel some attachment for HIPPIE and SPECIES. There, in fact, is where I have learnt the most about experimental physics. Over time, I have got acquainted with the specific features of these beamlines and I have realised that being fully aware of what a beamline is able to do, its technical characteristics and potential, is key to fine tuning one's research. This is the reason why I am presenting this very section, with the – perhaps too ambitious – aspiration of be of help to future beamline users.

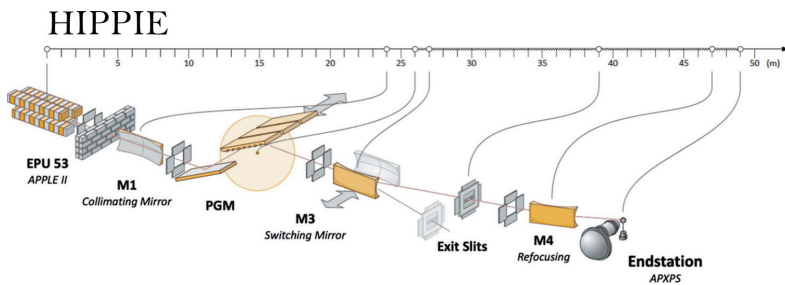


Figure 4.4 Optic layout of HIPPIE beamline. Adapted from ref.[79].

- HIPPIE

HIPPIE<sup>79</sup> is a soft x-ray beamline at the 3.0 GeV ring. It provides photon energy ranging from 250 eV to 2200 eV, with a resolving power up to 32000 (more details about the resolving power will follow). Photons are provided to HIPPIE via an elliptically polarising undulator, based on 70 full periods of dipoles, for a total length of approximately 4 m. The first optical component that photons meet is a toroidal mirror, M1 in Figure 4.4. Then photons meet a second mirror, a monochromator with a grating of 1200 lines/mm coated in gold, and another focusing mirror. As the name suggests,

the monochromator is needed to select the desired photon energy. Once the energy is set, the photon flux will reach the last refocusing mirror (M4), and an almost constant high flux of up to  $10^{13}$  photons per second will reach the endstation.

- SPECIES

SPECIES<sup>80</sup> beamline is in the small ring of MAX IV. SPECIES has a beamline setup similar to HIPPIE (c.f. Figure 4.4). The main difference can be found in the accessibility of photon energy: SPECIES can go from 30 eV to 1500 eV. This translates into two AP-XPS beamlines at MAX IV, covering the whole soft x-ray range. Resolving power of about 6500 and photon flux between  $10^{13}$  and  $10^{10}$  photon/s, makes SPECIES an excellent beamline.

- TEMPO

This section comes a little out of the blue, since TEMPO is not at MAX IV and this chapter was dedicated entirely to it. But it is fair to credit, and therefore adding a part of this thesis, to TEMPO beamline, that in these years provided me with three manuscripts (Paper IV, V and VI).

The TEMPO beamline, located at the SOLEIL synchrotron (France), is a soft x-ray beamline adapted to the dynamic studies of the electronic and magnetic properties of materials. The flux, which at the sample is about  $10^{13}$  photon/s, is in line with that at HIPPIE and SPECIES, but the resolving power is slightly lower. This can be appreciated by comparing the Hf 4f core-level spectra in Figure 1 in Paper IV.

#### 4.1.1 Flux and resolution

A significant aspect of the beamlines is their photon flux and energy resolution. I will start by discussing the photon flux. In order to simplify the reading, I will refer to HIPPIE beamline in this section, since the flux and

resolution are general aspects in common between HIPPIE, SPECIES and TEMPO.

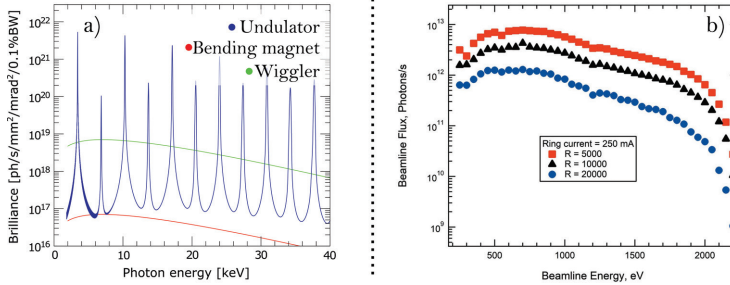


Figure 4.5 a) comparison of brilliance of an undulator (blue), a bending magnet (red), and a wiggler (green). B) HIPPIE beamline photon flux at the endstation for three different resolving power. Adapted from ref [79].

The photon flux, defined as the number of photons per second<sup>o</sup>, can be measured by inserting a photodiode in the photon path. At 250 mA ring current<sup>p</sup>, the photon flux is almost constant at 10<sup>13</sup> photons per second, between 500 to 1000 eV with a gradual decay toward 2000 eV. This is possible by using the first and third harmonic of the undulator spectrum. The undulator, in contrast to wiggler and bending magnets, produces a spectral flux with very narrow bands of radiation. A generic undulator spectrum, in comparison to one of a wiggler and bending magnets, is shown in Figure 4.6 a, while the photon flux of HIPPIE is shown in Figure 4.6 b.

Regarding the resolving power, it is measured from the x-ray adsorption spectra of N<sub>2</sub> (and Ne gas). This is usually done by filling a portion of the beamline with N<sub>2</sub> (or Ne) gas at around 10<sup>-2</sup> mbar. The N K-edge has a natural width<sup>81</sup> of about 120 meV. From a fit with a Voigt profile (see Chapter 3.1.2) the beamline contribution is estimated to be around 16 meV. Since the selected photon energy was 400 eV, a resolving power, defined as  $E/\Delta E$ , of approximately 25000 is achieved. However, when talking about

<sup>o</sup> Some definition includes the area, but this one does not!

<sup>p</sup> The nominal design ring current at the 5 GeV storage ring is 500 mA.

the resolution seen in XP spectra, this is only one of the main contributions to the overall energy resolution. Indeed, another main contribution needs to be included, and it is coming from the electron energy analyser. More discussion will follow in the next section.

## 4.2 Endstation

There are many similar aspects that can be found among the three beamlines presented. In fact, all of them have an endstation equipped with several ultra-high vacuum (UHV) chambers: a load lock, where samples can be transferred in UHV in a matter of minutes; a preparation chamber which includes a low energy electron diffraction (LEED) instrument, Ar ion sputter gun, electron beam heater. The electron energy analyser (EEA) at HIPPIE is a Scienta Omicron HiPP-3 analyser, and at the SPECIES and TEMPO beamlines a SPECS Phoibos 150 NAP analyser. All analysers feature a series of differential pumping stages that allows to measure samples in a gas environment with pressure up to 30 mbar, while keeping the EEA in UHV.

The heart of HIPPIE and SPECIES resides in its ambient pressure (AP) cell adapted in something called the “Lund cell” approach<sup>82</sup>. It is a cell-in-cell concept<sup>83,84</sup> where the sample environment is created inside an AP cell, which itself is placed inside a UHV vacuum chamber. The most common experiment type that can be performed in this cell revolves around measuring the interfaces between solids and gases. TEMPO, in contrast, has a backfilled chamber, where all the analysis chamber is filled with gas. More details about these approaches will follow. These chambers are interconnected, which allows transferring the samples between the different sections of the endstation without ever breaking the vacuum. HIPPIE, uses a radial distribution chamber (UFO) to interconnect them, while SPECIES, similarly to TEMPO, uses gate valves and linear transfer manipulator (c.f. Figure 4.7 a)

- Analyser mode

We are still missing an important point: how are the data collected? The general answer will be: via a detector. However, the detector changes depending on the beamline. The EEA at HIPPIE is equipped with a CCD camera; SPECIES and TEMPO feature delay-line detectors (DLDs). The analysers can operate in two different ways:

1. Swept mode: since the transmission and sensitivity of the detector are not uniform within the microchannel plate<sup>q</sup>, it is necessary to integrate every single kinetic energy in all the detector channels. This guarantees that each channel is used in the integration process and therefore removes the microchannel's dependency. This mode is favourable when high resolution, well-counted spectra are needed.
2. Fixed mode (also called "snapshot mode" in the SPECS lingo) is the mode you want to use when you aim to track chemical changes on your sample in "real time". Instead of sweeping the analyser voltages, the analyser is fixed on a specific kinetic energy range, the size of which is determined by the pass energy. As mentioned before, the allowed kinetic energy inside the detector is defined by the pass energy, the higher the pass energy, the higher the accessible photoelectrons with a variation in kinetic energy. As a rule of thumb, the variance in kinetic energy is 1/20 of the pass energy<sup>r</sup>. For example, a pass energy of 100 eV will allow electrons with kinetic energies of  $100 \text{ eV} \pm 5 \text{ eV}$  to be detected. The fixed mode has a significant advantage in terms of time spent collecting a spectrum, since the only limitation is the frame rate of the camera used<sup>s</sup>, and no time is spent in changing voltages; however, as a drawback, it

---

<sup>q</sup> A microchannel plate, like an electron multiplier, detect electrons and provide spatial resolution due to the several channels.

<sup>r</sup> In principle this number depends on several aspects, including the size of the camera and the lens. Therefore, it is not universal.

<sup>s</sup> This is valid in first approximation since the software which control the camera can and does limit the acquisition rate.

needs a sensitivity of the detector as uniform as possible, a condition seldom achieved. Improvements can be made in characterising the detector's sensitivity but, unfortunately, this depends on several parameters, including the kinetic energy, and it is not always easy to do.

Examples of spectra acquired in both the detector mode can be found in Paper II and Paper IV.

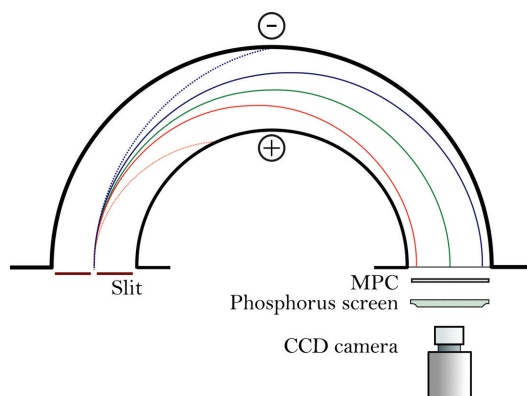


Figure 4.6 A hemispherical EEA selects only those photoelectrons within the proper kinetic energy range (green line), while the slower and faster electrons (blue and red) hit the detector in a slightly different position. Slower and faster is defined relative to the pass energy. On the left side, the slit select electrons arriving perpendicular to the entrance of the EEA.

- Energy resolution

Once the photoelectrons are ejected from the sample, their energy needs to be measured with the EEA. To do that, the electrons, after travelling towards a series of electrostatic lenses, are deflected between two concentric hemispherical electrodes, after which they hit a detector, which records their final position. It is essential to know how an electron energy analyser works in order to understand the experimental broadening. Between the two hemispheres, a potential is applied. The negative potential is on the outer side of the analyser, while the positive one is in the inner shell (c.f. Figure

4.6). Once the electrons enter the analyser, they will experience a potential that will bend their trajectory. For any given set of potential applied in the two shells of the analyser, also called pass energy, only one kinetic energy will make the semicircle and reach the detector. If the kinetic energy of the photoelectrons is too high, they will hit the outermost shell, contrary to electrons with not enough energy, that will hit the inner shell. However, if the electrons differ slightly from the perfect trajectory, they will still hit the detector but in a different position (see Figure 4.6 for a schematic of the energy electron analyser). This means that for a given potential (pass energy), only electrons with a kinetic energy of  $E_k \pm \Delta E_k$  are detected. Obviously, the resolution strongly depends on the pass energy: the higher the pass energy, the higher the spread in energy and the intensity, but the lower the experimental resolution. Other factors can affect the practical resolution of the analyser, and another important one is its slit. The analyser slit defines the solid angle of electrons entering the hemisphere. The higher the slit, the lower the resolution, since electrons with different angles, but same energy, will hit the detector in different position.

How can one measure kinetic energies that are not defined by the pass energy? Before entering the hemispheric analyser, the photoelectrons need to be slowed down by a potential called retardation potential<sup>†</sup>. The potential, negative with respect to the grounded sample is related to the actual kinetic energy of the electrons in the following:

$$U_{ret} \propto (E_k - PE). \quad (4.1)$$

The  $U_{ret}$  is then scanned to cover the region of interest.

To conclude, the overall experimental resolution, assuming no correlations and with Gaussian dispersion, will be a squared sum of all possible broadenings:

$$\Delta E = \sqrt{\Delta E_{beamline}^2 + \Delta E_{analyser}^2} \quad (4.2)$$

---

<sup>†</sup> In a Scienta, it could also be an acceleration voltage.



Typically, the experimental resolution in my manuscripts is around few hundreds of meV.

- APXPS setup

As previously mentioned, HIPPIE, SPECIES and TEMPO are equipped with an ambient pressure XPS setup. This means it is possible to acquire XPS spectra at pressures in the mbar range. If you are asking yourself why it is called ambient pressure XPS, even if the spectra are collected in mbar range, you are asking yourself a good question. The partial pressure of water is around 0.5 – 2.3 % of the total ambient pressure surrounding us, which is about  $10^3$  mbar. Therefore, XPS performed at pressures in the mbar range can be defined as APXPS. How does it work? XPS is an amazing surface-sensitive technique due to the small IMFP of the photoelectrons in a bulk material. In UHV, once the photoelectron has escaped from the sample, it can travel for kilometres before losing its entire energy due to inelastic and elastic scattering; however, when the surrounding pressure increases, the path becomes shorter. As an example, at 1 mbar of water pressure, a photoelectron with a kinetic energy of 100 eV, can travel for about 1 mm. This distance is, naturally, shorter than the typical distance between the sample and the

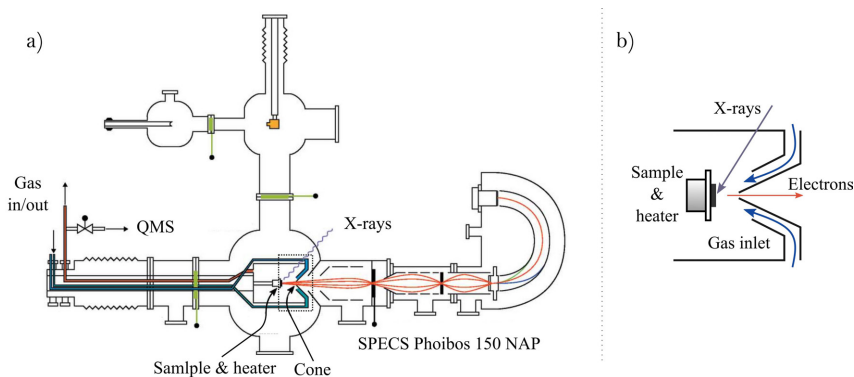


Figure 4.7 a) Schematic layout of the APXPS enedation at SPECIES, showing all the chambers. In orange, the path of the photoelectrons towards the analyser. b) Schematic view of the SPECIES cell with the double-cone system for gas inlet. Adapted from ref.[80].

electron energy analyser. Moreover, in order to work, the electron analyser, in more detail the detector, needs to be in high vacuum, between  $10^{-7}$  to  $10^{-9}$  mbar.

To increase the pressure gap between the sample's environment and the analyser, in order to keep the sample high pressure and the detector at low pressure, a series of differential pump stages are installed in between. A display of the SPECIES setup is sketched in Figure 4.7 a.

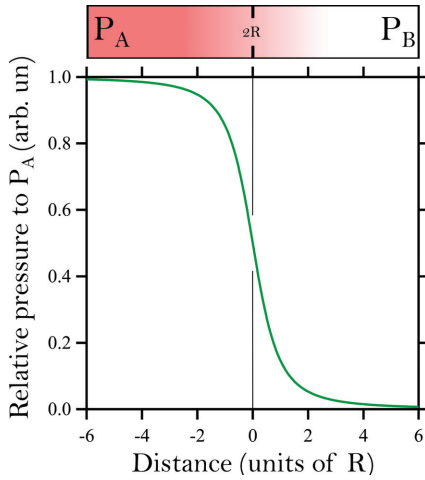


Figure 4.8 Pressure dependance between two chambers separated by an aperture of radius  $R$ .

To understand how the differential pumping stage works, one can resort to a simple ideal gas theory<sup>85</sup>. If one assumes an aperture with radius  $R$ , between two chambers (A and B) at a pressure  $P_A$  and  $P_B$  (with  $P_A > P_B$ ) one can calculate how the pressure varies between the two chambers using the following:

$$P(z) = \frac{1}{2} \cdot P_A \cdot \left(1 - \frac{z}{\sqrt{1+z^2}}\right), \quad (4.5)$$

where in  $z=0$  the aperture is placed. The function is also shown in Figure 4.8 where  $z$  is on  $R$  units, and the pressure is normalised to  $P_A$ . Interesting to notice is the fast drop on pressure close to the aperture  $R$ . At a distance of  $-3R$  (still in chamber A) from the aperture, the pressure is 97 % of  $P_A$ . Approaching the aperture, at a distance of  $R$ , the pressure drops to 85 % of

$P_A$ . On the other side, in chamber B, the pressure, just after a distance  $R$  from the aperture, is 14 % of  $P_B$ . This means that if pressure in A is 1 mbar, and the sample is placed at  $3R$  from the aperture, it will feel 0.97 mbar. However, even at a distance of more than  $10 R$  from the aperture, the pressure cannot drop fast enough to install the electron energy analyser. It is possible to calculate, for an ideal system, that the maximum ratio between  $P_A$  and  $P_B$  is around  $10^3$ . Therefore, a series of differential pumps is used, and the pressure can drop by 8 or 9 order of magnitudes in less than 1 meters!

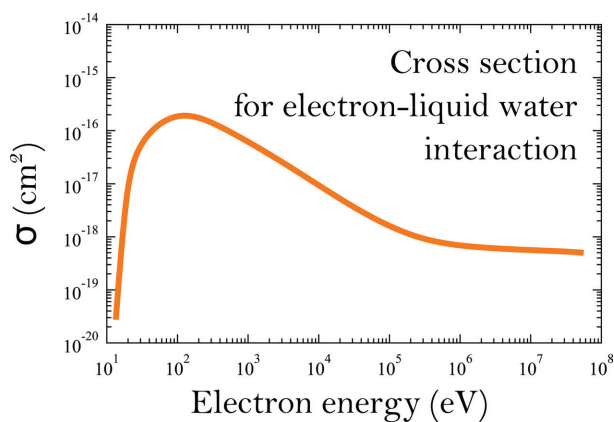


Figure 4.9 Total electron ionisation cross section for electron – water interaction. Adapted from ref.[87].

To enhance the XP signal even more, the HIPPIE beamline adopts a specific feature of the HIPP-3 analyser<sup>86</sup>, called swift acceleration mode, which significantly improves the analyser's performance under ambient pressure condition. A swift potential is located just after the first aperture between the sample and the electron energy analyser. This gives a kick to the photoelectrons by several keV, significantly increasing their kinetic energy, and consequently, reducing the cross section between the photoelectrons and the gas molecules present in their path (the cross section for interacting electrons with water as a function of their kinetic energy is shown in Figure 4.9)<sup>87</sup>. Thus, a higher transmission of the analyser is achieved, in ambient pressure condition, where the gain is about 20 times, and in UHV, where

the gain is a factor 2 or 4. Then, once the photoelectron gets close to the analyser, it is decelerated by the same energy applied before. The swift potential is "so good" that it is always on at HIPPIE.

All these precautions guarantee a time acquisition of any APXPS spectra close to the one acquired in UHV, with a reasonable count rate and high signal to noise ratio.

- Gas delivery system and APXPS setup: a comparison

The gas delivery system and the APXPS setup differ between the three endstation and this is an important aspect to consider when performing ALD experiments.

As mentioned before, the heart of HIPPIE and SPECIES resides in their AP cells. TEMPO, in contrast, adopts a backfilled chamber, where all the analysis chamber is filled with gas. The "Lund approach" has a significant advantage with respect to the backfilled chamber for ALD experiments. The small volume of the cell, around 200 ml (SPECIES) and 1 l (HIPPIE), allows fast gas exchange, while this is not possible at TEMPO beamline. However, TEMPO is based on a windowless analysis chamber, which ensures to keep a high vacuum on the beamline side, while having high pressure in the analysis chamber, via a differential pumping system similar to the one of the analyser. However, if having a bigger volume bring some disadvantages, not having a window which physically separate the beamline environments with the one of the cell, allow higher photon flux at the sample. Indeed, the AP cell at HIPPIE and SPECIES are equipped with exchangeable window, depending on the type of the experiments, which have a transmission dependent of the photon flux. This can reduce drastically the photon flux on the sample.

The gas delivery system at HIPPIE is composed of one inlet and one outlet. This setup is excellent for experiments in which a pulse of gases is used (Paper XI), and when a constant flow of gas is needed (Paper IX), as we did during the investigations of Assoc. Prof. Jan Knudsen and Dr Mattia

Scardamaglia. The gas delivery system at HIPPIE proved to be well suited for the ALD experiment but it showed some drawbacks in efficiency when the dosing of more than one precursor was needed. ALD requires two gas precursors dosed in sequence and without overlapping, and the single inlet causes interaction between the two precursors inside the inlet line before they reach the sample surface. This translates into an excellent first deposition but increasingly less efficient in further ALD half-cycles. The AP cell is continuously pumped via the first differential stage of the analyser and the outlet line, which can be closed, thus guaranteeing a constant flow of precursors during the experiment. In contrast, SPECIES and TEMPO have two inlets. It should be noted that ALD experiments at HIPPIE were done until the commissioning of the SPECIES beamline. Since 2020, almost all ALD experiments have migrated to SPECIES.

Another important aspect to take into account at SPECIES, is the dedicated ALD cell. In the cell, the flow of precursors, which points directly to the sample, as shown in Figure 4.5-b, behaves in a laminar-like flow across the entire surface. Dr Esko Kokkonen, beamline scientist at SPECIES, recently wrote a comprehensive review of the beamline, in which many insights can be found<sup>180,88</sup>.

### 4.3 Practical guide to do a beamtime

After more than twenty experiments conducted in beamlines in Sweden, France, Italy, and Germany, I have gained some confidence in how to prepare for a beamtime. Confidence, here, mainly deals with errors I have committed and that in hindsight, with some preparation, could have been avoided. I wished there was a practical guide transmitted by older doctoral students to tell me what to expect, how to behave, and what to avoid. For this reason, I have tried to distil the most salient notions to bring in mind before starting a beamline. What follows certainly does not aspire to be a

comprehensive guide, but it does aspire to help a little my future fellows, to spare them the whinging: “oh, I wish I knew it!”.

Let’s say that you have been granted five days of beamtime at SPECIES, MAX IV, where you will conduct an experiment that you planned when writing your proposal. You cannot get stuck in unplanned situations during your beamtime, nor you can get home with poor data to analyse. It is essential that you know what you will do: time is gold.

- ∴ Do you already know what core levels you want to measure? Good, now you need to start thinking about the photon energy you wish to use. When choosing photon energy, it is imperative to be aware of the cross section, the photon flux at that specific energy, the transmission of the windows between the cell, and the IMFP of the photoelectron. You may also want to check if at that specific photon energy, in your region of interest, an Auger line<sup>u</sup> is present. If this is the case, just move the photon energy by 10 or 20 eV so to shift the Auger out of your region of interest. If instead you are interested to keep the same kinetic energy so that the same depth is probed, be sure to save all the parameters that can influence the intensities of your core-levels due to the different photon energy.
- ∴ It is also crucial, at all times of the experiment, to be aware with all parameters you can tune at the beamline. For example, changing pass energy between two spectra will affect the resolution, the calibration, and the intensity. It will be tough to compare them! The same applies to the slits of the beamline and the slits of the analyser.
- ∴ A further essential point is to consider, and be prepared for, the sample preparation process. Do you know how to clean

---

<sup>u</sup> Auger are electrons generated by the relaxation of the system after photoexcitation. Once the system relax, a photon is generated which can cause the emission of a another electron.

(if the experiment requires cleaning) your sample? For example, anatase  $\text{TiO}_2$  crystals needs several cycles of sputtering and annealing to be clean and carbon-free. This process can take several hours and since it does not require photon beam, you may consider starting before the official beginning of the beamtime, to save some time.

- ∴ Make sure that all the data are calibrated. Take a known spectrum all the time you need to change photon energy, otherwise the calibration will be lost. Otherwise you can adapt a technique I personally called “cascade calibration”. I was taught by my supervisor Joachim Schnadt. It allows to acquire a metallic spectrum C (for calibration) only once, even if it is necessary to change photon energy in experimenting. Imagine collecting A, B and C core levels with photon energy “a”. Thus, all the core level will be calibrated. Then, collect B with “b” photon energy, and then calibrate it with the calibrate B acquired before. This approach, however, requires that the photon energies do not change drastically, otherwise you would compare photoelectrons from different depths, which can have different binding energies.
- ∴ If your experiment includes the deposition of new materials, keep in mind to take background spectra of the region where you are expecting the core level to rise. It will help a lot during future analyses.
- ∴ In an APXPS experiment, do not forget to measure, if possible, the gas phase spectra, with the same setting as the spectra on the solid.
- ∴ Organise well the shifts with your colleagues and friends. Let us assume an ideal case in which you can plan three eight-hour shifts, covering the whole day. But in this way, you will not have the chance to meet your teammates. Even in the

ideal case in which no issues have emerged, you will still need to be briefed about what has been going on in the previous shift. So, try to make each shift overlapping with the previous, to have a smoother communication on how to proceed with the beamtime.

- ∴ Write down everything, all the time, in the logbook. You will probably need to know some small details when analysing the data or writing the paper.
- ∴ It is easy to get distracted during a beamtime, especially if you are not collecting data and you are preparing something else. It is good practice to start plotting the data and comparing them to check if everything is going smoothly or you need to re-measure some core levels. This will save you some drama when back in the office.
- ∴ Maybe the most important of all the points: be patient. Beamtimes can be frustrating and tiring. You will not sleep properly or enough, work a lot, and try to find solutions to unexpected problems all the time. It is vital to be patient and never give up!
- ∴ This point has to be read once the data are collected and you are sitting in your office trying to figure them out. The main question you should ask is: how deep can you dig? In principle, the answer is: really, really deep. Developing results out from data starts with a fairly simple process: plot the data, check all of them, one fit there, another one there, and you find yourself with a decent number of results. The excitement can prevail, and you think you are able to build a nice story with what you think is a great analysis! Unfortunately, in my experiences, the details come out the moment you start writing. The writing process forces you to put together all the pieces obtained from the analysis. It forces you to read more



and more articles to check if the story you have in mind has any valid grounds. It forces you, most of the times, to go back to the data and double-check the analyses, looking for something that you might have lost in the initial enthusiasm. The whole process is long and intricate but, in the end, it often pays off in the best possible way!



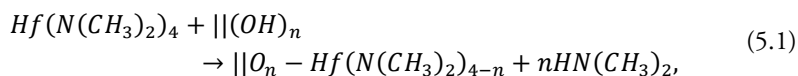
# 5 Insights from *in situ* and *operando* APXPS

The sections that will follow will trace the most important findings of the ALD manuscripts and published articles attached to this thesis. I will introduce new surface species found during the first half-cycle of ALD, and I will discuss in detail its possible origin. Then, specific subsections will expand on the surfaces of interest and their role during the deposition. Eventually, an exciting new finding during the water deposition will be reported. At the end, a result based on the adsorption of ethanol based on *in situ* measurements will be presented.

## 5.1 New surface species: the origin

As you probably have noticed in all the equations presented in chapter 2, ligands are always expressed with a single letter  $L$ , and remain unchanged before and after the reaction. However, since this was not the case, in any of the manuscript attached to this thesis, I decided to dedicate an entire section to the origin of new surface species.

As expressed in equation 2.2, and reported here with the atoms explicitly written:



the only possible ligands one should detect during the ALD is dimethyl-amido ligand  $-N(CH_3)_2^-$ , also called, in short, DMA $^-$ .

The DMA<sup>-</sup> ligand, on the right-hand side of the equation, is bonded to a hydrogen atom, which forms a dimethyl-amido molecule (DMA). Ideally, DMA should leave the surface as a by-product in the gas phase. The desorption temperature of DMA on a rutile TiO<sub>2</sub> surface is estimated to be around 180 °C; indeed, in Paper V, where ALD of HfO<sub>2</sub> on SiO<sub>2</sub> is performed at 180 °C, no trace of DMA was found. However, we observed DMA on the surface on ALD of HfO<sub>2</sub> on anatase TiO<sub>2</sub>, and on thermally oxidised InAs (Paper II, III, and, IV). All the experiments were conducted at temperatures higher than the desorption temperature on SiO<sub>2</sub>.

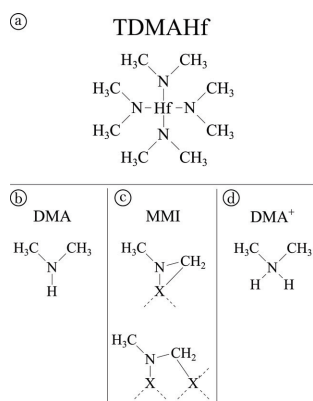


Figure 5.1 Scheme of a) TDMA-Hf, b) DMA, c) MMI, which can be in 3MR configuration (top) and in the bridge configuration between one, or two, metal complexes (bottom), d) DMA<sup>+</sup>.

However, it is imperative to emphasize that the formation of DMA species via an hydroxylate surface is not what is reported in the attached manuscripts. All the studied surfaces were hydroxyl free. Therefore, justifying the presence of DMA, without using hydroxyl from the surface, opens a new reaction pathway which has not been considered before.

As stated, a DMA is formed when a DMA<sup>-</sup> is bonded to a hydrogen atom; therefore, we need a source of hydrogen atoms. Every TDMA-Hf carries 24 H atoms (c.f. Figure 5.1-a). Assuming an insertion reaction of one of the hydrogens from a DMA<sup>-</sup> ligand, between the Hf-N bond of another DMA<sup>-</sup> ligand, a DMA and a new nitrogen species will be formed. The latter is called methyl-methylene-amine (MMI). MMI can be found, as suggested by the DFT calculations in Paper V, in two configurations: a three-

membered ring (3MR)<sup>89</sup> and a bridging bond. The derived MMI configurations are based on an intra- or inter- molecular reaction, respectively, as shown in Figure 5.1 c.

However, in Paper IV, on the ALD of HfO<sub>2</sub> on TiO<sub>2</sub>, another nitrogen species is found, at higher binding energy with respect to the others. The N species, identified as protonated DMA, is formed when protonating a DMA complex, from an hydroxyl on the surface.

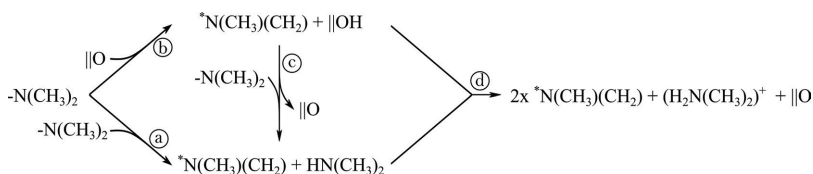


Figure 5.2 Suggested reaction path to form an MMI and DMA (a), MMI and hydroxyl (b), and connection between them (c). (d), suggested path for the formation of a DMA<sup>+</sup>.

Nevertheless, in the very same paper, evidence of hydroxyl formation during the first half cycle is found. In details, the hydrogen atom from the previous insertion reaction is now found on the surface, leading only to the formation of a MMI ligand. Consequently, if the hydroxyl is then used by a DMA, DMA<sup>+</sup> is formed. The suggested paths are shown in Figure 5.2.

It is also interesting to discuss how these species depend on the experimental parameters, such as precursor pressures and temperature of the substrate. In Paper IV, the influence of temperature and pressure is presented. One finding, which however still needs some additional verification, is based on the idea that physisorbed complexes such DMA and DMA<sup>+</sup> are unfavourable with respect to dissociative adsorption of a fresh TDMA-Hf molecule. If the adsorption energy of TDMA-Hf exceeds that of DMA (or DMA<sup>+</sup>), the high flux of impinging TDMA-Hf molecules on the surface at high pressure could lead to the displacement of more weakly adsorbed DMA (and DMA<sup>+</sup>) from the surface.

In conclusion, the formation of these new species during the first half cycle are not predicted by any of the current models used to describe ALD. These species, as shown in Paper II, IV and V, can be removed during the second ALD half-cycle, therefore, for a mere “device” perspective, they will not influence the resulting layer. However, it is imperative to be conscious about side reactions, which can lead to species which can be harder to remove during the second half-cycle by using different precursors.

## 5.2 The surface, does it do something?

One of the main findings of this thesis is that the surface may have an active role in the ALD process that goes beyond the static one that it has in conventional models of the ALD surface chemistry. Besides the type of reaction mechanism involved, either chemisorption, physisorption, or others, the surface always has a static role during the deposition, meaning it does not contribute to the reaction and is independent of the ALD precursors. "Static" in this context means that the constituent atoms of the surface are not directly involved in the reaction, but only possible ligands do, e.g. surface hydroxyls.

Several experiments will be presented here. As stated several times, they mainly focus on the first half-cycle of ALD of  $\text{HfO}_2$  on native and thermal oxides on an InAs(100) surface, anatase  $\text{TiO}_2$ (101), oxidised Si(111) and Si(111).

- InAs

The thermal and native oxide on an InAs(100) surface show an almost complete reduction of the oxide during the first half-cycle, in a process called self-cleaning<sup>12,13,15,23,90,91</sup>. The results obtained from the InAs surfaces can be found in Paper I, II and III. In the image plots of Figure 5.3 the In 3d, the As 3d and the Hf 4f/In 4d core-level intensities are shown as a function of

time<sup>v</sup> (Figure 5.3 a, b and c, respectively). In the In 3d and As 3d spectrum, the high binding energy components associated with the InAs native oxide decrease in intensity with the same characteristic time constant (bottom graphs in Figure 5.3). On the other side in Figure 5.3 c, the intensity of the broad doublet, associated with the Hf 4f core level, is increases. This correlation process suggests that the first half-cycle will end only when all the native oxide is consumed, consistent with the self-limiting nature of ALD. Interestingly, it seems as if the TDMA-Hf uses the oxygen from the native oxide to form HfO<sub>x</sub> already in the first half-cycle. In order to check the validity of this hypothesis, the binding energy of the Hf 4f line as a function of exposure time shows a fast downshift, followed by an upshift. DFT calculations suggest that TDMA-Hf on InAs chemisorbs only after a physisorption step, mediated by the lone pair of the N in the dimethyl amido ligands<sup>92,93</sup>. The physisorption step will lead the binding energy of the Hf 4f line towards a lower value (-0.15 eV with respect to the HfO<sub>x</sub> binding energy), since it will decrease the electron density of the N atom, and therefore increase the one of the Hf. In this experiment, N 1s and the O 1s core levels were not collected due to technical problem during the experiment, therefore a close examination of the possible hydroxylation of the surface prior to the deposition or the different surface species is not possible.

---

<sup>v</sup> Image plot: the energy scale is reported with respect the time. The intensity is encoded in the color scale, from blue to white.

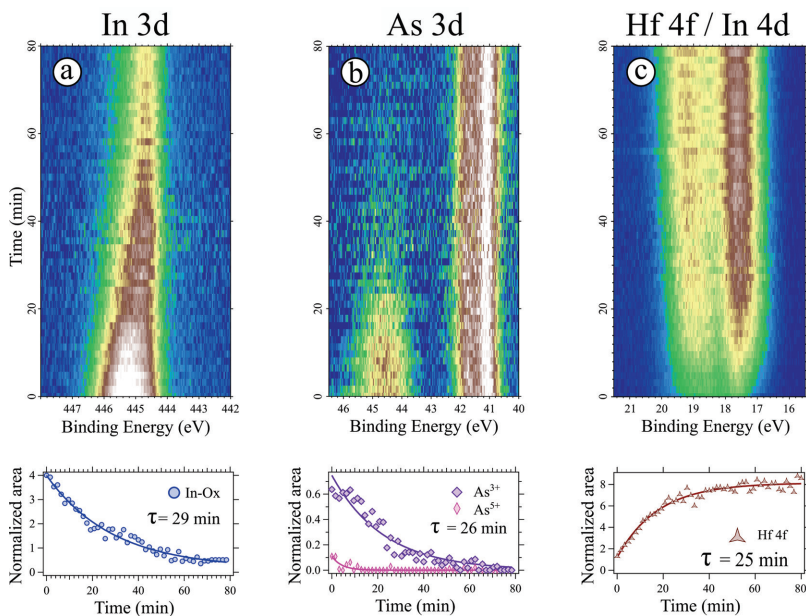


Figure 5.3 InAs oxide removal during the first half-cycle of  $\text{HfO}_2$  ALD on InAs. From left to right (top): APXPS image plot of In 3d, As 3d and Hf 4f/In 4d core-level spectra; (bottom) Intensities evolution for In 3d oxide and As 3d oxide components and the Hf 4f line. Reprinted with permission from ref. 12. Copyright 2020 American Chemical Society.

In order to understand even further the ALD of  $\text{HfO}_2$  on InAs oxide, a systematic study involving the TDMA-Hf interaction with eight InAs samples were performed. Four of the samples were prepared with a thin thermal oxide, which gives the ability to achieve any desired thickness of the oxide layer. In contrast, the remaining four were prepared with a thick native oxide. The different stoichiometry between the two classes of oxide can mainly be found in the possible oxidation states of the As and In atoms. In the thermal oxide, In is only found in In-As and  $\text{In}^{1+}$  state, whereas in the native oxide, an additional small component of  $\text{In}^{3+}$  is also present. Similarly, the As ion are only found in the  $\text{As}^{3+}$  oxidation state in the thermal oxide samples and in the  $\text{As}^{5+}$  state in the native oxide.



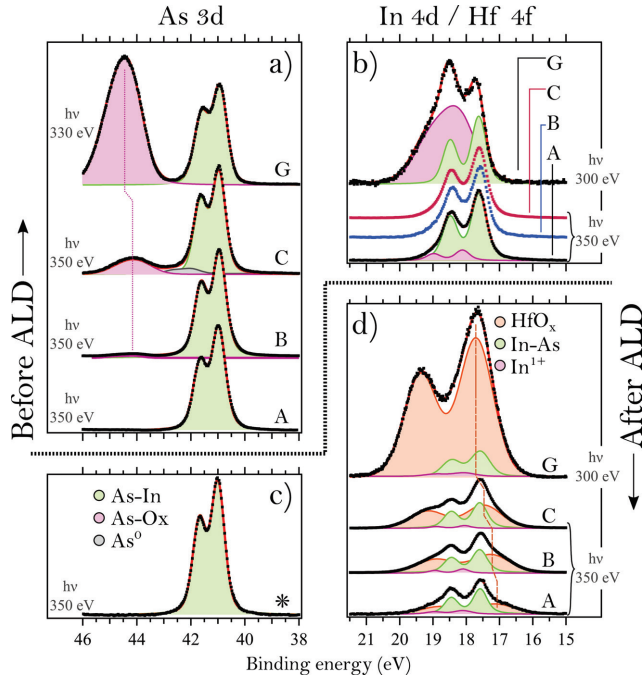


Figure 5.4 Core-level spectra before and after TDMAHf deposition. a) As 3d and b) In 4d spectra of four InAs samples acquired before TDMAHf deposition. The green doublet is associated with As-In, while the broad purple doublet is associated with As/In bonded to O. c) As 3d spectrum of one of the sample acquired after the first ALD half-cycle. Since the spectra of all other samples look like that of the shown sample, only this particular spectrum is shown. d) In 4d and Hf 4f spectra acquired after TDMAHf deposition. Adapted from ref.[13].

The O 1s spectrum of all samples does not show any component related to hydroxyl groups. Once the TDMA-Hf is deposited, a perfect self-cleaning is observed; therefore, the self-cleaning process is valid as it was valid for native oxide samples. In Figure 5.4, the As 3d and In 4d line before (a and b) and after (c and d) the ALD are shown.

However, what is described so far is not the key finding of this experiment. The most important result concerns the thickness of the final  $\text{HfO}_x$  layer. A correlation between the thickness of the oxide layer before the ALD and the  $\text{HfO}_x$  after is found. The results, presented in Figure 5.5, show a linear 1:1 correlation until the  $\text{HfO}_x$  layer reaches a thickness of around 5.6 Å, which is indeed about one monolayer<sup>94</sup> of  $\text{HfO}_2$ . Then, the thickness appears to be constant and independent from the initial oxide of InAs. These results suggest that, on the one hand, the thickness of the first layer of  $\text{HfO}_2$  can be controlled by tuning the thickness of the oxide layer of InAs; on the other hand, they open a new window for a deeper understanding of the ALD chemistry: what happens to the excess oxygen atoms that are not converted to  $\text{HfO}_2$ ? Some authors suggest that As-O dimers can leave the surface in the gas phase<sup>23,95</sup>; however, accepting such an interpretation can raise another question: what triggers the release of As-O to the gas phase? These are at least some of the questions that our results leave for future studies.

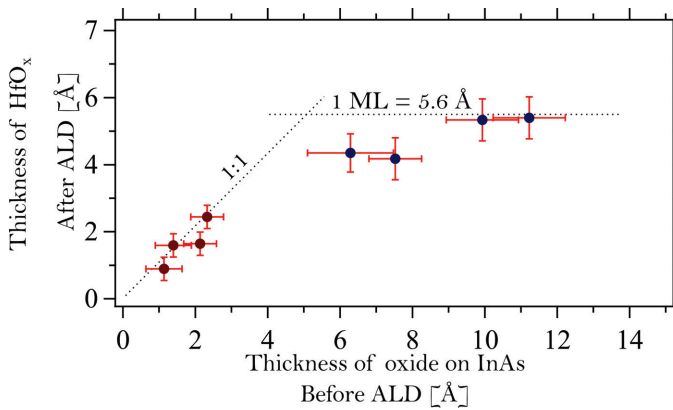


Figure 5.5 Correlation graph between the oxide thickness of InAs prior to the deposition and the thickness of the  $\text{HfO}_x$  layer after the first half-cycle. Adapted from ref.[13].

- $\text{TiO}_2$

The study of ALD of  $\text{HfO}_2$  on  $\text{TiO}_2$  was probably one of the more complicated experiments, followed by the most complicated interpretation I made during my PhD studies. I should not leave out the information that the manuscript about ALD of  $\text{HfO}_2$  on anatase  $\text{TiO}_2$  is the result of about three almost failed beamtimes, conducted at two different beamlines one year after the other. Which suggests that there are no useless or unsuccessful beamtimes. There is always something to understand or, even better, to discover.

I am saying “less expected” because what happened to the surface upon deposition of TDMA-Hf and water was indeed not hypothesized. The manuscript had already covered many interesting aspects of the chemical pathways to trace the formation of new surface species, as shown in Figure 5.2 and described in the previous section.

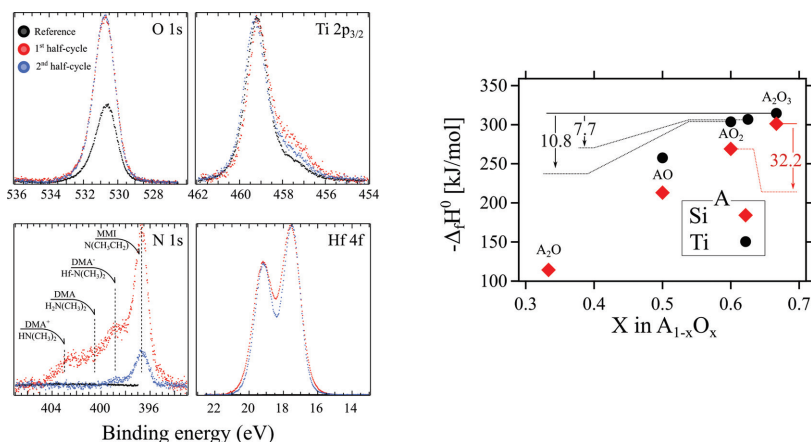


Figure 5.6 (left) O 1s, Ti 2p<sub>3/2</sub>, N 1s and Hf 4f core level spectra acquired before (black), after the first half-cycle (red) and after the second half-cycle. (right) calculated standard heat of formation for Si-O and Ti-O system as a function of O concentration.

However, here I will present new insights into the role of the surface. As already described in the subsection above dedicated to the InAs surfaces, the oxygen atoms of the InAs oxide were preserved before and after the first half-

cycle; in ALD of  $\text{HfO}_2$  on  $\text{TiO}_2$ , the oxygen is pulled out from the  $\text{TiO}_2$  bulk. At first, in Figure 5.6 left, one can notice a reduction in the intensity related to the Ti ions (the Ti  $2p_{3/2}$  core level shows an increase in shoulder intensity associated with  $\text{Ti}^{3+}$ ), and only when all the XP spectra are normalized, one can appreciate the oxygen migration from the stoichiometric  $\text{TiO}_2$  to the metal complex by looking at the increase in intensity of the O 1s core-level. By comparing the results obtained on  $\text{SiO}_2$ , where the atoms on the surface did not contribute the initial reaction, (see later), and the one on  $\text{TiO}_2$ , we address the differences by evoking the enthalpy of formation of the two surfaces as varying the oxygen concentration (c.f. Figure 5.6-right). The gaps in enthalpy between the existing configuration of the Ti-O and Si-O systems are lower in the first case, which suggests that Ti-O can be easily reduced upon ALD. Additional information can be attained from Figure 5.6 right, since one can also infer the energy released by the interaction of TDMA-Hf with the surface to be less than 32 kJ/mol.

- $\text{SiO}_2$

ALD of  $\text{HfO}_2$  on  $\text{SiO}_2$ , presented in Paper V, is the only study supported by DFT calculations. There, the key discovery is that the reaction mechanism involved is bimolecular in nature. The surface is not modified during the

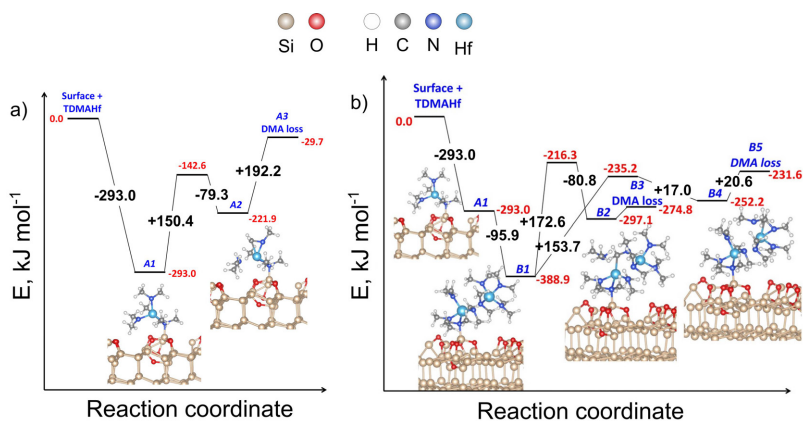


Figure 5.7 a) monomolecular and b) bimolecular pathways of TDMAHf to eliminate a DMA molecule.

reaction, however, it is still hydroxyl-free. The bimolecular nature of the reaction is favourable with respect a unimolecular alternative, as shown in Figure 5.7. The idea is to consider a TDMA-Hf molecule physisorbed, and another metal complex approaching the same site. Then, DMA is released by two possible pathways: i) formation of a bridging bond between the complexes to obtain Hf-C-N-Hf bond (B3 in Figure 5.7 and Figure 5.1-c); this is possible by considering a transfer of an H atom from two DMA<sup>-</sup> ligand of the two physisorbed molecules; ii) intramolecular hydrogen transfer between two DMA<sup>-</sup> of the same metal complex. This leads to the formation of a DMA molecule and a MMI ligand (B5 in Figure 4.9 and Figure 5.1 c). The reactions described here are in line with the reaction paths shown in Figure 5.2.

The obtained results are extremely important, since they expand the pool of ALD models and open several possibilities on metal oxide/surface combinations not “allowed” previously. One of the examples I am interested in, presented in the outlook chapter of the thesis, is the high- $\kappa$  oxide deposition via ALD on graphene, which, as for SiO<sub>2</sub>, does not allow a direct monomolecular reaction<sup>96,97</sup>.

Further consideration should be paid to the ALD of HfO<sub>2</sub> on SiO<sub>2</sub>, since it is part of the most complex analysis done during my PhD. This is reflected in the lengthy supporting information attached to the corresponding article. Once the DFT results suggested that the reaction was indeed bimolecular in nature, its validity needed to be verified experimentally. The main idea was to compare the experimental ratio between the N 1s and Hf 4f core level intensities and check if the expected ratio of 4 was indeed correct. Unfortunately, comparing intensities in XPS can vary in complexity depending on how deep your analysis must be. In this particular experiment, a ratio of 3.0 would suggest a chemisorption process, while a ratio of 4.0 physisorption. With this in mind, it was imperative to consider all the possible variables that can affect the intensities, including experimental values derived from the setup and theoretical values, which are typically

assumed to be constant for photoemission from the different core levels (as explained in chapter 3). Something at which I cudgelled my brains for a while was the internal electron attenuation of the atoms in a single complex. From the geometry of a single TDMA-Hf molecules, I derive the attenuation length for the Hf ion and the other atoms in the ligand; the results, which can be found in the SI of Paper V, are also summarized here in table 5.1.

It is fascinating to see that when the complex is chemisorbed, our calculation shows that the internal scattering is close to 1 (no attenuation). In contrast, for gas-phase molecules, is around 0.86.

	<i>TDMAHf</i>	<i>Hf(N(CH<sub>3</sub>)<sub>2</sub>)<sub>3</sub>OH</i>	<i>Surface-bonded Hf(N(CH<sub>3</sub>)<sub>2</sub>)<sub>2</sub></i>	<i>DMA</i>
$C_{Hf}$	0.792	0.807	0.792	//
$C_N$	0.678	0.703	0.745	0.795
$C_N/C_{Hf}$	0.856	0.871	0.941	//

Table 5.1 Correction factor describing the internal attenuation of the photoelectrons in different photomitting complexes.

- **Si(111)**

To conclude the series of ALD of HfO<sub>2</sub> on different surfaces, I will now discuss the ALD of HfO<sub>2</sub> on the Si(111) surface, using the same TDMA-Hf and water precursors as in the other experiments that I have discussed.

Out of the pool of the experiments discussed in this dissertation, the ALD of HfO<sub>2</sub> on Si(111) can be defined as the “least exciting”, not entailing any complexity regarding new chemistry or reaction mechanisms. A Si wafer was prepared in order to obtain a clean Si(111), with the well-known 7x7 reconstruction. However, moisture contamination influences the surface chemistry very significantly. Indeed, it was found that the Si(111) surface that had been cleaned by flash-annealing was largely hydroxylated by

reaction with residual water vapour in the experimental chamber (the hydroxyl coverage was estimated to be around 0.3 ML). This observation, whilst disappointing, triggers a reflection. The vacuum system used at the TEMPO beamline, where the experiment took place, consists of a series of turbomolecular and rough vacuum pumps, which allow achieving pressure lower than 10<sup>-8</sup> mbar. The vacuum is much better than the one used in most of ALD reactors, by several orders of magnitude. Therefore, it is fair to say that even if the Si(111) surface in the experiment was not precisely clean from a surface science perspective, it could be considered clean for ALD purposes.

It is found that the hydroxyl formed by the moisture contamination triggers the interaction of the TDMAHf with the surface, by means of the ligands exchange reaction mechanism. The chemisorption, however, appears to be preceded by a physisorption step, as observed and described in the ALD of HfO<sub>2</sub> on InAs. Interestingly, however, unlike in the other experiments, no side reactions or other reaction mechanisms were observed. Indeed, the MMI, which is found when intra- or inter-molecular reaction is considered, only appears as a minor component in the N 1s core-level spectra. Evidence of water contamination is also visible from the mismatch of the DMA-intensity in the N 1s core-level spectrum acquired after the first half-cycle, and before the water half-cycle. The intensity dropped by almost 50%.

Whilst not particularly appealing from a chemistry per se, this experiment is the closest to a real ALD reactor we, as a group, ever performed. It shows how moisture and residual vapours can highly influence the ALD chemistry in the environment where the ALD is performed.

### 5.3 Convolution of reaction mechanisms

In Paper II, ALD of HfO<sub>2</sub> on a thermally oxidised InAs is performed with APXPS in time-resolved mode. During the experiment, we were also able to obtain data from the second half-cycle, performed with water at a pressure of 10<sup>-1</sup> mbar.

The surface species were identified, and their nature and formation were already discussed in section 5.1. Here, I will mainly examine the second half-cycle. The second half-cycle of ALD follows a reaction as shown in the equation 5.2. However, if this was the reaction that correctly described the water interaction with the surface, one should expect to see a reduction of the surface species with the same rate of the formation of hydroxyl groups. It can be seen that for every water molecule reaching the surface, a DMA ligand will leave into the gas phase once protonated, and the -OH will bond to the metal ion



Above,  $n$  is the number of retained ligands per Hf ion, which is less than 4,  $L$  is the DMA ligand of the metal amido complex, and  $m$  is the number of interacting water molecules.

However, if one analyzes just the *in vacuum* spectra, in principle, one could state that the ligand exchange model is the right reaction mechanism that describes the second half-cycle of ALD of HfO<sub>2</sub> on InAs, since, as visible from Figure 5.8 a,b and c, the hydroxyls are formed, and the surface species are almost completely removed. Only when time-resolved APXPS is employed, the actual evolution of the reduction of the surface species and the formation of hydroxyl can be seen in “real time”. In Figure 5.8 e, the intensity of the N 1s and C 1s core levels is shown as a function of exposure time. The red line indicates the opening time of the water valve. Clearly, the reduction is efficient and almost immediate to the opening of the water valve. However, in the same Figure (d), the concentration of the hydroxyls evaluated from the O 1s spectrum shows a different behavior: the hydroxyl



component starts to increase in intensity as soon as the water valve is opened, but its formation is definitely slower.

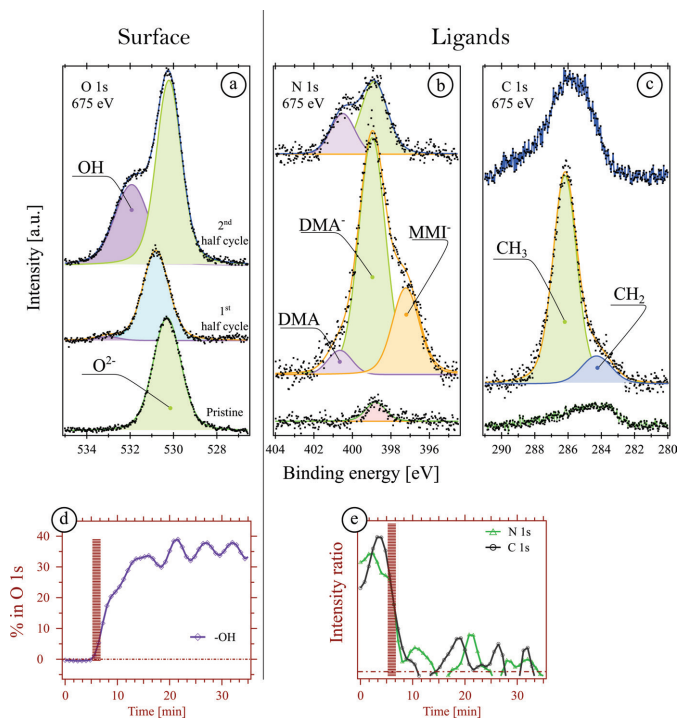
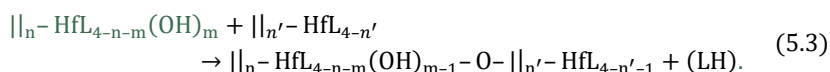


Figure 5.8 O 1s (a), N 1s (b) and C 1s (c) core level XP spectra acquired before the first half-cycle (bottom-green fit), after the first half-cycle (middle-orange fit) and after the water half-cycle (top-blue fit), of ALD of  $\text{HfO}_2$  on InAs thermal oxide. d) Time evolution of intensity of hydroxyl group visible in the O 1s. e) Time evolution of the intensities of the N 1s and C 1s lines, fingerprints of the surface species.

I believe that the water half-cycle must be described by more than one process: i) ligand exchange model, and ii) hydrogen insertion. The chemical equation describing i) is shown in equation 5.2, while in the following, the hydrogen insertion follows:



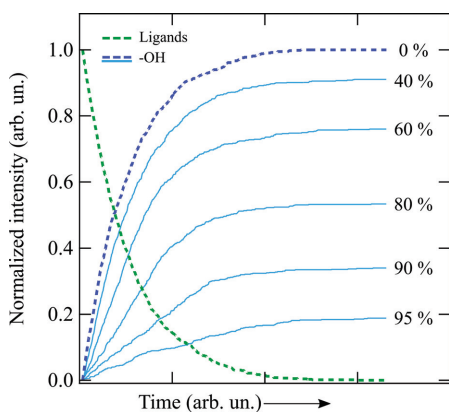


Figure 5.9 Simulated time evolution of surface ligand reduction (green) and -OH formation (blue).

To clarify, the green part of equation 5.2 and equation 5.3 are the same since the reaction expression in equation 5.3 follows the ligand exchange one (equation 5.2). A simulated model of reactions 5.3 and 5.2 is shown in Figure 5.9. The dotted lines represent the reduction of the nitrogen surface species (green) and the hydroxyl groups (blue) formation if only equation 5.2 is taken into account. Increasing the probability of reaction 5.3 (light blue in Figure 5.9), the hydroxyl formation is slower, as shown in the blue lines associated to each probability. Clearly, if the chemical reaction happens all the time after the ligand exchange mechanism, no hydroxyls will be present on the surface.

## 5.4 Consideration on APXPS for ALD experiments

*In situ* and *operando* APXPS, combined with *in vacuum* XPS, has proven to be extremely valuable for the study of ALD. It should be clear now that time-resolved data provide access to the fundamental nature of ALD, which otherwise can appear more straightforward than what it actually is.

In this section, I would like to cover another important aspect related to ALD experiments, not directly linked to the chemistry and the physics

involved, but, rather, related to the experimental setup. Can the reactors themselves modify the ALD layers and the growth mechanism?

During my doctoral years, I tried four ALD setups. One was a “real” ALD reactor, while the others were setups made to perform ALD *in situ* at the beamline. I refer to HIPPIE, SPECIES and TEMPO. The main question is: do different reactors produce different ALD layers, even if the parameters used are the same? In other words: is the chemistry influenced by the setup on where the ALD layer is grown? My hypothesis is, to some extent, yes, it is. I am not talking about completely different chemistry, but some detail in the reaction mechanism can be induced by the type of setup in use.

I believe that the length of the pipe, numbers of inlets and directions of them, the type of valve, the quality of vacuum, as well as the temperature of the pipe and the cylinders containing the precursors, and the volume of cell, are all essential parameters. These, of course, are parameters that I started to appreciate after several ALD beamtimes, and I began to realize only recently that they may play a crucial role. For example, the HIPPIE beamline, even with pipe of the same length of those at SPECIES, is equipped with only one inlet, which can cause a intermix of precursors in the gas line, and consequently ALD on the pipe itself. Or, another example, at TEMPO, where we saw broken precursors, and we determine that they can affect the ALD reactions (see SI of Paper V). There is also another import question that needs an answer: how “clean” are the real ALD reactors used in industry? And what about the sample’s preparation? These are some of the questions that with Dr Esko Kokkonen, others and I will try to answer in an upcoming beamtime.

Another comment regarding the ALD setups is based on the influence of the valves used during the ALD process. We recently tried to perform an experiment at TEMPO, which is equipped with a leak valve between the gas line and the analysis chamber. We followed the instructions about the temperature of the precursor, but we did not detect any of it on the surface. Most likely, the small leak in the leak valve prevented the correct flow of

precursor towards the surface. Indeed, at SPECIES beamline, that is equipped with a leak valve, we noticed that the vapour pressure of TDMA-Hf, with the gas line fully open, was about  $10^{-2}$  mbar, which is 2 orders of magnitude lower than that predicted by Hausmann et al<sup>98</sup>.

Therefore, it seems important to emphasize that, besides the nature of the experiment, it is also central to consider experimental factors that may sometimes appear obvious, or are taken for granted. This will lead to a more systematic approach to do science, with the final goal of reproducible and consistent results. Talking about reproducibility, I recently find myself reading about a survey conducted to over 1500 researchers<sup>99,100</sup>. It was asked their opinion about reproducibility of results, and it was quite surprising to read that more than 70 % have experienced that they failed to reproduce an experiment of someone else, and more than 50 % have experience of failing in reproducing one of their own experiments. The reasons behind the failure to reproduce experiments are manifold; among those that are serious are selective reporting, pressure to publish, and low statistical power and poor analysis. During my PhD I have learnt a lot about data analysis, which I consider very important. An analysis can almost always be done at different levels of complexity. My idea is to start simple and then, if necessary, increase the level of complexity step by step. Without being biased on what you want to find, build an idea of what the data is telling you.

## 5.5 Adsorption of ethanol on rutile TiO<sub>2</sub>(110)

Along with all the ALD based experiments just presented, there is also another *in situ* APXPS based investigation that I would like to discuss. It is based on the adsorption of ethanol (C<sub>2</sub>H<sub>5</sub>OH, EtOH) on a rutile TiO<sub>2</sub> surface. The aim is to verify whether the DFT calculations obtained so far agree with the experiments carried out at room temperature and ambient pressure conditions. Adsorption of ethanol is important in ALD since it can be used as an oxygen precursor<sup>101,102</sup>, as in the ALD of Al<sub>2</sub>O<sub>3</sub>, or as a model

system when  $M[\text{OC}(\text{CH}_3)_3]_4$  and M(IV) butoxide  $[\text{M}(\text{OC}_4\text{H}_9)_4]$  are used as metal (M) precursors in ALD<sup>103,104</sup>.

Some DFT suggests that dissociative adsorption of ethanol on the rutile  $\text{TiO}_2(110)$  surface is slightly more favourable than molecular adsorption at room temperature; some others, claim the reverse. However, the uncertainty of the DFT calculations with functional (B3LYP) report about  $\pm 0.18 \text{ eV}$ <sup>105</sup> suggested that error can be made for energies close to each other. Therefore, we did an experimental study that aims at elucidating whether dissociative or molecular adsorption is more favourable.

Using the O 1s spectral intensity assigned to molecular ethanol and ethoxy, the surface coverage of these species was estimated. Then, a calculation based on the distribution of Boltzmann, as reported here:

$$\frac{N_x}{N_y} \propto e^{-\frac{\Delta E}{k_b T}} \quad (5.4)$$

where  $N$  is the number of species  $x$  and  $y$ ,  $k_b$  is the Boltzmann constant and  $T$  the temperature, allows to find the difference in adsorption energy  $\Delta E$  to be between 0.02 and 0.04 eV, which are energies far from the theoretical one established by DFT.



# 6 Other related research

This chapter deals with topics apparently unrelated to this thesis. Perhaps, it could be read as a final appendix to it. The motivation of this final endeavour lies in the fact that, during these four years and (almost) a half, I have contributed to several other projects<sup>47,79,106–108</sup> besides mine, and some of them really took my interest. Thus, I aim to do this unrelated work justice by discussing it on the following pages.

I will not indulge in deep discussions on those research papers. Rather, I will try to provide at least a brief discussion of the methods, the results, and the motivation. Each of the subsequent sections is dedicated to a paper and the title of the sections indicates what I appreciated the most during those experiments and discussions. The motivation for the this chapter, however, will appear clear in the next one!

## 6.1 Fast process, smart setup I

Understanding how the catalyst structure and the catalyst composition influence heterogeneous catalysis is a key challenge that needs extreme caution to elaborate since pressure and temperature can strongly influence a system's dynamics. In this project, a new event-averaging-based method<sup>47</sup> employing time-resolved ambient pressure photoelectron spectroscopy to answer some of the questions around heterogeneous catalysis, was developed. The catalyst structure and local gas environment was mapped simultaneously, while reaction conditions were changed rapidly during an experiment conducted at the HIPPIE beamline<sup>79</sup>.

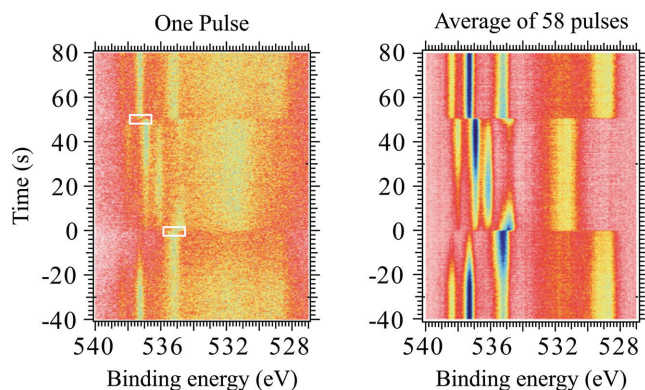


Figure 6.1 Image plots of O 1s before (left) and after (right) event-averaging. The white boxes on the left image plot are the events used to characterised the periodicity of the transitions. Adapted from ref. [47].

The method is based on an event averaging technique, which consists of averaging a periodic event. When adopting this method, it is essential to define the transition event. Such an event can be anything and, in our paper, we used the work function change which affect the binding energy position of the gas-phase peaks, measured with APXPS. We co-dosed CO and O<sub>2</sub> at different ratios 58 times onto a Pd(110) surface, and therefore we ended up with a single, extremely noisy, APXPS image plot. Then, an algorithm searches for the spectroscopic fingerprint chosen as event signal and determines the exact absolute time of each. Once all the changes are found, the averaging process can take place. Since the signal is directly proportional to  $N$ , where  $N$  is the number of events, and the noise is inversely proportional to the square root of  $N$ , the signal-to-noise ratio will improve by a factor  $\sqrt{N}$ . In Figure 6.1, the O 1s image plot of the time-resolved experiment before and after event-averaging 58 pulses is reported. Clearly, the image plot on the left does not allow any in-depth analysis, whereas the one on the right does. In the present case, the signal to noise ratio improved by a factor of almost 8.

Interesting about this approach is the time resolution that can be achieved. In principle, using the fixed mode of the electron energy analyser



(see chapter 3), the time resolution is limited only by the software and the camera's frame rate; therefore, ideally, upgrading the camera used should substantially increase the time resolution. As a drawback, it is essential that the non-averaged signal has a decent level of signal-to-noise ratio to be able to capture the event.

## 6.2 Fast(er) process, smart setup II

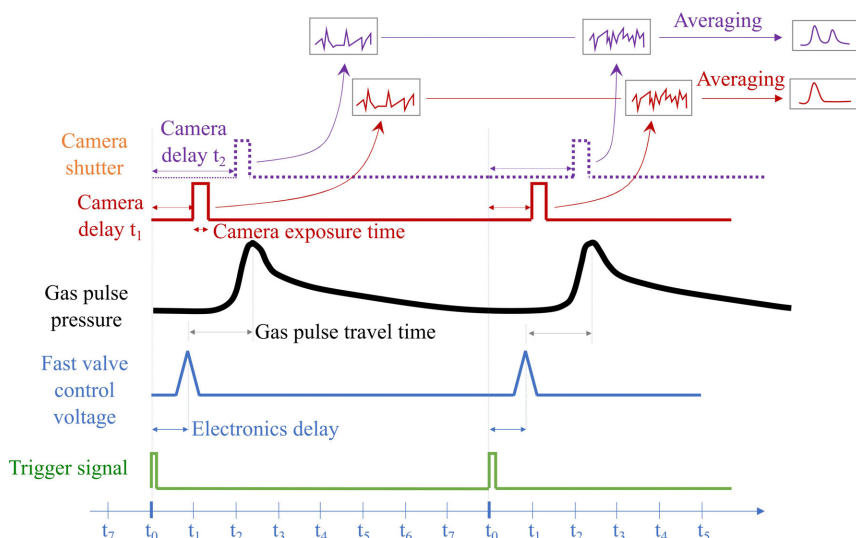


Figure 6.2 Time diagram for the time resolved APXPS. In green, the trigger signal, in blue, the voltages needed for the piezo valve delayed from the trigger signal. In black, the actual pressure of gas. In red and purple, the camera shutter from two delay times.

Reprinted with permission from ref. 109. Copyright 20201 American Chemical Society.

Here is another great experiment<sup>109</sup> in which I took part at HIPPIE. The motivation of this work overlaps with the previous one, but the focus was on testing a new APXPS setup capable of following structure and activity dynamics with  $20 \mu\text{s}$  time-resolution. A fast gas pulse with internal mbar pressure is generated by a piezo valve triggered by a signal/delay generator. The camera of the electron energy analyser is then synchronized to the valve's

trigger, and the exposure is defined by the frame rate of the camera used. Then, the delay between the trigger of the valve and the camera's shutter becomes the tuneable variable of the experiment. By periodically triggering the valve and slowly changing the time delay between the trigger and the camera's exposure time, and after an averaging process, incredibly fast XPS spectra can be obtained.

The similarities between the experiment described in section 6.1 and this one are several; however, differences can be found. Table 6.1 shows the main difference in terms of several aspects, including the need for extra hardware or software to use the methods.

	<b>Time resolution</b>	<b>Extra hardware</b>	<b>Dedicated software</b>	<b>Seed needed</b>
<b>Stroboscopic effect</b>	Up to 10 <i>ms</i>	No	Yes	Yes
<b>Pump and prob</b>	Tens of $\mu$ s	Yes	Yes	No

Table 6.1 Main differences between the two developed approaches to acquire time resolved APXPS data.

## 6.3 Graphene vs. hBN

The superlative properties of graphene are beyond the scope of this chapter; therefore, this paragraph takes them for granted. In this work<sup>106</sup>, graphene was compared to another two-dimensional (2D) material, hexagonal boron nitride (hBN), in the context of anti-corrosion coating. Before going into details, I would like to briefly clarify what a 2D material is.

As the reader may suspect, 2D materials are materials that can be described by only using two dimensions; essentially, they have the thickness of one single atom. They have exerted great attention in the scientific

community due to their peculiar structure and magnificent properties compared to similar 3D materials<sup>w</sup>.

The properties of graphene and hBN differ significantly in terms of electronic properties. The first is a conductor, and given its peculiarity of having the Dirac cone, it has a theoretical infinity electronic mobility<sup>110</sup>. hBN, on the other hand, is an insulator<sup>111</sup>. However, they both have similar properties regarding permeability and reaction to gases and liquids: both, and like all the other 2D materials, are involved in many chemicals and find application in the anticorrosive coating<sup>112,113</sup>.

Doctor and friend Mattia Scardamaglia, first author of this research paper, with the other authors of this work, exposed three samples to O<sub>2</sub> while linearly ramping up the temperature: a bare copper, one protected with a graphene (Gr) layer, and one with hBN. Copper under oxygen exposure follows a well-known oxidation process: i) dissociative adsorption of O<sub>2</sub>, followed by ii) formation of a Cu<sub>2</sub>O layer, ending with iii) the formation of CuO islands<sup>114,115</sup>. We were interested in understanding how these steps could be influenced by the presence of graphene and hBN deposited on the surface of copper metal. We employed APXPS in real time and followed the oxidation steps of Cu samples without and with Gr/h-BN coatings.

We demonstrated that both 2D materials work rather well for protecting the Cu metal sample by retarding the formation of the Cu<sub>2</sub>O layer to temperatures higher than 120 °C. The interesting aspect and novelty of this work regards the understanding of these protections' kinetics. The hBN/Cu sample is simple to explain: the Cu is protected until the hBN is intact, which happens until around 300 °C; then, the hot Cu is directly exposed to O<sub>2</sub>, and the steps i, ii and iii rapidly occur. Concerning the Gr/Cu sample, the

---

<sup>w</sup> A small note about 2D material: theoreticians were sceptical about the nature of 2D material, since, in 1968, Nathaniel David Mermin, Herbert Wagner, and Pierre Hohenberg stated, by means a theorem titled after them, that 2D crystals could not exist. However, 2D materials exist and graphene, since its first synthesis in 2004, really confused all theoreticians' panorama. The reason why graphene, as well as all other 2D materials exists, and "breaks" the Mermin-Wagner-Hohenberg theorem, is because it uses the third dimension to corrugate.

oxidation of Cu started before the etching of the Gr. This happens due to the interaction of oxygen beneath the Gr flakes, and undercover oxidation occurs (223 °C). Then, when the Gr is etched away, the Cu<sub>2</sub>O layer rapidly allows the formation of CuO islands (306 °C).

# 7 Outlook

It is said that a research is good when it brings about more new questions than answers. While the previous pages have focused on what I have found in my doctoral work, this chapter intends to focus precisely on what is yet to be found, what questions I could raise thanks to what has been accomplished so far, thereby setting a track for future research. Thus, I will try to have an outlook on what I think can be done next.

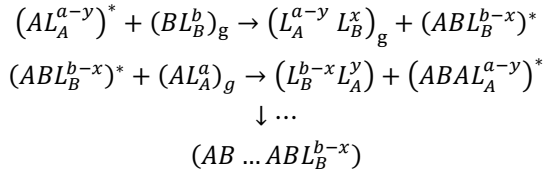
ALD has proven to be an excellent deposition technique all over the different fields of application, and with exponential growth in terms of interest from both the scientific and industrial community. However, even if I hope to have added a small contribution to the understanding of the ALD with this thesis, several open questions still need to be solved. Answers to them hopefully will lead to a complete picture of the reaction mechanism, kinetics, surface species, and dependence of experimental parameters of ALD.

This ambitious goal calls for adopting new solutions to investigate ALD reactions. During my years at Lund University, I have had several contacts with brilliant scientists who developed new techniques to study catalysis problems. In the following sections, these new techniques and results, already introduced in chapter VI, will be discussed for future implementation on experiments involving ALD.

## 7.1 Steady state during ALD

The event averaging technique developed by my supervisor Jan Knudsen appear relevant for ALD studies. If this thesis covered the first few cycles of ALD, where I demonstrate the high impact of the surface on the reaction mechanism, this first outlook would explain how the stroboscopic method can be implemented to understand the steady-state of ALD. A steady-state, in ALD experiments, is achieved when the deposited layer is completely decoupled from the surface where it is grown. And the changes in the system are periodic within an entire ALD cycle.

Let's consider two ALD precursors, Alice and Bob, interacting with a suitable surface, always in a sequential way. After several cycles, the surface will not affect the reaction mechanism anymore, and their nature will only drive the interaction between Alice and Bob with the support.



In the equations above,  $A$  and  $B$  are the ions of the precursors,  $L_{A,B}$  the ligands of  $A$  and  $B$ ,  $a$  and  $b$  indicate the number of ligands for Alice and Bob, respectively,  $x$  and  $y$  indicate the number of ligands lost during the ALD process,  $*$  and the subscript  $g$  indicate if the complex is on the surface or in the gas phase, respectively. The reactions shown here are assumed to follow the ligand exchange reaction mechanism.

Let us imagine, now, to perform  $2N$  half-cycles, as a final goal of achieving  $N$  layers of AB material. Ideally, each second half-reaction will look identical, and the stroboscopic operando APXPS technique appears perfect for this type of system. While collecting the data, in time-resolved with the higher acquisition rate available, Alice and Bob's core level spectrum will appear with a low signal-to-noise ratio. However, assuming that the  $2N$  pulse follows an almost periodic behaviour, the signal to noise ratio can

drastically increase. As explained before, the signal to noise ratio will be improved by a factor  $\sqrt{N}$ .

From a technical point of view, and from previous experience on performing ALD experiments, performing more than a couple of cycles in a single beamtime is already a challenge. However, by warming all the gas lines and using a bubbler or a unique design gas delivery system, it is in principle feasible to perform 10/15 cycles for each core level of interest during the same beamtime.

By using a camera of 120 Hz, an incredible time resolution of 8 ms is achievable. New details will certainly be elucidated. My interest would be to use this method on the ALD of  $\text{HfO}_2$ , using TDMA-Hf and water, since I could only perform two complete cycles of ALD during my PhD. I am curious to check if the mechanism involved will follow the ligand exchange reaction or something else. As already observed in Paper II, I hypothesise that the reactions involved in the half-cycles are more than one, and what we could observe is actually a convolution of them.

A step forwards can be made by implementing the methods explained in chapter VI, section II, to increase further the time resolution, from *ms* to  $\mu\text{s}$ , so to mimic the real ALD reactor used in industry.

## 7.2 Graphene and ALD

This last section moves out from the experimental technique and introduces a variation of ALD, called photo-assisted ALD. The reason will be clarified soon, but a small introduction to motivate this outlook is needed.

To use the outstanding properties of graphene in modern devices, such as optical and electronic devices, it is sometimes necessary to couple the graphene with a dielectric thin film. During the work on this thesis, a particular emphasis was posed on the excellent properties of ALD on deposition thin film with high quality, conformity, and control over the

deposited layer's thickness. However, graphene is a two-dimensional material, with strong  $\sigma$  bonds in the plane and a weak  $\pi$  bonds out of the plane. This, whilst securing a great electron mobility, does not allow the direct deposition of materials via ALD, since no active sites can be used<sup>97</sup>. Other deposition techniques, such as PVD, sputtering, e-beam evaporation, can quickly damage or, in the worst-case scenario, even destroy the graphene layer. This thesis showed that ALD of the dielectric film is typically made using metal-amido complexes and water as precursors; however, the precursor needs an active site to initiate the reaction. Active sites can be found in the intrinsic defects site of graphene, including single and multiple vacancies, Stone-Wales defects, and out of plain carbon atoms. However, using defective sites as an active site for ALD leads to a non-uniformity of the ALD overlayer, limiting the device performance.

Several aspects were considered to deposition dielectric film on the graphene layer during the years. The most successful one adopted the sacrificial layer, or functionalisation of the graphene by forming a so-called graphene oxide layer. However, both these approaches are time-consuming and still far from being ideal.

An approach yet to be tested would be to use photo-assisted ALD<sup>116</sup> for the first few half-cycles, followed, if necessary, by thermal ALD. Photo-assisted ALD uses UV light to supply energy to the surface reaction. The rising development of photo ALD precursors allows the deposition of several transition metal oxide layers, which will enable the deposition of materials with desired properties. For example,  $\text{HfO}_2$  can be grown using Hf-t-butoxide  $\text{Hf}[\text{OC}(\text{CH}_3)_3]_4$  and  $\text{TiO}_2$  using a similar precursor with Ti ions instead of Hf.

Ideally, the exposure of these precursors to a graphene layer will lead to a uniform physisorbed molecular layer, which will start forming  $\text{HfO}_2$  once the precursors split out their ligands when irradiated to UV light, with no need to heat the surface. Moreover, even if a water pulse is required, as discussed in chapter 6.3, graphene can hold oxidation and hold to



temperatures up to 220 °C, guaranteeing a safe ALD without breaking the graphene layer.



## 8 Concluding remarks

It has been a long journey, and I hope this thesis has been as light and precise as I would have liked. Throughout the different chapters, we have seen how x-ray spectroscopy is a characterisation technique that, while seeming simple, has various nuances of complexity that can only be appreciated if it is fully understood. Like the technique itself, the results can also be seen and observed with varying levels of complexity and allow for excellent results. These results, shown in chapter V, exhibit how this deposition technique is much more complicated than I, at least, could have imagined. I think it is part of the deal you make when you decide to do research and find the unexpected in what is considered trivial. With ALD of  $\text{HfO}_2$  on InAs, we have seen how even the surface plays a fundamental role during growth, providing oxygen to obtain a single layer of  $\text{HfO}_2$  already from the first half cycle. Similar is what happens during the deposition of  $\text{HfO}_2$  on  $\text{TiO}_2$ .

Even more complex than expected, the surface species can only be justified if the surface itself, and the interaction between several molecules, is taken into consideration. Indeed, even with DFT support, we found evidence of a bimolecular reaction in nature, which is favourable to the unimolecular one predicted by the different models used to describe ALD. We have also seen that, when a known preconception is eliminated, based on the fact that the surfaces in which ALD is performed are hydroxylated, new paths and new types of reactions can be opened.

Another aspect comes from the possibility of obtaining these results while the reactions take place, through *in situ* and *operando* APXPS. HIPPIE and SPECIES beamline, at MAX IV, and TEMPO at SOLEIL, are excellent beamlines that allow such experiments, without which it would have been

impossible to demonstrate that it is necessary to lengthen the dosage times. In fact, we have seen how the reduction of InAs oxide is closely correlated with the formation of Hf oxide, or how exposure of the co-reactant leads to the formation of a uniform layer of hydroxyl only after all surface species are been eliminated.

There are still many open questions, and many curiosities yet to be found and some of these will answered as explained in the previous chapter.

In conclusion, ALD proved to be a deposition technique that allows the growth of uniform layers on almost any type of surface, even when "theoretically" this should not be assumed. At the same time, it has shown a level of complexity that requires multidisciplinary knowledge, from the physics of matter to organic and non-organic chemistry, which if well weighed, allows a detailed description of the ALD process/reaction mechanism.

## 9 References

1. Dombey, N. The Nobel Prize in Physics. *Nature* vol. 300 106–107 [http://www.nobelprize.org/nobel\\_prizes/physics/laureates/1956/](http://www.nobelprize.org/nobel_prizes/physics/laureates/1956/) (1982).
2. Gutierrez-Aitken, A. High-Speed InP-Based Heterojunction Bipolar Transistors. *Compr. Semicond. Sci. Technol.* **1–6**, 114–175 (2011).
3. Riordan, M. The lost history of the transistor. *IEEE Spectr.* **41**, 44–49 (2003).
4. Dawon, K. Electric field controlled semiconductor device. *U.S. Patent 3102230 4* (1963).
5. Handy, J. How Many Transistors Have Ever Shipped? *Forbes.com* <http://www.forbes.com/sites/jimhandy/2014/05/26/how-many-transistors-have-ever-shipped/> (2014).
6. Moore, G. M. Cramming more components onto integrated circuits With unit cost. *Electronics* **38**, 114 (1965).
7. Wilk, G. D., Wallace, R. M. & Anthony, J. M. High- $\kappa$  gate dielectrics: Current status and materials properties considerations. *J. Appl. Phys.* **89**, 5243–5275 (2001).
8. Than, O. R. E. & Paper, H. International Roadmap for Devices and Systems - More than Moore - IRDS. *Ieee* 1–41 <https://irds.ieee.org/editions/2020> (2020).
9. Zaera, F. Mechanisms of surface reactions in thin solid film chemical deposition processes. *Coord. Chem. Rev.* **257**, 3177–3191 (2013).
10. Raiford, J. A., Oyakhire, S. T. & Bent, S. F. Applications of atomic layer deposition and chemical vapor deposition for perovskite solar cells. *Energy Environ. Sci.* **13**, 1997–2023 (2020).
11. Johnson, R. W., Hultqvist, A. & Bent, S. F. A brief review of atomic layer deposition: From fundamentals to applications. *Mater. Today* **17**, 236–246 (2014).

12. D'Acunto, G. *et al.* Atomic Layer Deposition of Hafnium Oxide on InAs: Insight from Time-Resolved in Situ Studies. *ACS Appl. Electron. Mater.* **2**, 3915–3922 (2020).
13. D'Acunto, G. *et al.* Oxygen relocation during HfO<sub>2</sub> ALD on InAs. *Faraday Discuss.*, *in press* (2022) doi:10.1039/d1fd00116g.
14. Timm, R. *et al.* Self-cleaning and surface chemical reactions during hafnium dioxide atomic layer deposition on indium arsenide. *Nat. Commun.* **9**, 1–9 (2018).
15. Timm, R. *et al.* Reduction of native oxides on InAs by atomic layer deposited Al<sub>2</sub>O<sub>3</sub> and HfO<sub>2</sub>. *Appl. Phys. Lett.* **97**, 2008–2011 (2010).
16. Troian, A. *et al.* InAs-oxide interface composition and stability upon thermal oxidation and high-k atomic layer deposition. *AIP Adv.* **8**, 125227 (2018).
17. Kirk, A. P., Milojevic, M., Kim, J. & Wallace, R. M. An in situ examination of atomic layer deposited alumina/InAs(100) interfaces. *Appl. Phys. Lett.* **96**, 2008–2011 (2010).
18. Del Alamo, J. A. Nanometre-scale electronics with III-V compound semiconductors. *Nature* **479**, 317–323 (2011).
19. Ko, H. *et al.* Ultrathin compound semiconductor on insulator layers for high-performance nanoscale transistors. *Nature* **468**, 286–289 (2010).
20. Johansson, S., Memisevic, E., Wernersson, L. E. & Lind, E. High-frequency gate-all-around vertical InAs nanowire MOSFETs on Si substrates. *IEEE Electron Device Lett.* **35**, 518–520 (2014).
21. Hasegawa, H. & Akazawa, M. Interface models and processing technologies for surface passivation and interface control in III-V semiconductor nanoelectronics. *Appl. Surf. Sci.* **254**, 8005–8015 (2008).
22. Houssa, M., Chagarov, E. & Kummel, A. Surface defects and passivation of Ge and III-V interfaces. *MRS Bull.* **34**, 504–513 (2009).
23. Chang, C. H. *et al.* Interfacial self-cleaning in atomic layer deposition of HfO<sub>2</sub> gate dielectric on In<sub>0.15</sub>Ga<sub>0.85</sub>As. *Appl. Phys. Lett.* **89**, 2–5 (2006).
24. Ahvenniemi, E. *et al.* Review Article: Recommended reading list of early publications on atomic layer deposition—Outcome of the “Virtual Project on the History of ALD”. *J. Vac. Sci. Technol. A* **35**, 010801 (2017).
25. Suntola, T. & Antson, J. United States Patent (19). *Geothermics* vol. 14

- 595–599 (1977).
26. Puurunen, R. L. A short history of atomic layer deposition: Tuomo Suntola's atomic layer epitaxy. *Chem. Vap. Depos.* **20**, 332–344 (2014).
  27. Leskelä, M. & Ritala, M. Atomic layer deposition (ALD): From precursors to thin film structures. *Thin Solid Films* **409**, 138–146 (2002).
  28. Asundi, A. S., Raiford, J. A. & Bent, S. F. Opportunities for atomic layer deposition in emerging energy technologies. *ACS Energy Lett.* **4**, 908–925 (2019).
  29. Miikkulainen, V., Leskelä, M., Ritala, M. & Puurunen, R. L. Crystallinity of inorganic films grown by atomic layer deposition: Overview and general trends. *J. Appl. Phys.* **113**, (2013).
  30. Randich, E. & Gerlach, T. M. Chemical vapor deposition. *Bull. Alloy Phase Diagrams* **3**, 140 (1982).
  31. Mittal, M., Sardar, S. & Jana, A. Nanofabrication techniques for semiconductor chemical sensors. *Handb. Nanomater. Sens. Appl.* 119–137 (2021) doi:10.1016/b978-0-12-820783-3.00023-3.
  32. Deposition Technologies: An Overview. *Handb. Depos. Technol. Film. Coatings* 1–31 (2010) doi:10.1016/B978-0-8155-2031-3.00001-6.
  33. Pottathara, Y. B., Grohens, Y., Kokol, V., Kalarikkal, N. & Thomas, S. Synthesis and processing of emerging two-dimensional nanomaterials. *Nanomater. Synth. Des. Fabr. Appl.* 1–25 (2019) doi:10.1016/B978-0-12-815751-0.00001-8.
  34. Meng, X. An overview of molecular layer deposition for organic and organic-inorganic hybrid materials: Mechanisms, growth characteristics, and promising applications. *J. Mater. Chem. A* **5**, 18326–18378 (2017).
  35. Meng, X. & Elam, J. W. (Invited) Atomic Layer Deposition of Nanophase Materials for Electrical Energy Storage. *ECS Meet.* **02**, 980–980 (2015).
  36. Marichy, C., Bechelany, M. & Pinna, N. Atomic layer deposition of nanostructured materials for energy and environmental applications. *Adv. Mater.* **24**, 1017–1032 (2012).
  37. Niu, W. *et al.* Applications of atomic layer deposition in solar cells. *Nanotechnology* **26**, 064001 (2015).
  38. Cheng, N. *et al.* Platinum single-atom and cluster catalysis of the hydrogen evolution reaction. *Nat. Commun.* **7**, 1–9 (2016).

39. Minkel, J. The Magic Ingredients in Intel's New, Tinier Transistor - Scientific American. *Scientific American* <https://www.scientificamerican.com/article/the-magic-ingredients-in/> (2007).
40. Mistry, K. *et al.* A 45nm logic technology with high-k+ metal gate transistors, strained silicon, 9 Cu interconnect layers, 193nm dry patterning, and 100% Pb-free packaging. *Tech. Dig. - Int. Electron Devices Meet. IEDM* 247–250 (2007) doi:10.1109/IEDM.2007.4418914.
41. Kim, H., Lee, H. B. R. & Maeng, W. J. Applications of atomic layer deposition to nanofabrication and emerging nanodevices. *Thin Solid Films* **517**, 2563–2580 (2009).
42. Schneider, J. R., Baker, J. G. & Bent, S. F. The Influence of Ozone: Superstoichiometric Oxygen in Atomic Layer Deposition of Fe<sub>2</sub>O<sub>3</sub> Using tert-Butylferrocene and O<sub>3</sub>. *Adv. Mater. Interfaces* **7**, 1–10 (2020).
43. Liu, X. *et al.* ALD of Hafnium Oxide Thin Films from Tetrakis(ethylmethylamino)hafnium and Ozone. *J. Electrochem. Soc.* **152**, G213 (2005).
44. Richey, N. E., De Paula, C. & Bent, S. F. Understanding chemical and physical mechanisms in atomic layer deposition. *J. Chem. Phys.* **152**, 1–17 (2020).
45. Bartram, M. E., Michalske, T. A. & Rogers, J. W. A reexamination of the chemisorption of trimethylaluminum on silica. *J. Phys. Chem.* **95**, 4453–4463 (1991).
46. Lu, J. & Elam, J. W. Low Temperature ABC-Type Ru Atomic Layer Deposition through Consecutive Dissociative Chemisorption, Combustion, and Reduction Steps. *Chem. Mater.* **27**, 4950–4956 (2015).
47. Knudsen, J. *et al.* Stroboscopic operando spectroscopy of the dynamics in heterogeneous catalysis by event-averaging. *Nat. Commun.* **12**, 1–8 (2021).
48. Lizzit, S. & Baraldi, A. High-resolution fast x-ray photoelectron spectroscopy study of ethylene interaction with Ir(1 1 1): From chemisorption to dissociation and graphene formation. *Catal. Today* **154**, 68–74 (2010).
49. Zhang, K., Zhu, G. R., Kong, Y. C. & Chen, T. S. 100 nm Gate-Length AlGaIn/GaN FinFETs with High Linearity of G<sub>m</sub> and f<sub>T</sub>/f<sub>max</sub>. *2018 Int. Conf. Microw. Millim. Wave Technol. ICMMT 2018 - Proc.* **39**, 179–180 (2018).



50. Sze, S. M. & Ng, K. K. Appendix F Properties of Important Semiconductors. in *Physics of Semiconductor Devices* 789–789 (John Wiley & Sons, Inc., 2006). doi:10.1002/9780470068328.app6.
51. Siegbahn, K. & Edvarson, K.  $\beta$ -Ray spectroscopy in the precision range of 1 : 105. *Nucl. Phys.* **1**, 137–159 (1956).
52. Nobel Foundation. The Nobel Prize in Physics 1921. *Nobelprize.org* [http://www.nobelprize.org/nobel\\_prizes/physics/laureates/1921/index.html](http://www.nobelprize.org/nobel_prizes/physics/laureates/1921/index.html) (1921).
53. Nordling, C., Sokolowski, E. & Siegbahn, K. Precision Method for Obtaining Absolute Values of Atomic Binding Energies. *Phys. Rev.* **105**, 1676–1677 (1957).
54. Dombey, N. The Nobel Prize in Physics. *Nature* vol. 300 106–107 <https://www.nobelprize.org/prizes/physics/1915/summary/> (1982).
55. Hertz, H. Ueber einen Einfluss des ultravioletten Lichtes auf die electriche Entladung. *Ann. Phys.* **267**, 983–1000 (1887).
56. Einstein, A. Über einen die Erzeugung und Verwandlung des Lichtes betreffenden heuristischen Gesichtspunkt. *Ann. Phys.* **322**, 132–148 (1905).
57. Hüfner, S. *Photoelectron Spectroscopy*. (Springer Berlin Heidelberg, 2003). doi:10.1007/978-3-662-09280-4.
58. Eastman, D. E. & Nathan, M. I. Photoelectron spectroscopy. *Phys. Today* **28**, 44–51 (1975).
59. Koopmans, T. Über die Zuordnung von Wellenfunktionen und Eigenwerten zu den Einzelnen Elektronen Eines Atoms. *Physica* **1**, 104–113 (1934).
60. Sawatzky, G. A. & Antonides, E. the Electronic Structure and Electron Correlation Effects Studied By Xps. *Le J. Phys. Colloq.* **37**, C4-117-C4-123 (1976).
61. Travnikova, O. *et al.* The ESCA molecule - Historical remarks and new results. *J. Electron Spectros. Relat. Phenomena* **185**, 191–197 (2012).
62. Gelius, U., Basilier, E., Svensson, S., Bergmark, T. & Siegbahn, K. A high resolution ESCA instrument with X-ray monochromator for gases and solids. *J. Electron Spectros. Relat. Phenomena* **2**, 405–434 (1973).
63. Tanuma, S., Powell, C. J. & Penn, D. R. Calculation of electron inelastic

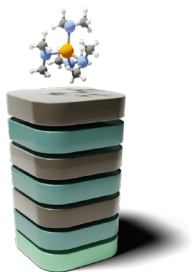
- mean free paths (IMFPs) VII. Reliability of the TPP-2M IMFP predictive equation. *Surf. Interface Anal.* **35**, 268–275 (2003).
64. Tanuma, S., Powell, C. J. & Penn, D. R. Electron Inelastic Mean Free Paths in Organic Materials Especially for Polyethylene and Guanine. *Hyomen Kagaku* **15**, 175–180 (1994).
  65. Yeh, J. J. & Lindau, I. Atomic subshell photoionization cross sections and asymmetry parameters:  $1 \leq Z \leq 103$ . *At. Data Nucl. Data Tables* **32**, 1–155 (1985).
  66. Cooper, J. W. Photoionization from outer atomic subshells. a model study. *Phys. Rev.* **128**, 681–693 (1962).
  67. Shirley, D. A. High-resolution x-ray photoemission spectrum of the valence bands of gold. *Phys. Rev. B* **5**, 4709–4714 (1972).
  68. Tougaard, S. Practical algorithm for background subtraction. *Surf. Sci.* **216**, 343–360 (1989).
  69. Doniach, S. & Sunjic, M. Many-electron singularity in X-ray photoemission and X-ray line spectra from metals. *J. Phys. C Solid State Phys.* **3**, 285–291 (1970).
  70. Minnhagen, P. Increased phonon broadening of XPS lines of metals due to finite core-hole lifetime. *J. Phys. F Met. Phys.* **6**, 1789–1800 (1976).
  71. Andersen, J. N. *et al.* Vibrational fine structure in the C 1s core level photoemission of chemisorbed molecules: Ethylene and ethylidyne on Rh(111). *Chem. Phys. Lett.* **269**, 371–377 (1997).
  72. Groot, F. De. Multiplet effects in X-ray spectroscopy. *Coord. Chem. Rev.* **249**, 31–63 (2005).
  73. Greczynski, G. & Hultman, L. Compromising Science by Ignorant Instrument Calibration—Need to Revisit Half a Century of Published XPS Data. *Angew. Chemie - Int. Ed.* **59**, 5002–5006 (2020).
  74. The Nobel prize organization. The Nobel Prize in Physics. *Science* vol. 72 [https://www.nobelprize.org/prizes/physics/1901/summary/%0Ahttp://www.nobelprize.org/nobel\\_prizes/physics/laureates/1901](https://www.nobelprize.org/prizes/physics/1901/summary/%0Ahttp://www.nobelprize.org/nobel_prizes/physics/laureates/1901) (1930).
  75. Dombey, N. The Nobel Prize in Physics. *Nature* vol. 300 106–107 [http://www.nobelprize.org/nobel\\_prizes/physics/laureates/1914/index.html](http://www.nobelprize.org/nobel_prizes/physics/laureates/1914/index.html) (1982).
  76. Kerst, D. W. Historical development of the betatron. *Nature* **157**, 90–95

- (1946).
77. Elder, F. R., Gurewitsch, A. M., Langmuir, R. V. & Pollock, H. C. Radiation from electrons in a synchrotron [8]. *Phys. Rev.* **71**, 829–830 (1947).
  78. Tavares, P. F., Leemann, S. C., Sjöström, M. & Andersson, Å. The max iv storage ring project. *J. Synchrotron Radiat.* **21**, 862–877 (2014).
  79. Zhu, S. *et al.* HIPPIE: A new platform for ambient-pressure X-ray photoelectron spectroscopy at the MAX IV Laboratory. *J. Synchrotron Radiat.* **28**, 624–636 (2021).
  80. Kokkonen, E. *et al.* Upgrade of the SPECIES beamline at the MAX IV Laboratory. *J. Synchrotron Radiat.* **28**, 588–601 (2021).
  81. Feifel, R. *et al.* Role of stray light in the formation of high-resolution resonant photoelectron spectra: An experimental and theoretical study of N 2. *J. Electron Spectros. Relat. Phenomena* **134**, 49–65 (2004).
  82. Knudsen, J., Andersen, J. N. & Schnadt, J. A versatile instrument for ambient pressure x-ray photoelectron spectroscopy: The Lund cell approach. *Surf. Sci.* **646**, 160–169 (2016).
  83. Starr, D. E., Liu, Z., Hävecker, M., Knop-Gericke, A. & Bluhm, H. Investigation of solid/vapor interfaces using ambient pressure X-ray photoelectron spectroscopy. *Chem. Soc. Rev.* **42**, 5833–5857 (2013).
  84. Schnadt, J. *et al.* The new ambient-pressure X-ray photoelectron spectroscopy instrument at MAX-lab. *J. Synchrotron Radiat.* **19**, 701–704 (2012).
  85. Ogletree, D. F. *et al.* A differentially pumped electrostatic lens system for photoemission studies in the millibar range. *Rev. Sci. Instrum.* **73**, 3872 (2002).
  86. HiPP-3 - Scienta Omicron. <https://scientaomicron.com/en/Instruments/Electron-Analysers/HiPP-3>.
  87. Plante, L. & Cucinotta, F. A. Cross sections for the interactions of 1 eV–100 MeV electrons in liquid water and application to Monte-Carlo simulation of HZE radiation tracks. *New J. Phys.* **11**, (2009).
  88. Urpelainen, S. *et al.* The SPECIES beamline at the MAX IV Laboratory: A facility for soft X-ray RIXS and APXPS. *J. Synchrotron Radiat.* **24**, 344–353 (2017).

89. Li, K., Li, S., Li, N., Dixon, D. A. & Klein, T. M. Tetrakis(dimethylamido)hafnium adsorption and reaction on hydrogen terminated Si(100) surfaces. *J. Phys. Chem. C* **114**, 14061–14075 (2010).
90. Ye, L. & Gougousi, T. In situ infrared spectroscopy study of the interface self-cleaning during the atomic layer deposition of HfO<sub>2</sub> on GaAs(100) surfaces. *Appl. Phys. Lett.* **105**, 121604 (2014).
91. Hinkle, C. L. *et al.* GaAs interfacial self-cleaning by atomic layer deposition. *Appl. Phys. Lett.* **92**, 1–4 (2008).
92. Rodríguez-Reyes, J. C. F. & Teplyakov, A. V. Surface transamination reaction for tetrakis(dimethylamido)titanium with NH<sub>x</sub>-terminated Si(100) surfaces. *J. Phys. Chem. C* **111**, 16498–16505 (2007).
93. Rodríguez-Reyes, J. C. F. & Teplyakov, A. V. Mechanisms of adsorption and decomposition of metal alkylamide precursors for ultrathin film growth. *J. Appl. Phys.* **104**, (2008).
94. Wang, Y., Zahid, F., Wang, J. & Guo, H. Structure and dielectric properties of amorphous high- $\kappa$  oxides: HfO<sub>2</sub>, ZrO<sub>2</sub>, and their alloys. *Phys. Rev. B* **85**, 1–5 (2012).
95. Ye, L. & Gougousi, T. Indium diffusion and native oxide removal during the atomic layer deposition (ALD) of TiO<sub>2</sub> films on InAs(100) surfaces. *ACS Appl. Mater. Interfaces* **5**, 8081–8087 (2013).
96. Li, Z., Su, J. & Wang, X. Atomic layer deposition in the development of supercapacitor and lithium-ion battery devices. *Carbon N. Y.* **179**, 299–326 (2021).
97. Vervuurt, R. H. J., Kessels, W. M. M. E. & Bol, A. A. Atomic Layer Deposition for Graphene Device Integration. *Adv. Mater. Interfaces* **4**, 1700232 (2017).
98. Hausmann, D. M., Kim, E., Becker, J. & Gordon, R. G. Atomic layer deposition of hafnium and zirconium oxides using metal amide precursors. *Chem. Mater.* **14**, 4350–4358 (2002).
99. Stoddart, C. Is there a reproducibility crisis in science? *Nature* **533**, 452–454 (2016).
100. Baker, M. & Penny, D. Is there a reproducibility crisis? *Nature* **533**, 452–454 (2016).
101. Xu, W., Lemaire, P. C., Sharma, K., Hausmann, D. M. & Agarwal, S. Surface reaction mechanisms during atomic layer deposition of zirconium

- oxide using water, ethanol, and water-ethanol mixture as the oxygen sources. *J. Vac. Sci. Technol. A* **38**, 012401 (2020).
102. Seo, S. *et al.* Reaction Mechanisms of Non-hydrolytic Atomic Layer Deposition of Al<sub>2</sub>O<sub>3</sub> with a Series of Alcohol Oxidants. *J. Phys. Chem. C* **125**, 18151–18160 (2021).
  103. Kukli, K., Ritala, M. & Leskelä, M. Low-temperature deposition of zirconium oxide-based nanocrystalline films by alternate supply of Zr[OC(CH<sub>3</sub>)<sub>3</sub>]<sub>4</sub> and H<sub>2</sub>O. *Chem. Vap. Depos.* **6**, 297–302 (2000).
  104. Elam, J. W. *et al.* Mechanism for zirconium oxide atomic layer deposition using bis(methylcyclopentadienyl)methoxymethyl zirconium. *Appl. Phys. Lett.* **91**, 253123 (2007).
  105. Wang, J. & Durbeej, B. How accurate are TD-DFT excited-state geometries compared to DFT ground-state geometries? *J. Comput. Chem.* **41**, 1718–1729 (2020).
  106. Scardamaglia, M. *et al.* Comparative study of copper oxidation protection with graphene and hexagonal boron nitride. *Carbon N. Y.* **171**, 610–617 (2021).
  107. Larsson, A. *et al.* Thickness and composition of native oxides and near-surface regions of Ni superalloys. *J. Alloys Compd.* **895**, 162657 (2022).
  108. Temperton, R. H. *et al.* Resonant X-ray photo-oxidation of light-harvesting iron (II/III) N-heterocyclic carbene complexes. *Sci. Rep.* **11**, 1–14 (2021).
  109. Shavorskiy, A. *et al.* Gas Pulse-X-Ray Probe Ambient Pressure Photoelectron Spectroscopy with Submillisecond Time Resolution. *ACS Appl. Mater. Interfaces* **13**, 47629–47641 (2021).
  110. Allen, M. J., Tung, V. C. & Kaner, R. B. Honeycomb carbon: A review of graphene. *Chem. Rev.* **110**, 132–145 (2010).
  111. Zhang, K., Feng, Y., Wang, F., Yang, Z. & Wang, J. Two dimensional hexagonal boron nitride (2D-hBN): Synthesis, properties and applications. *J. Mater. Chem. C* **5**, 11992–12022 (2017).
  112. Camilli, L., Yu, F., Cassidy, A., Hornekær, L. & Bøggild, P. Challenges for continuous graphene as a corrosion barrier. *2D Mater.* **6**, 022002 (2019).
  113. Shen, L. *et al.* A long-term corrosion barrier with an insulating boron nitride monolayer. *J. Mater. Chem. A* **4**, 5044–5050 (2016).
  114. Lampimäki, M., Lahtonen, K., Hirsimäki, M. & Valden, M. Nanoscale

- oxidation of Cu(100): Oxide morphology and surface reactivity. *J. Chem. Phys.* **126**, 034703 (2007).
115. Zuo, Z. J., Li, J., Han, P. De & Huang, W. XPS and DFT studies on the autoxidation process of Cu sheet at room temperature. *J. Phys. Chem. C* **118**, 20332–20345 (2014).
  116. Miikkulainen, V., Vehkamäki, M., Mizohata, K., Hatanpää, T. & Ritala, M. Highly Material Selective and Self-Aligned Photo-assisted Atomic Layer Deposition of Copper on Oxide Materials. *Adv. Mater. Interfaces* **8**, 2100014 (2021).



ISBN 978-91-8039-230-3  
Division of Synchrotron Radiation Research  
Department of Physics  
Faculty of Science  
Lund University

